Development of a Thermal Lag Test Engine

Edward Vandermeersch, Michael Calcoen

Promotoren: prof. dr. ir. Michel De Paepe, prof. dr. ir. Sebastian Verhelst
Begeleider: Carlos Fernandez Aballi Altamirano

Masterproef ingediend tot het behalen van de academische graad van
Master in de ingenieurswetenschappen: werktuigkunde-elektrotechniek

Vakgroep Mechanica van stroming, warmte en verbranding
Voorzitter: prof. dr. ir. Roger Sierens
Faculteit Ingenieurswetenschappen
Academiejaar 2009-2010

UNIVERSITEIT
GENT

Development of a Thermal Lag Test Engine

Edward Vandermeersch, Michael Calcoen

Promotoren: prof. dr. ir. Michel De Paepe, prof. dr. ir. Sebastian Verhelst
Begeleider: Carlos Fernandez Aballi Altamirano

Masterproef ingediend tot het behalen van de academische graad van
Master in de ingenieurswetenschappen: werktuigkunde-elektrotechniek

Vakgroep Mechanica van stroming, warmte en verbranding
Voorzitter: prof. dr. ir. Roger Sierens
Faculteit Ingenieurswetenschappen
Academiejaar 2009-2010

UNIVERSITEIT
GENT

Ghent, June 2010

The authors

Michaël Calcoen Edward Vandermeersch

Acknowledgments

We would like to express our gratitude to a number of people, without whom this project would have never been realised.

First, we would like to thank prof. dr. ir. Michel De Paepe and prof. dr. ir. Sebastian Verhelst for giving us the opportunity to work on this subject and for their support and advice throughout the year.

Also, we would like to express our sincere gratitude to ir. Carlos Fernandez-Aballi Altamirano for his ongoing guidance and energy. His insights have given a different perspective on things more than once.

The project also would have never succeeded without the experience and enthusiasm of Robert Gillis. Many thanks go out to him for helping us out on many occasions.

We thank Patrick De Pue for his work. He has been of great assistance in implementing the electronics of the rig.

ir. Jonas Galle is thanked for his help on the problems with the data acquisition, during late nights and long weekends.

Special thanks go out to our girlfriends Kim and Ann-Julie, our parents and many friends for their patience and persistent support all year.

Last but not least, many thanks go out to Steve Clissold, sales manager at Marsh Bellofram Corporation (UK), who was extremely generous to provide us with a number of their rolling seals.

Michaël Calcoen
Edward Vandermeersch

Abstract

In this master thesis experimental research is done on the Thermal Lag Engine. In first instance, a literature study is performed, in which a stark contrast in opinions on the working principle of the engine is revealed. An experimental test rig design is presented. It was designed and constructed, based on the statements about the possible working principles and previously built engines described in literature. The first pressure versus volume diagrams of this engine that were obtained are presented. An important step is taken, as suggestions about statements in literature are made based on experimental results for the first time.

Development of a Thermal Lag Test Engine

Michaël Calcoen and Edward Vandermeersch

Supervisor(s): Michel De Paepe, Sebastian Verhelst and Carlos Fernandez-Aballi Altamirano

Abstract—**After a short introduction to Peter Tailer's Thermal Lag Engine (TLE) is given, the discussion in literature about the TLE is briefly touched. It has led to the development of a Thermal Lag test engine that was designed and built within the scope of the thesis project. The first pV-diagrams obtained from experiments that were performed on the test rig are presented.**

Keywords—**Thermal lag engine, Stirling engine, Alternative energy resources**

I. INTRODUCTION

IN the light of a growing awareness of environmental degradation the world is looking for solutions. Stirling engines are external combustion engines that have inherent advantages such as fuel flexibility, continuous combustion with clean emissions, silent operation amongst other things. The Thermal Lag Engine (TLE) represents a mechanical simplification of the Stirling engine, which adds a new, social dimension to the concept. The TLE could make a difference in developing countries, where the need for low cost site built engines running on local resources can be met. In a joint research between Ghent University and the Higher Polytechnic Institute of Havana, a project was launched to investigate numerically and experimentally the inner workings of the TLE.

II. BACKGROUND

In 1995, Peter Tailer patented an elegantly simple external combustion engine, the Thermal Lag Engine [1]. It represents a mechanical simplification of common Stirling engines as it exhibits only a single moving piece, the piston. He realised that the limiting factor of Stirling engines' power output is the time it takes for gas to exchange heat. This so called 'thermal lag' is what inspired Tailer to build an engine that, instead of being limited by it, uses it as a driving phenomenon. The engine consists of a hot space connected to a cold space in which a piston runs, see figure 1. West describes the working principle of the engine based on the engine speed relative to the heat transfer in the cold space [3]. At the right speed, the heat transfer from the gas to the heat exchangers lags behind the piston movement. Because of the time shift between the movement of the fluid and the heat transfer, expansion takes place at a higher temperature and pressure than the compression. Therefore the engine produces a net work output. West and Tailer claim that the main effect of the TLE is the bulk motion of the fluid from the hot to the cold space and back. This flow regime leads to the heat transfer that drives the engine. Fourteen years later, in 2007, Allan Organ published an alternative approach in his book [2]. With a background in the area of pulse tube refrigeration devices, Organ explained the engine from a completely different perspective. He identified the connecting space between the hot and cold spaces of Tailer's TLE as a pulse tube and contradicted the previously stated working principles. He considers the flow

Fig. 1. Picture taken from the original Thermal Lag Machine patent, granted to Tailer in 1995 [1].

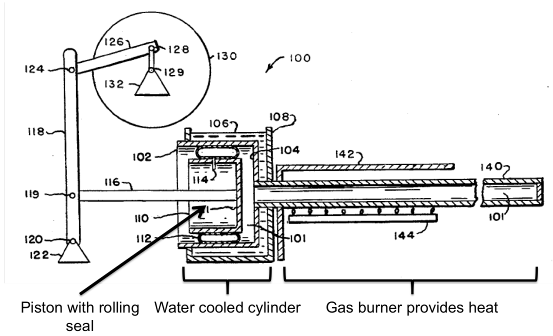

as being very laminar and stratified and divides the fluid into multiple control volumes, hereby neglecting the bulk fluid mixing throughout the engine. Organ stresses that the pulse tube is essential to the functioning of the engine. Different working principles were claimed in literature, but all of these researchers lack the experimental proof to back up their statements. Thorough analysis of the proposed working mechanisms further revealed that they are not explicitly contradictory, but represent different implementations of the same effect. Discussions in literature about minor differences in effects overlook the essence, which is the de-phasing of the heat transfer and the movement of the piston. Further research should focus on these different implementations and investigate which renders maximum power and efficiency.

III. EXPERIMENTAL WORK

A thermal lag test engine was designed and built to perform experiments and to obtain the first pressure versus volume diagrams of this type of engine. The requirements for the test rig were based on claims concerning the possible working principles and descriptions of previously built engines in literature. The design incorporates the possibility to adopt the engine configurations of both Organ and Tailer. It allows to reproduce their experiments and investigate optimal operating conditions. Furthermore, the rig is equipped with a variety of sensors to measure inside the engine in order to derive pV-diagrams and acquire a more profound insight in the inner workings of the TLE. A schematic overview of the test rig that was built is shown figure 2.

A. *Experimental Results*

Two sets of experiments were conducted in the time span of the thesis. The first data set was recorded when the heater did not meet the specifications. One of the pV-diagrams obtained from the first session is shown in figure 3. Expansion curves are always represented in red, compression curves in blue. At the end

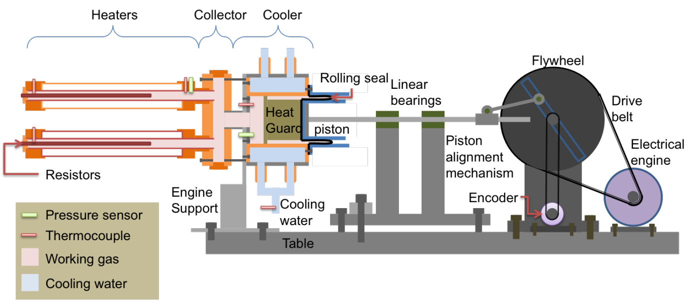

Fig. 2. Schematic overview of the test rig that was built.

of the expansion, the curve tends to bend downward. Cooling has increased towards bottom dead centre (BDC), making pressure drop. At the beginning of the compression stroke, cooling continues due to the thermal inertia of the gas. As cooling becomes optimal after BDC, the trend of lowered pressure carries on along the compression line, creating a 'belly' that opens up the cycle (a). Compression occurs at a lower mean pressure than expansion. Toward the end of the compression stroke, the gas

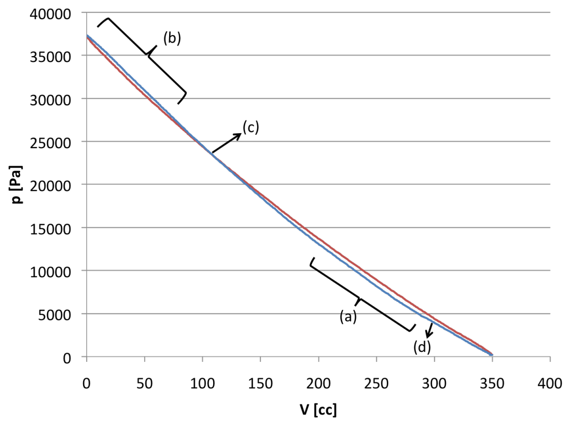

Fig. 3. pV-diagram at 3 Hz with a 5.5 cm stroke.

is already heating up and pressure rises. The expansion stroke that follows happens faster, so the heater cannot heat the gas fast enough to compensate the pressure drop resulting from the increasing volume. As a result, the expansion line drops below that of compression after TDC (b). The cycle is going too fast to allow the heater to deliver heat to the gas. If the heater were fast enough, pressure would rise at TDC, lifting the expansion line over the compression line and thus opening up the cycle. Further along the expansion stroke heat input improves again when gas pressure and thus temperature drops, increasing the temperature difference between heater and gas. This gives the expansion a more isothermal character. Furthermore, cooling has not yet increased significantly. As a result, the expansion line crosses the compression line and a butterfly shaped cycle is created (c). This pV-diagram represents a motor cycle, because the cycle is opened up due to cooling at BDC. It has an indicated work output of 0.071 J. At 3.2 Hz the indicated power output is of 0.227 W with an error of 0.186 W. The cycle has an efficiency of 1.14%

Tailer and Organ state that the most significant pressure changes occur at bottom and top dead centre. The pV-diagram in figure 3, however, shows that the cycle opens up at a certain point (d) *during* compression. This observation could be linked to the flow dynamics in the cylinder. It is only when the piston starts recompressing the gas that vortices occur near the cylinder walls, increasing convection coefficients. In figure 4 one

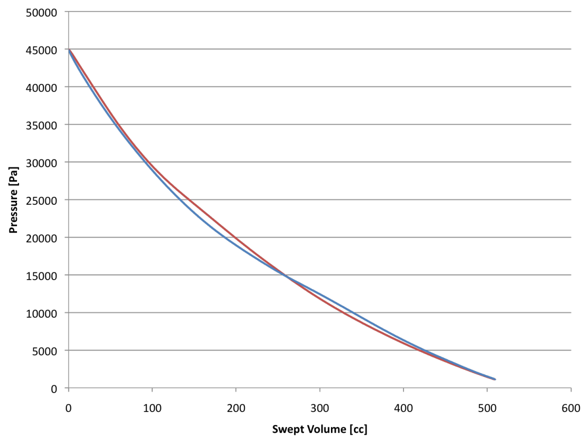

Fig. 4. pV-diagram at 3 Hz with an 8 cm stroke.

of the pV-diagrams of the second set of experiments is shown. For this session the heater was improved by providing additional heating elements. On the pV-diagram it can be seen that the previously observed cooling effect is lost completely. This indicates that the additional heating elements undermined the proper functioning of the cooler. Around top dead centre, however, a positive heater effect is observed. Heat is given to the gas after TDC, lifting the expansion line above the compression line. The absence of a positive cooling effect, however, keeps the cycle from opening up completely. With proper adjustments of the rig, both effects could be combined and reinforced. Cycles with significantly higher work outputs and efficiencies could then be expected.

IV. Conclusions

Up until this point, researchers have only viewed the TLE as a black box. The pV-diagrams that were obtained thus represent an important first step. To improve engine performance, the driving phenomena of this engine need to be fully understood. Future research should investigate the different claims that have been made in literature to identify which implementation of the thermal lag effect can maximise engine performance.

References

[1] Peter Tailer, *Thermal Lag Machine, U.S. Patent*, Patent No 5414997, 1995.
[2] Allan Organ, *The Air Engine, Part 2: Some light on the inner workings of the thermal lag engine*, Woodhead Publishing Ltd, 2007.
[3] Colin D. West, *Some Single-Piston Closed-Cycle Machines and Peter Tailer's Thermal Lag Engine, Proceedings of the 28th Intersociety Energy Conversion Engineering Conference*, American Society of Mechanical Engineers, Atlanta, USA, 1993.

Nederlandstalige Samenvatting

Deze thesis behandelt de ontwikkeling van een experimentele opstelling van een 'thermal lag motor', of Thermal Lag Engine (TLE) in het Engels. Dit project past in een grotere context van het groeiend ecologisch bewustzijn van de impact van de mensheid op het milieu. Daarom wordt in de wereld meer en meer gezocht naar alternatieve oplossingen. Stirling motoren zijn uitwendige verbrandingsmotoren die inherente voordelen vertonen zoals flexibiliteit in brandstof, continue verbranding met controle over uitstoot en stille werking onder andere. De TLE vertegenwoordigt een mechanische vereenvoudiging van de Stirling motor, waardoor een nieuwe, sociale dimensie toegevoegd wordt aan het concept. De TLE zou een verschil kunnen maken in ontwikkelingslanden, waar de behoeft kan ingevuld worden aan goedkope, ter plaatse geproduceerde motoren die draaien op lokaal beschikbare energiebronnen. De Universiteit Gent heeft in samenwerking met het Higher Polytechnic Institute of Havana een project gelanceerd om numeriek en experimenteel onderzoek te voeren naar de onderliggende werkingsmechanismen van de TLE.

In 1995 werd aan Peter Tailer een patent toegewezen voor een uiterst eenvoudige uitwendige verbrandingsmotor, de 'Thermal Lag Engine'. Het vertegenwoordigt een vereenvoudiging van de Stirling motor, aangezien slecht een enkel bewegend deel heeft, de zuiger. Tailer realiseerde zich dat de beperkende factor op de vermogensoutput van Stirling motoren de tijd was die het duurde voor het gas om warmte uit te willen in de motor. Dit zogenaamde 'thermal lag' effect inspireerde Tailer om een motor te bouwen die, in plaats van beperkt te worden door dit effect, er net zijn voordeel uit haalde. De motor bestaat uit twee ruimtes: een warme ruimte die verbonden is met een gekoelde cylinder, waarin de zuiger beweegt, zie figuur 1.

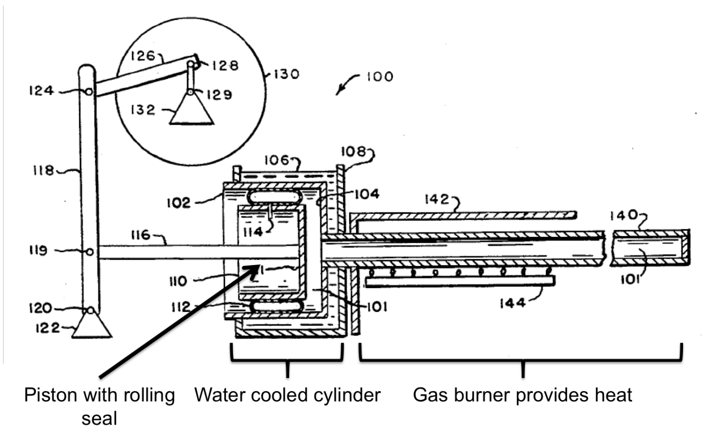

Figure 1: Figuur uit het originele 'Thermal Lag Machine' patent, toegekend aan Peter Tailer in 1995.

West beschrijft het werkingsprincipe van de motor gebaseerd op de snelheid van de motor relatief ten op zichte van de warmte-overdrachtssnelheid van de koude warmtewisselaar. Aan de juiste snelheid ijlt de warmteoverdracht tussen het gas en de warmtewisselaars na op de beweging van de zuiger. Door deze tijdsverschuiving van de beweging van de vloeistof en warmteoverdracht gebeurt expansie op een hogere temperatuur en druk ten op zichte van compressie. Hierdoor produceert de motor arbeid. West en Tailer claimen dat het drijvende effect achter de motor in de beweging van een grote massa gas naar de koude ruimte en terug. Dit stromingsregime leidt tot tot de warmte overdracht die de drijvende kracht vormt van de motor. Veertien jaar later, in 2007, publiceerde Allan Organ een alternatieve aanpak in zijn boek. Met zijn achtergrond in het domein van de 'pulse tube' cryo-koelers legde Organ de motor uit vanuit een volledig ander perspectief. Hij identificeerde de verbindingsruimte tussen de warmte en de koude ruimtes in de TLE van Tailer met een 'pulse tube' en sprak de voorheen geformuleerde werkingsprincipes tegen. Dit mondde zelf uit in de uitspraak van Organ dat de toekenning van Tailers patent niet in overeenstemming was met de werking van de motor. Hij beschouwt de stroming als zijnde zeer laminair en gestratifieerd en deelt de vloeistof op in meerdere controlevolumes, waarbij onderlinge menging van gas in de motor verwaarloosd wordt. Organ benadrukt dat de 'pulse tube' essentieel is voor de werking van de motor. Verschillende stelling werden geformuleerd in de literatuur, maar al deze onderzoekers hebben een gebrek aan experimenteel bewijs om die stelling hard te maken. Een grondig onderzoek van de voorgestelde werkingsmechanismen legde verder bloot dat de gemaakte stelling niet per se tegenstrijdig zijn, maar eerder verschillende implementaties zijn van hetzelfde effect. Discussies in de literatuur over kleine verschillen in effect gaan voorbij aan de essentie: de defasering van de warmteoverdracht en de beweging van de zuiger. Verder onderzoek zou de nadruk moeten leggen op deze verschillende implementaties en onderzoeken welke de optimale vermogensoutput en rendement vertonen.

Een testopstelling van een TLE werd ontworpen en gebouwd om experimenten uit te voeren en om de eerste pV-diagramma's van deze motor te bekomen. De eisen voor de testopstelling werden gebaseerd op de claims betreffende de mogelijke werkingsprincipes en de beschrijving van voorheen gebouwde testopstellingen in de literatuur. Het ontwerp incorporeert de mogelijkheid om de verschillende configuraties van Organs en Tailers motoren over te nemen. Het laat toe om hun experimenten te reproduceren en de optimale werkomstandigheden te onderzoeken. Verder werd de opstelling voorzien van sensoren om binnenin te motor te meten. Dit laat toe pV-diagramma's af te leiden een diep inzicht te verkrijgen in de interne werking van de TLE. Een schematisch overzicht van de testopstelling is te zien in figuur 2.

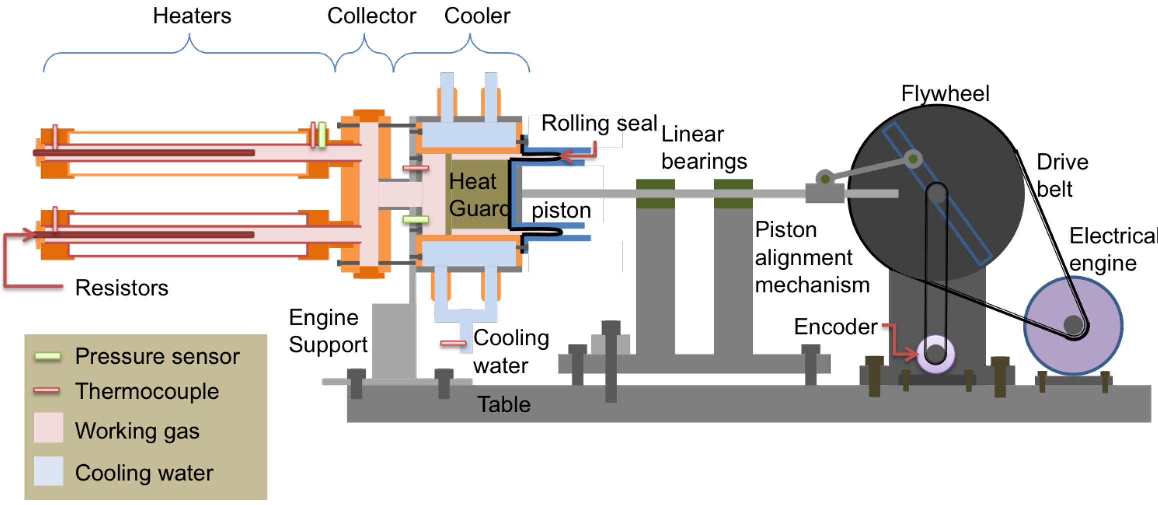

Figure 2: Schematisch overzicht van de gebouwde testopstelling.

Twee sets van experimenten werden uitgevoerd in de tijdspanne van de thesis. De eerst data set werd opgemeten toen de verhitter nog niet voldeed aan de eisen. Een van de pV-diagramma's die verkregen werd tijdens deze eerste sessie is te zien in figuur 3. De expansie curves zijn altijd afgebeeld in het rood, de compressiecurves in het blauw. Tegen het einde van de expansie neigt de expansielijn naar beneden. De koeling is verbeterd naar het onderste dode punt toe, waardoor de druk daalt. Wanneer de koeling optimaal wordt na het onderste dode punt, wordt de trend van verlaagde druk voortgezet en versterkt langsheen het eerste deel van de compressielijn. Dit creëert een 'buik' die de cycles opentrekt (a). De compressie gebeurt op een gemiddeld lagere druk dan expansie. Tegen het einde van de compressieslag wordt het gas reeds opgewarmd in de verhitter en de druk stijgt. De expansieslag die volgt gebeurt sneller, waardoor de verhitter het gas niet vlug genoeg kan opwarmen om de drukval tegen gevolge van de volumetoename te compenseren. Het resultaat is dat de expansielijn onder de compressielijn valt na het bovenste dode punt (b). De cyclus gaat te snel om de verhitter toe te laten warmte te leveren aan het gas. Indien de verhitter snel genoeg was, zou druk stijgen na het bovenste dode punt, waardoor de expansielijn boven de compressielijn getild wordt en de cyclus meer opgetrokken wordt met resulterende arbeidsoutput. Verder langsheen de expansielijn verbetert de warmteinput terug een beetje door de dalende druk en dus temperatuur van het gas. De expansie krijgt dus een iets iets isothermer karakter. Verder is de koeling nog niet op gang gekomen. Het resultaat is dat de expansie en compressielijn elkaar kruisen en een vlindervormige cyclus gevormd wordt (c). Het positieve effect van de koeler is net sterker dan het negatieve effect van de slecht presterende verhitter, waardoor netto arbeid geleverd wordt. Aan 3.2 Hz is de geïndiceerde vermogensoutput 0.227 W met een fout van 0.186 W. De cyclus heeft een rendement van 1.14%.

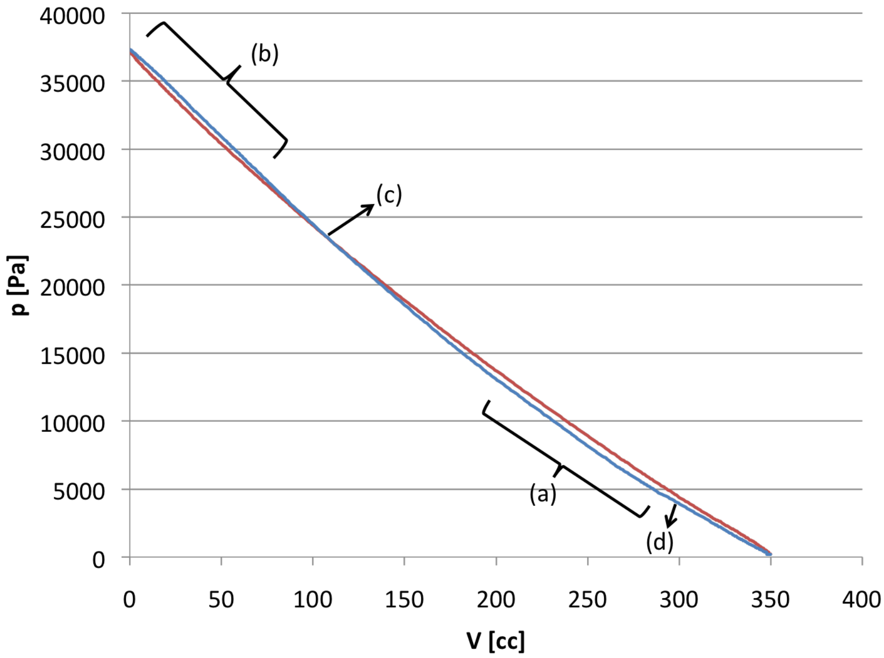

Figure 3: pV-diagram opgemeten aan 3 Hz met een slaglengte van 5.5 cm.

Tailer en Organ stellen dat de meest significant drukveranderingen voorkomen op het bovenste en onderste dode punt. Het pV-diagramma van figuur 3, echter, toont dat de cyclus echt opent vanaf een punt (d), *tijdens* compressie. Deze observatie zou kunnen gelinkt worden aan de stromingsdynamica in de cylinder. Het is pas wanneer de zuiger begint te recomprimeren dat er wervels voorkomen nabij de cilinderwanden, waardoor de convectiecoëfficiënten verhoogt worden. Figuur 4 toont een pV-diagram opgemeten in de tweede set van experimenten. In deze sessie was de verhitter verbeterd ten opzicht van de eerste sessie. Extra verwarmingselementen werden voorzien om de warmteinput naar het gas te verhogen. Op het pV-diagramma, echter, kan worden gezien dat het positieve koeleffect van het eerste pV-diagramma volledig afwezig is. Dit toont aan dat de extra verwarmingselementen de goede werking van de koeler ondermijnd hebben. Rond het bovenste dode punt, echter, kan een positief verhittereffect geobserveerd worden. Warmte wordt toegevoerd aan het gas na het bovenste dode punt, waardoor de expansielijn boven de compressielijn getild wordt. Het ontbreken van een positief koelereffect zorgt er echter voor dat de cyclus niet volledig open is. Het resultaat is terug een vlindervormig verloop van de cyclus. Met de nodige aanpassing aan de testopstelling zouden beide geobserveerde positieve effecten kunnen gecombineerd en versterkt worden. Open cycli met significant hogere arbeidsoutput en rendementen kunnen dan verwacht worden.

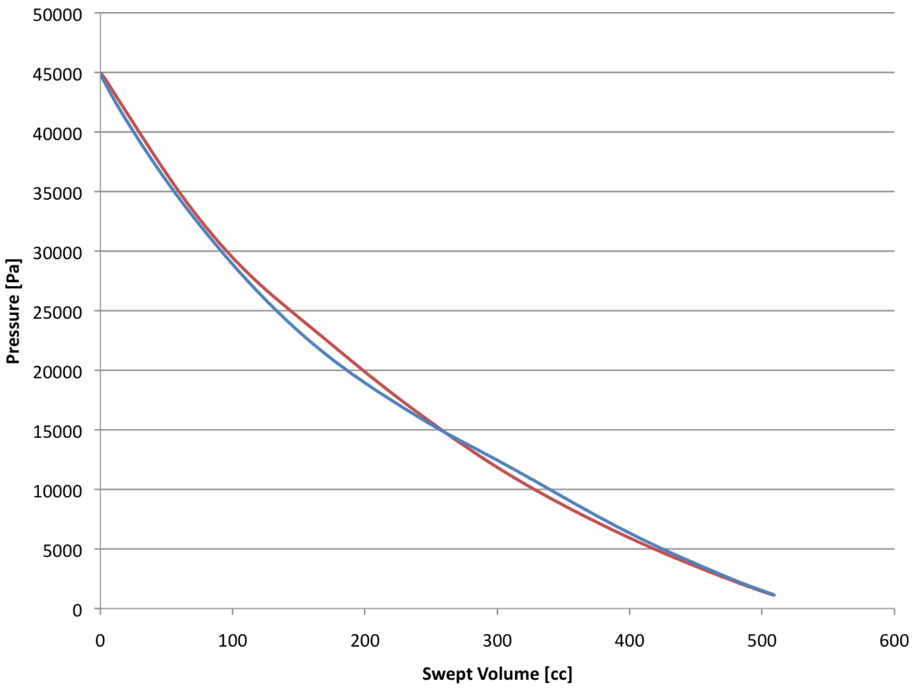

Figure 4: pV-diagram opgemeten aan 3 Hz met een slaglengte van 5.5 cm.

Tot op heden werd de TLE door onderzoekers beschouwd als een zwarte doos. De opgemeten pV-diagramma's vertegenwoordigen dus een belangrijke eerste stap in het begrijpen van de werkingsmechanismen van de TLE op basis metingen binnenin de motor. Om motorprestaties te verbeteren dienen de drijvende fenomenen van de TLE volledig begrepen te worden. Toekomstig onderzoek zou de verschillende claims die gemaakt werden in de literatuur moeten onderzoeken om uit te maken welke implementatie van het 'thermal lag' effect de prestaties kan maximaliseren.

Nomenclature

Abbreviation	Dimension	Description
T	$[K]$	Temperature
Q	$[J]$	Heat flow
U	$[\frac{W}{m^2K}]$	Overal heat transfer coefficient
A	$[m^2]$	Heat transfer area
R	$[\frac{mK}{W}]$	Thermal resistance
k	$[\frac{W}{mK}]$	Thermal conductivity
p	$[Pa]$	pressure
V	$[m^3]$	volume
$\dot{m}$	$[\frac{kg}{s}]$	Mass flow
c_p	$[\frac{J}{kgK}]$	Specific heat capacity
TDC	$[-]$	Top dead centre
BDC	$[-]$	Bottom dead centre
Pr	$[-]$	Prandtl number
Ra	$[-]$	Rayleigh number
β	$[\frac{1}{K}]$	Thermal expansion coefficient
ν	$[\frac{m^2}{s}]$	Kinematic viscosity
Subscript		**Description**
c，$cold$		Cooler
h，hot		Heater
g		Gas
w		Pulse tube wall
in		Input, inlet
out		Output, outlet
$conv$		Convection
ax		Axial
rad		Radial
$insul$		Insulation
CF		Ceramic fiber
RW		Rock wool

Contents

Chapter 1

Introduction

This master thesis is part of a joint research project on the Thermal Lag Engine (TLE) between the Department of Flow, Heat and Combustion Mechanics at Ghent University and the Centre for the Study of Renewable Energy Technologies (CETER) at the Polytechnic University of Havana (Cujae).

The subject of our work is embedded in a broader context of environmental and social concern. As the TLE represents a mechanical simplification of classic Stirling engines, it holds numerous assets. In addition to the environmental benefits displayed by classic external combustion engines, the mechanical robustness of this engine could provide a breakthrough in a new generation of thermal energy converters.

The objective of this master thesis is threefold.

First, to make a detailed analysis of literature to gather information of the state of the art and identify the claims made by others on the TLE.

Second, to design and construct an experimental rig that allows to capture the important phenomena that were identified in the literature study.

Third, to test the functionality of the rig and acquire the initial set of measurements in order to gain profound insight in the mechanisms that drive the engine. Also, to recommend improvements for the rig and further research in order to develop a sound experimental base that can provide the required understanding which will permit to develop a competitive TLE for renewable energy applications.

This work was carried out in close cooperation with doctoral student Carlos Fernandez-Aballi Altamirano, who is currently developing a mathematical model of the TLE and will continue the experimental work.

In order to reach the objectives, the thesis is divided in three main parts.

In the first part a literature review is performed where information is gathered and an analysis is made of the statements on the working principle of the engine. In the broader context of this project, the most important technologies based on alternative energy resources are touched. From there, we focus on the broader Stirling family. After a historical overview, a discussion of its main configurations is held, to arrive at the TLE. A thorough analysis is performed of both theoretical and experimental results presented in literature. A stark contrast is revealed in the opinions on how the TLE works. The statements made by the researchers are analysed in greater detail. A principle is put forward which gives a clear view of the essence of the thermal lag concept. The different claims are linked to this principle. What follows is a motivation as to why this machine deserves further research. The objectives for the experimental part of the project are then formulated based on this motivation.

In the second part, requirements for a flexible experimental rig are defined based on this analysis. The final design is presented along with the motivations to prove the requirements are met.

In the third part, the experimental work that has been performed is described and the data is analysed. Two data sets are presented, each with its energy balance and pV-diagrams. Conclusions and suggestions are then made based on the obtained results.

After a critical review of the rig that has been constructed, recommendations are given to improve the current rig and future designs. Also, a path is proposed in which future research should be headed.

Part I

Literature Review

Chapter 2

Broader Context

2.1 Environmental concerns

When the global annual mean temperature curve began to increase steeply in the late 1980's global warming theory rapidly gained popularity. The 'greenhouse effect theory' took shape and the Intergovernmental Panel on Climate Change (IPCC) was founded by the United Nations Environmental Programme and the World Meteorological Organization.

The probable effects of global warming have already been extensively studied by numerous scientists and are covered in the Assessment Reports of the IPCC [1]. Many of those effects pose serious threats to human, biological and geophysical systems.

The world's primary international agreement on climate change is the Kyoto Protocol, negotiated in 1997, which forced the signing countries to reduce the emissions of greenhouse gases [2]. The impact of this agreement however, should not be overestimated as some of the biggest CO_2-emitters, such as the United States, did not sign it. Furthermore, in 2008 the European Commission agreed that by the year 2020 each member of the EU should attain the following goals [3]:

- Cut greenhouse gas emissions by 20% of 1990 levels.
- Increase the use of renewable energy to 20% of total energy production.
- Reduce energy consumption by 20% of projected 2020 levels by improving energy efficiency.

In December 2009, the United Nations Climate Change Conference was held in Copenhagen (COP15). The participation of the United States and China was perceived as a positive evolution that has injected newfound optimism. Nevertheless, the conference failed to produce compulsory measures to restrict greenhouse gas emissions on a global level.

2.2 Renewable energy technologies

The aspiration to reduce greenhouse gas emissions drives the development of new technologies. These developments take place in all areas of energy production. Scientists and engineers are improving the efficiency of current power plants and address new energy sources. Cogeneration (also combined heat and power, CHP) is the use of a heat engine or a power station to simultaneously generate both electricity and useful heat. It is one of the most common forms of heat recovery.

Solar energy, radiant light and heat from the sun, has been harnessed by humans since ancient times using a range of ever-evolving technologies. However, only a minuscule fraction of the available solar energy is used. Solar powered electrical generation relies on heat engines or photovoltaic panels. Both methods have applications in the whole power range, from a few watts to several megawatts. Solar energy represents 0.29% of the world's electricity generating capacity [4].

Wind power has known an exponential growth over the last twenty years. It has gained a competitive status as the technology reaches new levels. Onshore units are now generating up to 6 MW and future plans for major offshore plants are being made. Global wind power installed capacity will be 152 gigawatts by the end of 2009. This represents 3.2% of the world's electricity generating capacity. Consultancy group Frost & Sullivan estimates offshore installed capacity will reach 18,769 MW by 2015 [5] [6].

Stirling engines deserve special attention. After all, they can be driven by any external heat source, providing a multitude of possibilities to harness renewable energy sources or waste heat. Applications range from energy generation to driving pump systems. Its future mainly lies in low power applications.

Chapter 3

Stirling Engines

3.1 History

Hot air engines have been known as early as 1699. They were revolutionised by the invention of the Stirling brothers called the 'economiser' or 'regenerator', patented in 1816. The driving force behind the invention was the concern of one of the brothers, Rev. Robert Stirling, regarding the health of his parishioners, who were often injured in steam engine accidents. By 1843, the brothers had pressurized the engine and had sufficiently increased power to drive all the machinery at an iron foundry in Dundee, Scotland [7]. Although these engines have known significant success, they faded into obscurity as steam engines became safer with the introduction of high quality steel. Some eighty years later, the internal combustion engine was invented, ready to outrun the competition.

More than a century later, in the 1960's, renewed interest in Stirling engines was shown. Several engine types regarding piston and cylinder configuration, displacer movement mechanisms and the like were developed. One of these new developments was the free piston engine, developed by researchers, specifically William T. Beale, from the Mechanical Engineering Department of Ohio University in 1964. The team left the university to create Sunpower Inc in 1974, with the intent of developing commercially feasible free piston engines for low-tech applications [8]. In its mission statement, Sunpower Inc shows a distinct sense of social awareness by stating that it primarily pursues applications in developing countries. It is a clear response to the general unawareness of Stirling capabilities and limitations, as sponsors were expecting an engine competing with internal combustion engines.

"Ironically, there is a real promise in Stirling applications, not so much in the most difficult applications, but in those which are so simple and so technically unchallenging that they are often ignored. The community of Stirling advocates sometimes appears to be like the thirsty man who labours to reach the snow at the top of a high peak rather than stooping to drink from the stream at his feet", William T. Beale [8].

The oil crisis of 1973 revealed a painful dependency on imported fossil fuels, which has further encouraged research in Stirling engines during that period. Sunpower Inc's major funded project resulted in an inertia compressor Stirling Rankine system intended as a home heating and cooling device. A working prototype was delivered to General Electric Company in 1975, which started developing an attractive heat pump for the marketplace in the 1980's [9].

At the high-tech end of the Stirling engine spectrum, an entirely new member of the Stirling family appeared in the field of thermoacoustics. The new technology disposed of moving parts completely. Research and development was primarily done by NASA, using these engines in spacecraft applications, such as cryo-coolers for rocket fuel.

As the Stirling community steadily grew throughout the years, more ideas and fields of research opened up. In the early 1980's, Professor Ivo Kolin of the University of Zagreb, Croatia, demonstrated the first low temperature differential (LTD) Stirling engine. The audience was amazed. It only stopped running when the temperature difference dropped below 20°C. During the late 1980's and early 1990's Professor Senft of the University of Wisconsin joined forces with Professor Kolin resulting in the Ringbom engine. NASA showed persistent interest and asked Senft to design and build a new engine, the N-92, with a temperature difference as low as 6°C to power it [10].

The youngest descendant of the Stirling engine is the Thermal Lag Engine (TLE). Patented in 1995 by Peter Tailer, it represents a mechanical simplification of the Stirling engine. It uses only a single piston and thereby eliminates the need for a complex linkage mechanism [11]. The piston sits in a cooled volume, which omits the need for high temperature sealing mechanisms, found in classical Stirling engines. It is a fairly unexplored field of research, although hobbyists all around the world have constructed numerous small-scale engines. The underlying phenomena, however, are persistently ignored.

3.2 Previous research

A thorough search in databases gave an idea of what the information landscape of the Stirling family looks like. About five hundred scientific publications relate to Stirling engines. These cover all aspects, from optimisation to various implementation possibilities. Stirling engines are well understood and product development is ongoing to bring them to the market.

Thermoacoustic machines have also been extensively studied, resulting in over three hundred papers and reviews. Initial research and investments by NASA in the 1970's have matured the technology. It is still an active area of research. Present-day publications address very specific technological details of applications in cryogenics and space engineering.

The amount of publications on TLE's is in stark contrast to those on Stirling and thermoacoustic engines. Besides its inventor Peter Tailer, only a handful of researchers have tried to analyse this machine. To this point, research has only led to a proof of concept and possible improvements.

3.3 The Stirling family

Stirling engines produce work by compressing and expanding a working fluid at different temperature levels. The Stirling cycle is made up of the following four processes, see figure 3.1:

Process 1-2: isothermal compression. The cold section cools the working fluid that is being compressed. The compression thus happens at constant low temperature. Work is done onto the fluid.

Process 2-3: constant volume regenerative transfer process. The working fluid shifts through the regenerator at a constant volume towards the hot section. The regenerator delivers heat to the working fluid, which causes a rise in fluid temperature from T_{min} to T_{max}. There is an increase in internal energy and entropy.

Process 3-4: isothermal expansion. The fluid is heated and expands at a high constant temperature. The fluid performs work.

Process 4-1: constant volume regenerative transfer process. The working fluid shifts back through the regenerator towards the cold section at constant volume. Heat is recovered from the fluid by the regenerator. No work is done and there is a decrease in internal energy and entropy.

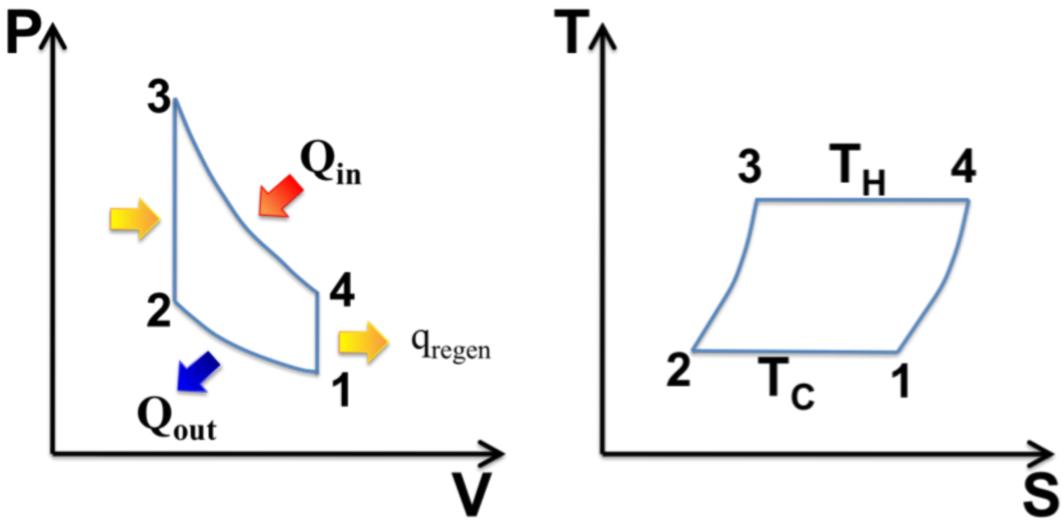

Figure 3.1: Stirling cycle pV-diagram and Ts-diagram

This highly idealized theoretical cycle is never valid for actual engine operation. The assumption of isothermal work requires perfectly effective heat exchangers with heat exchange at an infinite rate. The cycle is assumed reversible, which requires zero heat transfer between walls and working fluid.

Displacement type	Type of piston sealing technique (to atmosphere) found in literature			
	Classic piston seal	Liquid seal (liquid piston)	Annular rolling Seal	Closed system
Mechanical	✓	✓	✓	
Gas spring				✓
Acoustic				✓

Figure 3.2: Classification of Stirling engines and comparison of piston sealing techniques

We have classified the different Stirling engines according to displacement type, see figure 3.2.

This allows us to compare the different sealing techniques found in literature.

Stirling engines with mechanical displacers are commonly divided into three classes according to cylinder coupling. These comprise alpha, beta and gamma configurations. Gas spring driven displacers are found in free piston engines. Thermoacoustic engines use sound waves to transfer mass. The displacement is therefore acoustically driven. We will now briefly explain the sealing methods and the aforementioned configurations.

Most of the hot air engines have a mechanical displacer, allowing different types of seals. Apart from classic piston or rod seals, annular rolling seals were developed for very low friction applications. The use of a liquid piston omits the need for conventional sealing. Engines with gas spring or acoustic displacement do not have an outgoing shaft. The engine volume can thus be completely closed off from the surroundings. No dynamic seal is needed. Sealing methods for engines like the TLE are similar to those of engines with mechanical displacers.

In the following paragraphs, the Stirling engine configurations that were mentioned will be briefly described.

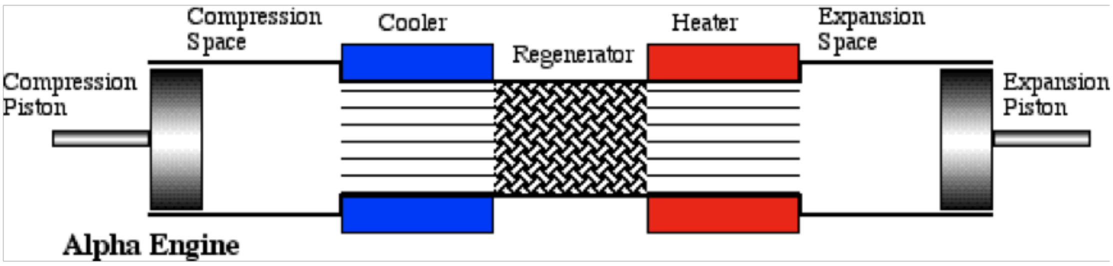

Figure 3.3: Schematic representation of an alpha configuration [12]

Alpha coupling: Alpha engines have a compression and expansion piston in separate cylinders, as shown in figures 3.3 and 3.7(a). The out of phase movement of the pistons makes the different processes possible. The working fluid shuttles from one cylinder to another through the regenerator. The decoupled cylinders make this engine very sensitive to leakage. Multiple cylinders can be coupled in series, which enables a high specific power output. Such a compact multicylinder engine could be a candidate for (hybrid) automotive purposes, see figure 3.4. Efficiencies of around 30% have been attained, producing over 60 hp at full load [13].

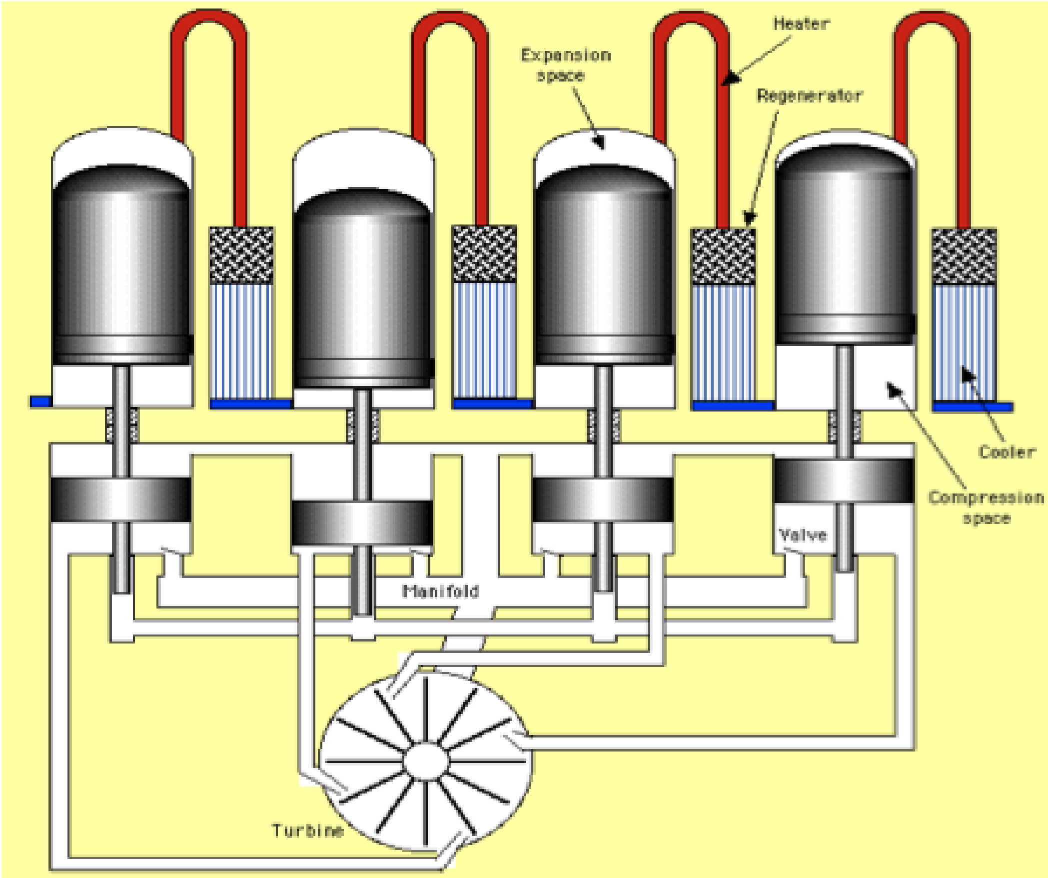

Figure 3.4: V- type multicylinder alpha configuration [12]

Beta coupling: A single cylinder holds both the displacer and a power piston, see figures 3.5 and 3.7(b). Unlike the alpha engine, there is only one power piston. The displacer is used to keep the working fluid at constant volume and displace it from one space to another. The power piston and displacer may not physically touch. They are connected to the crankshaft by a separate linkage mechanism to maintain the required phase angle. These engines are often used in cogeneration units in rural areas [12].

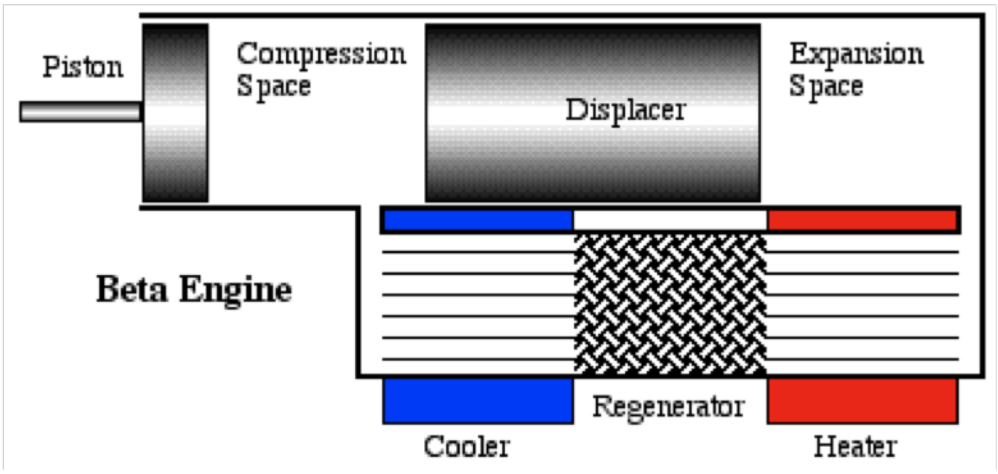

Figure 3.5: Schematic representation of a beta configuration [12]

Gamma coupling: Gamma type engines are similar to beta engines, but use different cylinders for displacer and power piston. They each have there own crank mechanism, so there is no need for complex linkage. In between the passage from displacer cylinder and power cylinder the cooler, heater and regenerator are connected in series. This is shown in figures 3.6 and 3.7(c). Gamma engines have lower performance and are large, but are nonetheless used when the aspect of separate cylinders outweighs the disadvantages. They are commonly favoured in low temperature difference Stirling engines [12].

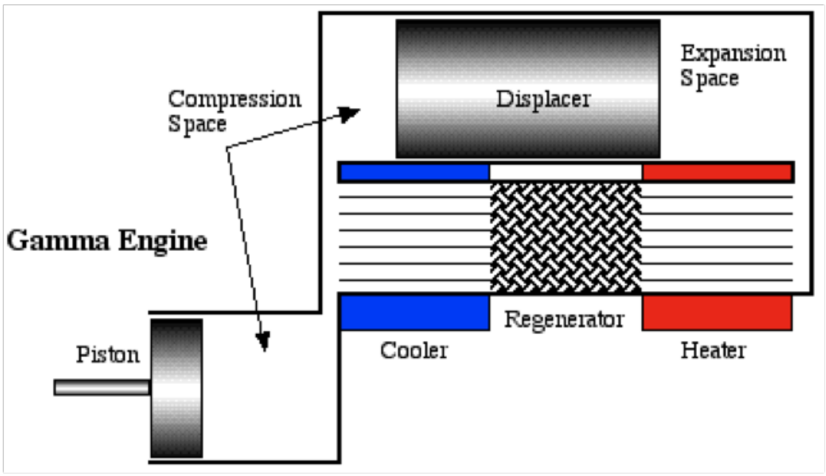

Figure 3.6: Schematic of gamma configuration [12]

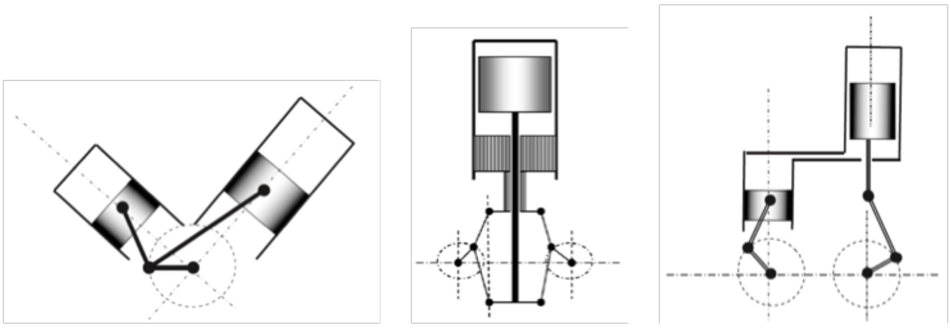

(a) Alpha Coupling (b) Beta coupling (c) Gamma coupling

Figure 3.7: Mechanical coupling configurations

Free piston engine: In 1964 William T. Beale invented a stirling engine that has no mechanical linkage, the free piston engine. Instead of a mechanical link, the piston and displacer are dynamically coupled by a gas spring. Running on waste heat, these engines can be used for power generation [14]. They have proven to be reliable and capable of delivering over 1 kW in a FPSE/linear alternator system [15]. The free piston concept is currently also being implemented in a controlled internal combustion electricity generating module[1].

Thermo acoustic Stirling engine: If the free piston engine reduced the number of mechanical parts, than the thermoacoustic engine abolished all of them. Not a single part is moving in this machine. The driving force behind it is a peculiar thermoacoustic phenomenon. A schematic overview is given in figure 3.8. A temperature gradient along the length of a pipe induces a sound wave. Simply put, if this pipe has half the length of the wavelength a standing wave is created. The input of heat at the high pressure point and rejection of heat at the low pressure point tend to enhance the amplitude of the pressure wave. This induces pulses that can be converted to electricity by a piezoelectric transducer. Other more sophisticated configurations used as heat pumps are based on travelling waves [16].

[1]Pempek Systems, 2007

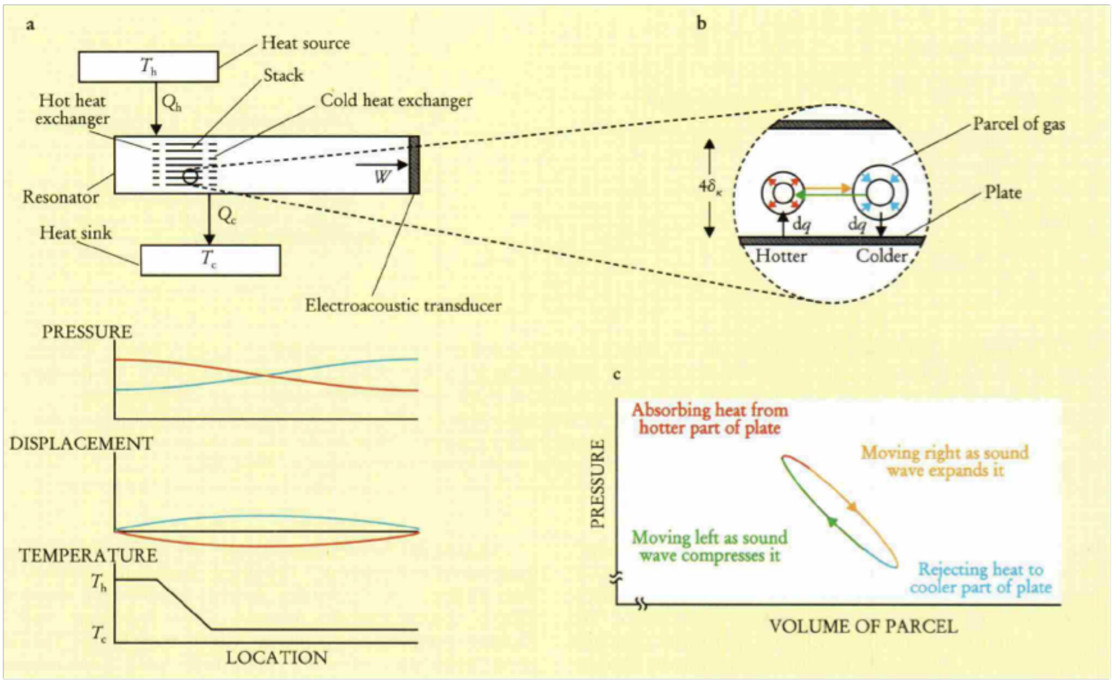

Figure 3.8: Explanatory schematics of thermo acoustic phenomenon [16]

Thermal Lag Engine: This new concept is a mechanical simplification of the classic Stirling engines with mechanical displacers, see figure 3.9. The engine invented by Tailer consists of two spaces: a hot space where the heat is supplied to power the engine and a cooled cylinder in which the piston moves [19]. Because of the piston's motion, the gas is exposed intermittently to the cold heat exchange area. Compared to the standard Stirling configurations, there is only one moving part. The piston adopts the role of the displacer and power piston. Thus, there is no need for a complex linkage mechanism. The heat transfer delay time superimposed on the piston motion separates the different processes in time, hence the name 'Thermal Lag Engine'. The driving phenomena behind the engine are subject to discussion.

In the next chapter, a literature study on the TLE is performed and both qualitative and quantitative results are analysed.

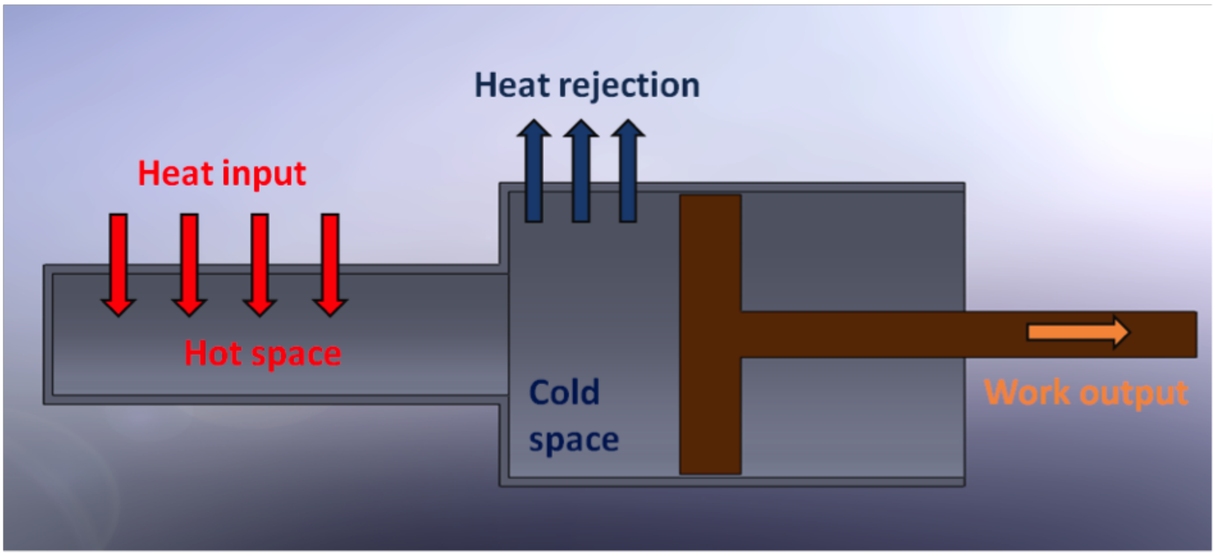

Figure 3.9: Thermal Lag Engine concept

Chapter 4

Focus on TLE

4.1 Origin of the thermal lag concept

In 1991, Peter Tailer presented a very simple and low friction internally pressurised annular rolling seal developed for heat engines [17]. A large gamma type Stirling engine was built using this sealing technique. It consisted of two cylinders, a power cylinder with a power piston and a displacer cylinder with a displacer. To test the seal, several experiments were conducted. One of the experiments consisted of moving the displacer while the power piston remained locked in position. Upon rapid movement of the displacer, Tailer noticed that the pressure gauge needle had a noticeable time delay between the movement of the displacer and the rise in pressure in the engine volume. Tailer realised that this resulted from the low rate of heat transfer in the Stirling engine heater compared to the displacer speed. It was then that the idea of using this so-called 'thermal lag' as a driving force arose. Instead of being limited in engine speed and thus power because of limited heat transfer, as is the case for Stirling engines, Tailer hoped to use this effect to drive an engine.

4.2 Qualitatively

In 1987 N. C. J. Chen along with co-author C.D. West described a theoretical single-cylinder valveless heat engine [18]. This engine combines consecutive isothermal and adiabatic compression and expansion to provide net work. Because their engine has a single port that connected to the atmosphere, they could identify certain states in the cycle which allowed them to postulate a unique triangular P-V diagram.

Inspired by that effort, Peter Tailer presented the audience of the 28th Intersociety Energy Conversion Engineering conference in 1993 a working prototype of an elegantly simple external combustion engine, the Thermal Lag Engine [19]. Having only one piston that acts as a power and displacement piston, it immediately showed its mechanical simplification compared to the Stirling Engine. Because of the time shift between the movement of the fluid and the heat transfer, expansion takes place at a higher temperature and pressure than the compression. Therefore the engine produces a net work output. Chen, West and Tailer all agree on this basic reasoning. Tailer, however, has a different opinion on the theoretical cycle that takes place in the engine. He stated that the cycle consists of an adiabatic expansion and compression (fast piston movement), an isochoric cooling and an isochoric heating process. This represents the Otto-cycle.

At the same conference, C. D. West presented a paper in which he tried to cast some light on the possible modes of operation for the engine built by Tailer [20]. According to West, these different modes are achieved by varying the engine speed relative to the rate of heat transfer in the cylinder. If the engine speed is too low or too high, all the working gas will behave isothermally or adiabatically. The engine then behaves as a gas spring and the net work output is zero. At an intermediate speed, however, the thermal inertia of the gas will ensure that the gas temperature exceeds the cylinder walls at the end of expansion. This allows further cooling in the cylinder during compression which makes the gas temperature drop despite the tendency of the increasing pressure to cause an (adiabatic) temperature rise. Therefore, the average gas temperature and pressure during the expansion is higher than during compression and a net amount of work is done on the piston. West also performed a simple calculation, which provides a rough estimate of the indicated work available. In this calculation, he acknowledged that losses occur during the expansion as some of the expanding gas is already cooled in the cylinder.

In 1994, one year after the conference, Frank Wicks and Carlos Caminero developed a computer simulation in which they tried to analyse the working principle of the TLE [21]. They used a model with two control volumes: a heated part with constant volume and a cooled part with a variable volume. The heated part receives a constant heat flow, while the cold part receives a cyclic heat flow. This is caused by the reciprocating action of the piston. While the authors believe that they have developed a reasonable model and simulation, they admit that their results are highly dependent on heat transfer characteristics which they could not estimate with much confidence. They were the first, however, to publish a detailed simulation of the pV- and Ts-diagram.

Peter Tailer was granted a US Patent on the TLE in 1995 [11], in which he still hangs on to the concept of the engine operating on the Otto-cycle. In an effort to increase the engine efficiency, he proposed the use of a cam which provides longer dwelling times of the piston in top and dead centre and gas diodes to improve gas circulation. In the same year Tailer built two new test engines, one that was vertically set up and one horizontally [22]. These were the first TLE's from which a power output could be measured. In the paper that presented the results of these experiments, he compared the power densities of those test rigs with Ericsson and traditional Stirling engines. Although his TLE's only reach a power density of 40% of that of Stirling Engines, Tailer sees much potential for them as there is a lot of room for improvement and they have a much greater mechanical simplicity.

In 2009 Carlos Fernandez-Aballi Altamirano proposed another control volume based simulation [23]. His model assumes a fixed volume hot space and a varying volume cold space which are coupled by their time dependent mass and energy balances. The gas temperatures of both spaces can be different but it is assumed that the pressure, as it equalizes throughout the system at the speed of sound, is uniform inside the engine volume. Altamirano describes the engine's theoretical cycle as being a hybrid of the Otto- and Stirling-cycle: By slowing down the expansion, it becomes isothermal and by speeding up the compression, it becomes adiabatic. However, the displacement now is not sinusoidal anymore. As a result the efficiency also lies in between those of the Otto- and Stirling-cycle: $\eta_{Otto} < \eta_{TLE} < \eta_{Stirling}$.

All these researchers claim that the main effect of the TLE is the bulk motion of the fluid from the hot to the cold space and back. This flow regime leads to the heat transfer that drives the engine. But in 2007 Allan Organ published an alternative approach in his book [24]. He proposed a solution that extended the theory developed for thermoacoustic engines to TLE's. He considers the flow as being very laminar and stratified and divides the fluid into multiple control volumes, hereby neglecting the bulk fluid mixing throughout the engine. Organ sees the disequilibrium between temperature gradients in the walls and fluid as the important effect.

4.3 Quantitatively

4.3.1 Numerical results

Chen and West were the first to calculate power output and efficiency for an engine with a total engine volume of 2400 cc in 1987 [18]. With a hot source temperature (T_{hot}) of 923.15K and a cold sink temperature (T_{cold}) of 298.15K, their calculations led to an indicated power output of 5.9 kW and an indicated efficiency of 11%. This provides a power density of 2458 mW of indicated power per cc of engine volume.

Organ made his calculations in 2007 for a very small engine with a total engine volume of 35.966 cc, T_{hot} = 900K and T_{cold} = 300K [24]. The indicated work is 4.1598 W. This leads to a power density of 116 mW of indicated power per cc. As the heat input is not specified, the engine's efficiency can not be calculated.

Altamirano's calculations for a small engine of 125.66 cc with T_{hot} = 600K and T_{cold} = 302K lead to an indicated power output of 1.8 W with an efficiency of 4.4% [23]. This gives a power density of 14.3 mW of indicated power per cc.

The calculations done by West are done for an engine volume of 1570 cc, T_{hot} = 850 K. T_{cold} = 325 K [20]. The result is an indicated power output of 12 W and thus a power density of 7.64 mW/cc.

4.3.2 Experimental results

Peter Tailer's first test engine from 1993 did not provide enough power to be actually measured [19]. In 1995 he built two new test engines, one that was set up horizontally and one vertically. These two engines provided enough work output to be measured accurately [22]. The horizontal engine had a volume of 2425 cc and produced a power output of 4 W. This gives a power density of 1.65 mW/cc. The hot temperatures is T_{hot} = 700.15 K. The vertical engine had a volume of 2150 cc with a power output of 7.5 W. This means a power density of 3.49 mW/cc. The hot temperature was 903.15 K. Cold temperatures are not given, but can be assumed to be equal to atmospheric temperature. An indication of heat input is not available as the test engines were heated with a gas burner.

After modelling the TLE in 2007, Organ also built an experimental test engine [24]. The internal dimensions are the same as the ones he used for his calculations, which means that the engine volume is 35.966 cc. The engine produced a maximum of about 0.47 W with a heat input of 43 W. This means a global efficiency of 1.093%. As a result, the power density is 13.1 mW/cc. The hot source had a temperature of T_{hot}= 753.15K. Cold source temperature is not specified.

All experimental and numerical results are condensed into tables 4.1 and 4.2. Although Tailer and Organ do not specify T_{cold}, it is reasonable to assume that this will not have differed much from atmospheric temperature.
Several remarks can be made about these tables. First, there is no correspondence between the engines, both experimental and numerical.

Looking at the numerical results, the engine of Chen and West seems unrealistic, because

Table 4.1: Experimental results found in literature

Parameter	Tailer (horizontal)	Tailer (vertical)	Organ
Engine Volume [cc]	2425	2150	35.966
T_{hot} [K]	700.15	903.15	753.15
T_{cold} [K]	$\pm T_{atm}$	$\pm T_{atm}$	$\pm T_{atm}$
Effective Power Output [W]	4	7.5	0.47
Effective Power Density [$\frac{mW}{cc}$]	1.65	3.49	13.1
Efficiency	N/A	N/A	1.093%

Table 4.2: Numerical results found in literature

Parameter	West	Chen/West	Altamirano	Organ
Engine Volume [cc]	1570	2400	125.66	35.966
T_{hot} [K]	850	923.15	600	900
T_{cold} [K]	325	298.15	302	300
Indicated Power Output [W]	12	5900	1.8	4.1598
Indicated Power Density $[\frac{mW}{cc}]$	7.64	2458	14.3	116
Efficiency	N/A	11%	4.4%	N/A

of its extremely high power output and Organ mentions no heat input. Therefore, only Altamirano's result is fully described. This makes comparison impossible.

The experimental results lack even more information. Peter Tailer did not have means to estimate heat input properly as he used a gas burner. Therefore no comparison can be made with Organ's engine.

The only conclusion to be made of these results is that there is no sufficient data to make proper statements. The goal of the experiments was merely proof of concept.

Chapter 5

Project Motivation

5.1 Background

Coming back to the environmental concerns, it is unmistakable the world is looking for solutions. These have emerged in many forms. Renewable energy resources, improved insulation and building methods, combined heat and power generation, etc. And industries are not the only ones to commit themselves. The interest of the public in new and better technology results in passive housing, micro-CHP for residential use, etc. [25].

One of the broader concepts is a super decentralized system of renewable power generation. This means a serious shift of the energy generation paradigm, but the idea is gaining public support. A recent publication affirms that thirty-one (US) states could meet all their electric energy demand relying on nearby renewable energy sources [26].

But climate issues tend to overshadow other severe problems. Still today, around thirty percent of the world population has no access to electricity [27]. Often accompanied by a lack of fresh water, these problems create an enduring state of poverty for as many as 2 billion people. Closing the gap of technological development has become too difficult for most of these countries.

5.2 Potential of the Thermal Lag Engine

Clearly, the TLE technology is still in its infancy. However, great potential has often been cited. Stirling technology can be implemented when it comes to heat exchangers, sealing solutions and optimization of the engine: pressurization of the engine, the use of different working fluids, improved heat exchangers, new materials, etc. In addition, the TLE has a few advantages, such as the extreme mechanical simplicity and the absence of moving parts in the hot space. Very high temperature resistant materials like ceramics can be used with crude tolerances. This is not the case for Stirling engines, where moving parts demand low tolerances and high surface finishes that cannot be easily attained for these materials. The expected lower cycle efficiency compared to a Stirling cycle engine can thus be alleviated by operating at higher temperatures. This results in a higher thermal efficiency. The relatively unrestricted flow of the TLE also enables higher operating speeds [22]. The piston in a TLE does not require high temperature sealing methods, as the piston sits in the cooled cylinder. This allows the use of simple rubber seals, such as Tailer's annular rolling seal [17].

TLE's could be used in solar applications. Photovoltaic cells are expensive primarily due to the cost of highly purified silicon. This is not the case for a TLE as they can be made with common materials such as steel and rubber.

Inherent to external heat engines is that they can run on any kind of fuel. Combustion is continuous, so they run quietly and smoothly with high control of emissions.

Another important aspect to be taken into account is cost effectiveness. This is represented by the symbolic cost for hydrocarbon energy generation: 1$/W. An optimised TLE has the potential to achieve this goal because of its low initial and maintenance cost.

The prospects mentioned above, reveal several applications for the TLE. If all the advantages are fully exploited, it could be part of a hybrid power generation system that captures solar heat by day and runs quietly on any kind of fuel by night. Furthermore, the need for low cost site built engines running on local resources in non-industrialized regions can be met. Coal, wood, agricultural or solar powered TLE's could enable remote or impoverished communities worldwide to generate electricity or drive modest applications.

The problems and developments cited uncover vast opportunities for low-tech machines like the TLE to become a sustainable engine for the future.

5.3 Objectives

The previous discussions make it clear that a great deal of research needs to be done to understand the driving phenomena behind the engine. Apart from some guesses to its working principle, very few people have tried to analyse and model the engine. Even fewer experiments have been conducted. Up until now, these experiments have considered the TLE as a black box. The researchers tried to make the engine run and measured the work output. Basic parameters were changed and an interpretation was given to the observations. No attempts have been made, however, to measure the cycle on which the engine runs to obtain experimental verification of the claims that have been made.

To allow better understanding of the engine, measurements must be made inside the engine. Therefore, a test rig will be designed from which pV-diagrams and energy balances can be obtained. At this point, mathematical models are not available to provide guidance in the design process. Therefore, a detailed investigation of the test rigs described in literature needs to be performed. These test rigs have only been made by Tailer and Organ. To have a better understanding of their design choices, a profound analysis of their conceptions of the working principle is done. After that the construction of their test rigs is evaluated. Design requirements are then put forward. Subsequently the result of the design process is presented along with the calculations that prove they meet the requirements.

Chapter 6

Underlying Physics

6.1 Thermal lag effect

From literature, there is a stark contrast in opinions on how the TLE functions. They are represented by Tailer and Organ, see table 6.1.

Tailer	**Organ**
Bulk mixing	Stratified flow
Strict separation of hot and cold	Pulse tube separates hot and cold
Shifting bulk mass	Shifting temperature gradients
High temperature differences between the space and gas that is pushed into it.	Low temperature differences between the space and gas that is pushed into it.

Table 6.1: Thermodynamics according to Tailer and Organ [22] [24]

Both working principles, however, essentially create the same thermal lag effect: the dephasing in time of the net heat transfer to the gas and the piston movement.

To explain how the phase shift results in producing work, let us consider the following thought experiment. If we assume heat transfer and volume function to be sinusoidal, maximum efficiency is obtained when the phase shift is 90°, see figure 6.1. Of course, this exposition is purely illustrative of the thermal lag effect. A perfect sinus does not occur in a real engine, as it would mean that heat input equals heat output over a cycle, which results in zero net work.

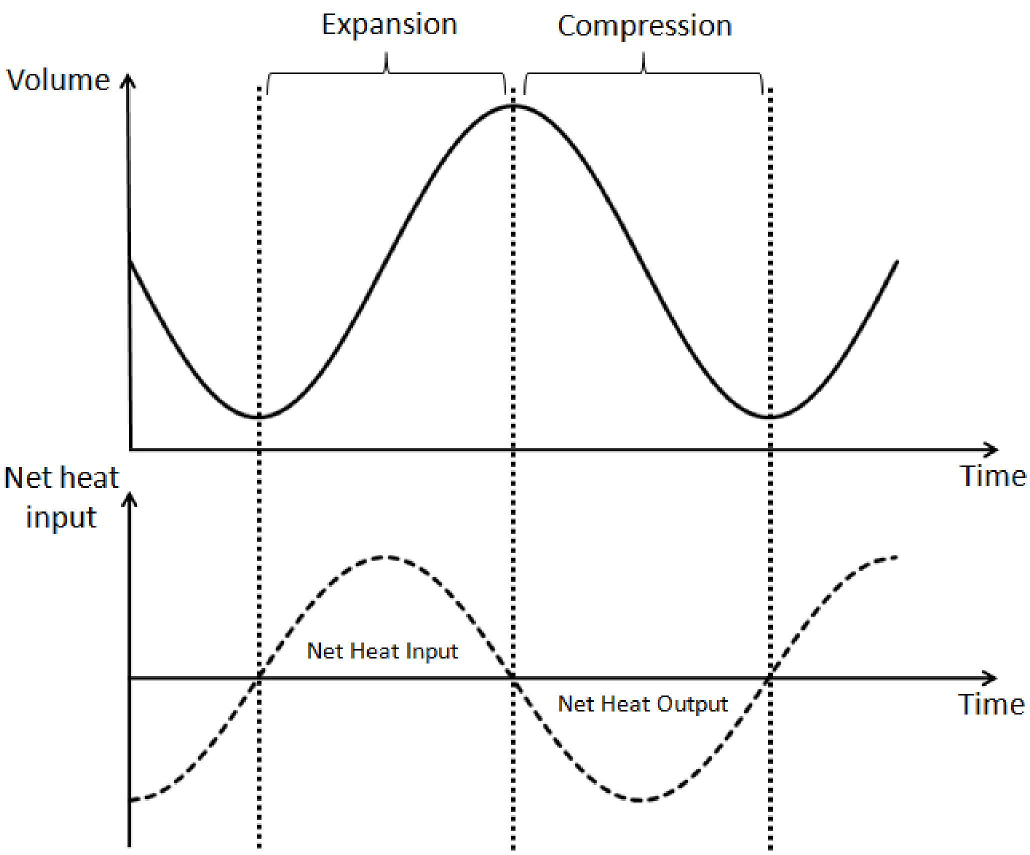

Figure 6.1: The thermal lag effect with the assumption of sinusoidal volume and heat transfer function.

During expansion, there is net heat input into the gas. Therefore pressure is higher than for adiabatic expansion. During compression, heat is drawn from the gas. Therefore pressure is below the adiabatic case. As a result, the engine produces a net work output. If the phase shift differs from 90°, then heat is drawn from the gas during expansion and heat is added during compression, see figure 6.2. This will inevitably reduce the engine's performance, as the pressure during expansion decreases and the pressure during compression increases. These considerations give an insight in the inherent losses of a TLE.

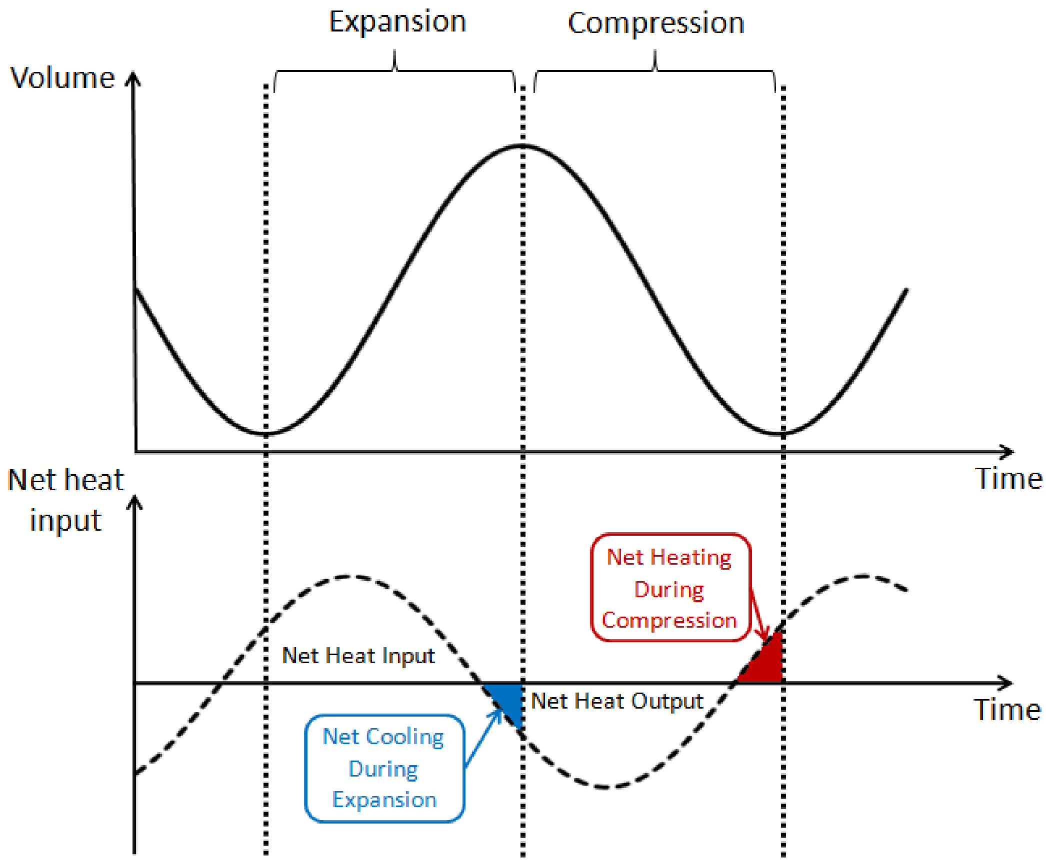

Figure 6.2: Phase shift differs from 90° with the assumption of sinusoidal volume and heat transfer function.

The discussed principle lies at the basis of the functioning of the TLE. Tailer and Organ have a different idea of how this can be achieved. In the next sections, their claims on how the thermal lag effect is implemented in their engine are described.

6.2 The physics behind Tailer's engine

Tailer explains his vision of the fundamental TLE cycle in four steps, see figure 6.3 [19]. The enclosed engine volume consists of a long heater connected to a cooled cylinder space of much higher diameter. Starting with the piston at bottom dead centre, there is a temperature difference between the gas in the cooled cylinder and the heater. Going from (a) to (b), the gas is being compressed and the cold portion of gas is shifted into the hot space. At top dead centre (c), the gas takes time to heat up. Consequently, temperature and pressure rise. The gas expands and pushes the piston back (d), delivering work. Because the hot section keeps dumping heat into the gas, this expansion takes place at a higher temperature than if it were adiabatic. Because of the piston's motion, the cold section of the engine starts to increase in volume inducing a gas flow from the heater towards the cylinder. The gas expands into the cylinder where bulk mixing takes place due to the gas inertia and the movement of the piston. This increases temperature diffusion and heat transfer with the cold cylinder walls. However, because of its thermal inertia, the gas does not instantly drop in temperature. This happens gradually and continues when the piston starts recompressing the gas. This time shift between the displacement of the gas and its change in internal energy, is the key to the functioning of this engine. Compression should take place at the lowest gas temperature possible. This will maximize the net work output of the engine.

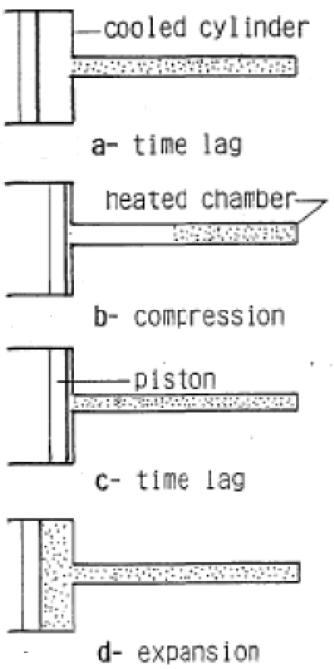

Figure 6.3: Tailer's TLE cycle [19]

Tailer speculates with this explanation that the engine runs on the Otto-cycle [19]. He assumes that piston movement is too fast to allow heat transfer during compression and expansion so that these processes are adiabatic. In top and bottom dead centre, piston movement is slower. This leaves time for isochoric heating and cooling. Tailer states that sinusoidal piston movement is already sufficient to create this behaviour. As isochoric heating and cooling gives the cycle the highest efficiency, providing higher dwelling times at top and bottom dead center would increase the engine's performance. He proposes the use of a cam to attain this effect.

In 1993, he reported the following experiment [19]: *On rapid removal of the piston, a tem-*

perature probe inserted from the cylinder into the cooler indicated a progressive increase in temperature from top to bottom of the chain in the cooler. This would indicate that, as air shuttles back and forth through the cooler, the cylinder and the heated chamber, there is no temperature change interface but a progressive temperature change. Designing a thermal lag engine with a sharper temperature interface should increase its power and efficiency.

This statement can be understood by considering what happens when gas is pushed into the hot space with a 'spread out' temperature interface between heater and cooler. Part of the gas will not come into contact with the highest temperature of the engine. Therefore it does not receive heat at the highest temperature possible. The same holds for the cooling. Part of the gas will not dump heat at the lowest temperature possible. Therefore, efficiency will be lower than it would be if the engine had a sharp temperature interface.

Another observation made by Tailer in [19], is: *Smaller pore sizes or more closely spaced heat exchange fins in heated chambers and coolers can increase the frequency, but power declines in these specific test engines. Larger pore sizes reduce the frequency.*

Tailer does not make any statements to explain this behaviour. It seems however that when varying heat exchanger pore size, a compromise must be made between flow resistance and heat exchange capacity. When the pore size is reduced, two things happen: The additional flow losses decrease the engine's performance. Heat transfer area will rise however, increasing the possible heat transfer rates in the engine. This will enhance the engine's ability to run at higher frequencies.

Colin West also made an effort to explain the principle of Tailer's engine [20]. He made two important assumptions about heat transfer throughout the engine:

- The hot heat exchanger consists of small tubes, mesh, plates or other partitions. This increases the heat transfer area so dramatically that the gas temperature is always very close to the heater temperature, i.e. the gas behaves isothermally.
- Heat transfer within the cooled cylinder is low enough, so that during rapid movements of the piston the gas behaviour is almost adiabatic. There is not enough time for the gas to exhange a significant amount of heat with the cylinder walls. Only during a sufficient dwell period, or slow movements, does the gas temperature reach the wall temperature.

The working principle of the engine is then explained by West with the following thought experiments [20]:

First consider an engine with a high rate of heat transfer in the cylinder relative to the engine speed. The gas in the cylinder now behaves almost isothermally. If the motion of the piston were sinusoidal, pressure and volume variation would be 180° out of phase. Consequently, the net work output or the integral of pV over a cycle would be zero. The engine works as a simple gas spring. The compression work equals the work output during expansion.

Second, consider the engine speed to be very high relative to the rate of heat transfer in the cylinder. Now, there is very limited heat transfer in the cylinder. The system would act as a nearly adiabatic gas spring with some losses due to mixing of gas at different temperatures.

Finally, consider the following situation:

- The engine runs at intermediate speed.
- The temperature difference between the heater and the cooler is high.
- The ratio of cold to hot volume is not too low.

Under these conditions, the gas temperature in the cylinder T_g at the end of expansion will always be higher than the cylinder wall temperature T_c. This is the case, because during the expansion more hot gas is being transported into the cylinder. The resulting heat transfer makes temperature and pressure drop below the adiabatic expansion case. This would lower expansion work. At the right speed, however, this heat transfer lags behind the piston motion. In this case, T_g will still exceed T_c during the compression stroke. This way, cooling continues even with the tendency of rising temperature due to compression. Therefore, mean gas temperature and pressure during the expansion is higher than during the compression with a net amount of work done on the piston.

Comments on the de-phasing of Tailer's engine It is possible to relate Tailer's statements to the thermal lag effect that was introduced in the section 6.1. For Tailer, the phase shift is obtained primarily because of the top and bottom dead center dwell times. The gas is *given time* to cool down after expansion and to heat up after compression. During expansion and compression, the piston's speed is too high to allow any heat transfer in the cooled cylinder. If an engine would work exactly as Tailer describes, the phase shift between heat transfer and volume function would thus be exactly 90°.

Tailer describes an idealised TLE, without making any statements about the inherent losses that occur. West does [20]. He describes the effect of heat transfer occurring in the cylinder during expansion which lowers expansion work. West thus acknowledges the fact that some of the gas is cooled in the cylinder during expansion. *At the right speeds*, however, the thermal inertia of the gas ensures that gas temperature stays above cooler temperature at the end of expansion, which allows cooling to happen during compression. West is the first to stress the importance of the relationship between the speed at which the gas temperature in the cooler drops during expansion and the speed of the engine. This is an important statement. It means that when the engine speed is too low, the thermal inertia of the gas will not be sufficient to keep its temperature and pressure high during expansion. Expansion work will thus decrease. The temperature difference between gas and wall will be smaller at the end of expansion, reducing the potential for cooling during compression. Compression work will thus increase. Relating to the thermal lag effect, this means that the highest cooling rate is shifted towards the expansion stroke. The ideal phase shift of 90° is then lost.

Furthermore, heat transfer in Tailer's engine is not only dephased by the dwell times and thermal inertia. There are two additional phenomena in this engine which reinforce the thermal lag effect.

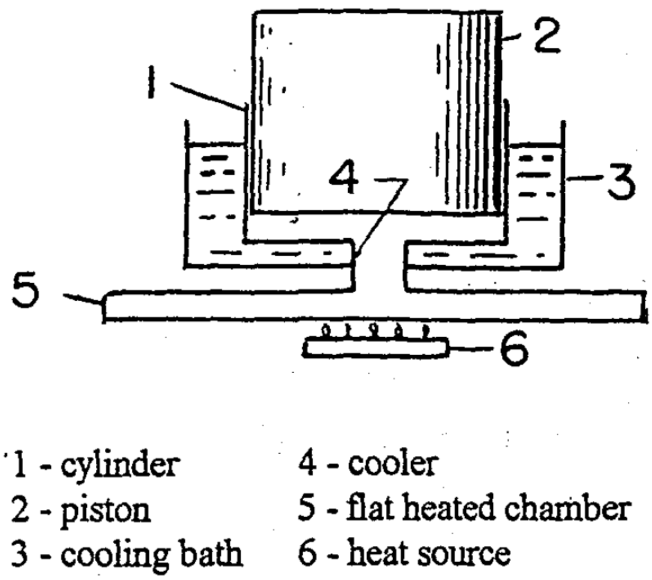

Figure 6.4: Tailer's vertical TLE [22]

To illustrate the first effect, it is necessary to have a look at the cooler in Tailer's TLE, see figure 6.4. The entire piston cylinder and the duct leading to it is cooled. It is important to notice that part of the cold heat transfer area is fixed and a part is variable. The heat transfer area, and thus the heat transfer capacity of the cooler is maximised at bottom dead center because of the piston's motion. This shifts the cooling of the gas towards the end of expansion, thus reinforcing the thermal lag effect. In Tailer's engine [19], the ratio between variable and fixed cold heat transfer area is only 0.23, as the piston stroke is only 1.9 cm. The effect of the variable cooler area in his engine may thus not be overestimated. Nonetheless, it would be interesting to investigate how much power output can be improved using this effect. To achieve this, thermal lag test engines with long strokes would be necessary.

The second phenomenon is due to the nature of the gas flow inside the changing geometry. When hot gas expands into the piston chamber, the incoming mass flow is central of the piston chamber and velocities at the cylinder walls are relatively low, see figure 6.5(a). There is some cooling due to temperature diffusion, but this is minimal because of the gas's low thermal conductivity. It is only when the piston starts recompressing the gas that vortices are induced due to the mass inertia of the gas, see figure 6.5(b). Much higher velocities now occur at the cylinder walls and convection coefficients increase. Furthermore, the gas is now being compressed against the cylinder head, which adds a lot of effective heat transfer area to cool the gas during the compression stroke, see figure 6.5(c). This phenomenon thus shifts the highest cooling rates towards the compression. This is beneficial for the thermal lag effect.

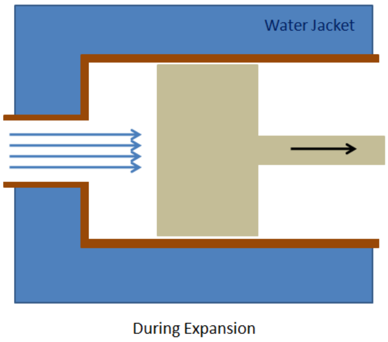

(a) Gas flow during expansion

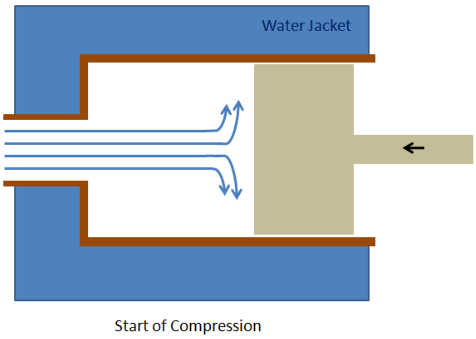

(b) Gas flow at start of compression

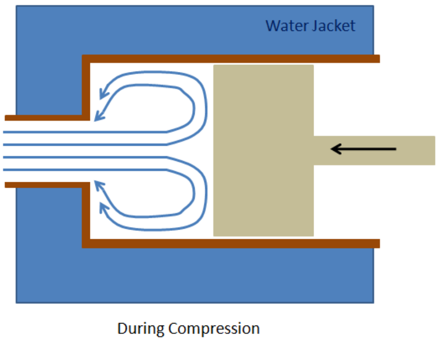

(c) Gas flow during compression

Figure 6.5: Circulating air flow.

Functioning of the heater Tailer and West focus their analysis on the heat transfer in the cooler. It is however interesting to analyse the heat transfer in the heater. The functioning of the heater during expansion is rather simple. If gas behaviour is isothermal, the heater keeps dumping heat into the gas so that $T_{gas} = T_{heater}$. If the heat transfer capacity of the heater is insufficient to achieve this, the pressure in the heater will drop below isothermal and less expansion work will be produced. To maximise the engine's performance, gas behaviour inside the heater should be isothermal during expansion.

During compression, two effects come into play:

- Temperature of the gas inside the heater will go up due to compression.
- Temperature of the gas inside the heater will drop because of mixing with the cold gas that enters from the cylinder.

The first effect will tend to minimise heat transfer in the heater, which is beneficial for the compression work. The second effect will do the exact opposite. Limiting the heat transfer capacity of the heater would thus be beneficial, however it must not jeopardize having isothermal gas behaviour during expansion, as discussed above. From this perspective, an ideal heater would consist of two sections: an isothermal section to enable optimal isothermal expansion and a non-isothermal section into which the cold gas can be compressed.

6.3 The physics behind Organ's engine

The configuration of Organ's engine [24] is different from Tailer's, see figure 6.6. The piston cylinder is assumed adiabatic and the cooler is placed in front of the cylinder head. Unlike Tailer's engine, the cold heat transfer area does not change because of the piston's motion. The section between the heater and the cooler is referred to as the pulse tube, which exchanges heat with the gas only. In contrast to Tailer, who minimises this volume as it increases dead space, Organ designs the pulse tube to have a certain length and heat transfer capacity. For a more profound description of Organ's engine, see section 7.3.

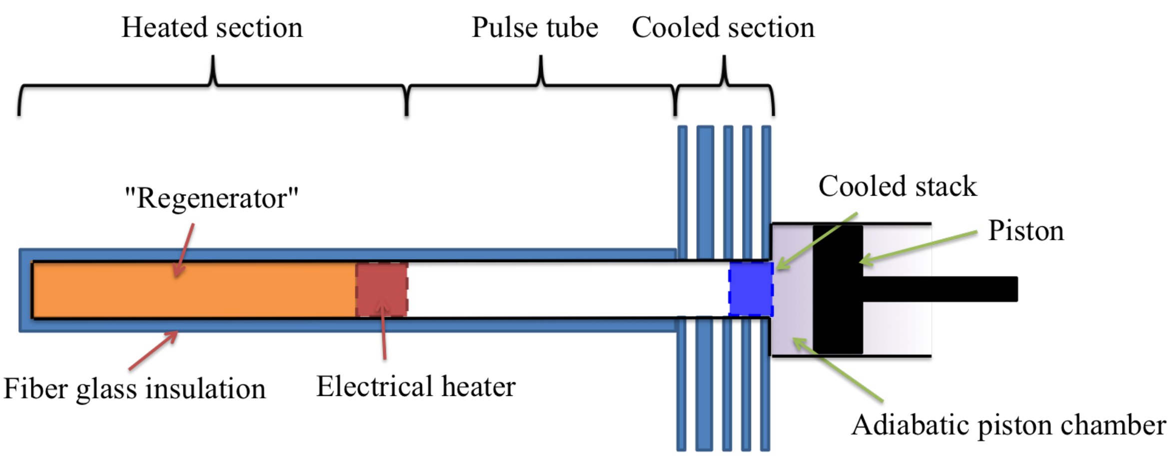

Figure 6.6: Representation of Organ's basic pulse tube TLE.

To understand how Organ attains the thermal lag effect, the temperature profile of the gas in the pulse tube throughout the cycle should be looked at more closely. Three assumptions were made by Organ concerning the working principle of the engine [24]:

1. The rate of heat transfer in the regenerator is sufficiently high to maintain a gas temperature gradient that is constant in time along the regenerator. In other words, the gas in the regenerator behaves isothermally.

2. Heat transfer between the walls of the pulse tube and the gas is restricted, implying a low rate of heat transfer. This enables temperature differences to persist temporarily between the gas and the pulse tube wall.

3. Flow is assumed laminar. In Organ's original 1D model, this implies gas molecules to be in the same cross section throughout the cycle. Compression and expansion can thus be seen as cross sections getting closer together and further apart. One might think of an accordion-like behaviour. This is important, as it implies that the portion of gas in the regenerator never enters the piston chamber.

T_h is the heater temperature and T_c the cooler temperature. In between, the pulse tube has a wall temperature profile T_w. At the beginning of the expansion, we have the situation shown in figure 6.7. During the dwell period at top dead center, the gas has had time to exchange heat with the pulse tube wall and take its temperature, so $T_g = T_w$. Hence, there is no heat transfer between the pulse tube and the gas.

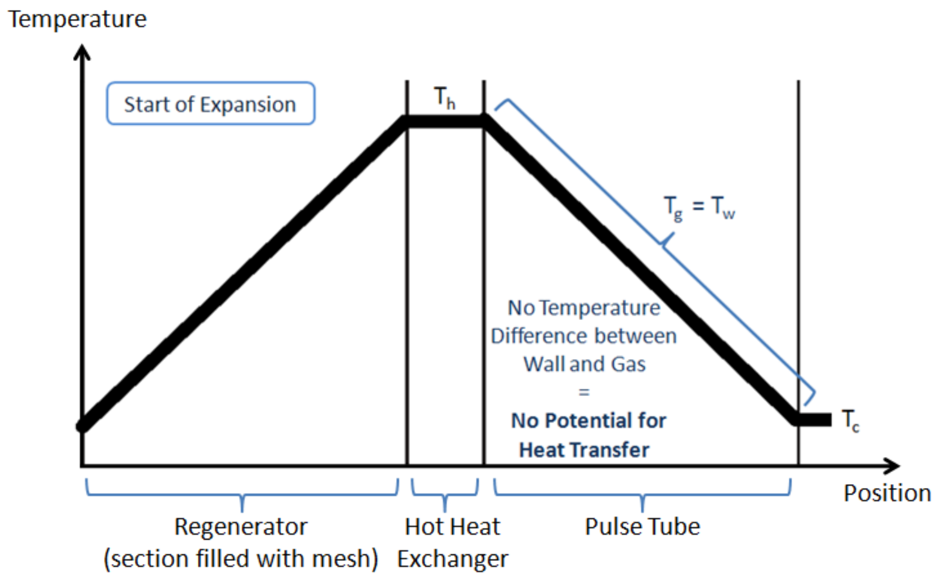

Figure 6.7: Temperature profile at start of expansion.

During the outward stroke, gas expands out of the heater at temperature T_h. The gas moves through the pulse tube, shifting its temperature profile along, see figure 6.8. Now, the temperature difference between the gas and the tube wall is increased. This raises the potential for heat transfer from the gas to the pulse tube. Organ states in his ideal thermodynamic cycle that expansion is adiabatic because of high piston velocity [24].

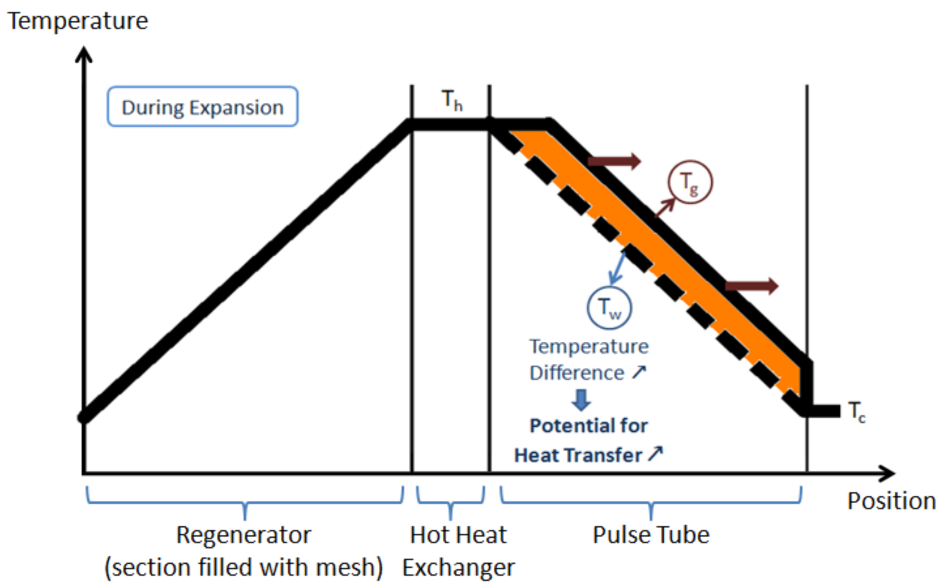

Figure 6.8: Temperature profile shift during expansion.

At the end of the expansion, the gas temperature profile has shifted to a maximum position. From figure 6.9, it can be seen that the temperature difference and thus heat transfer potential is now at a maximum. During the dwell period at bottom dead center, the gas has time to dump heat into the walls and adopt its temperature profile.

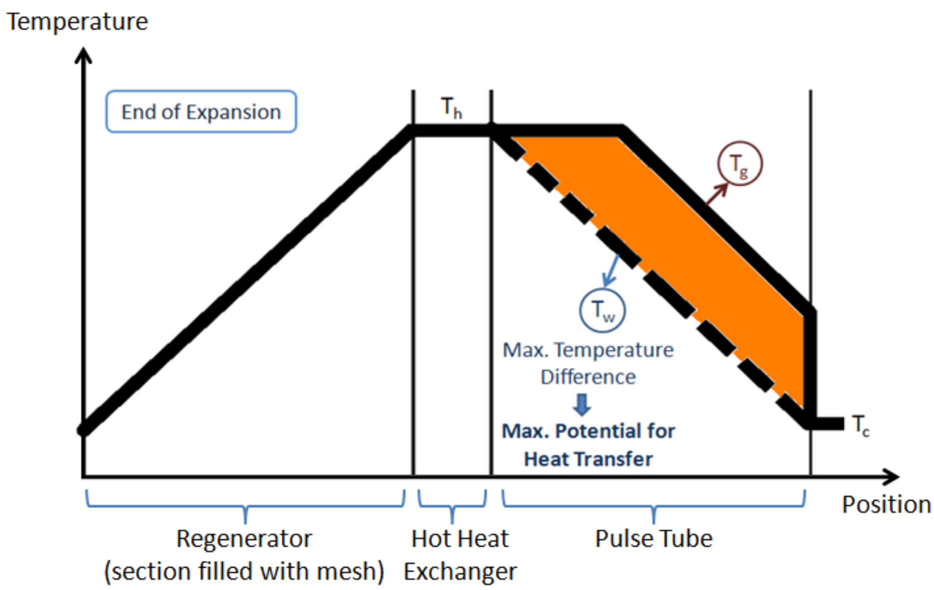

Figure 6.9: Gas temperature profile at end of expansion.

During compression, an analogous phenomenon occurs. The gas is shifted out of the cooler at temperature T_c due to its high rate of heat transfer. This can be seen in figure 6.10. After compression, at top dead centre, the gas is given time to receive heat from the pulse tube wall and adopt its temperature profile.

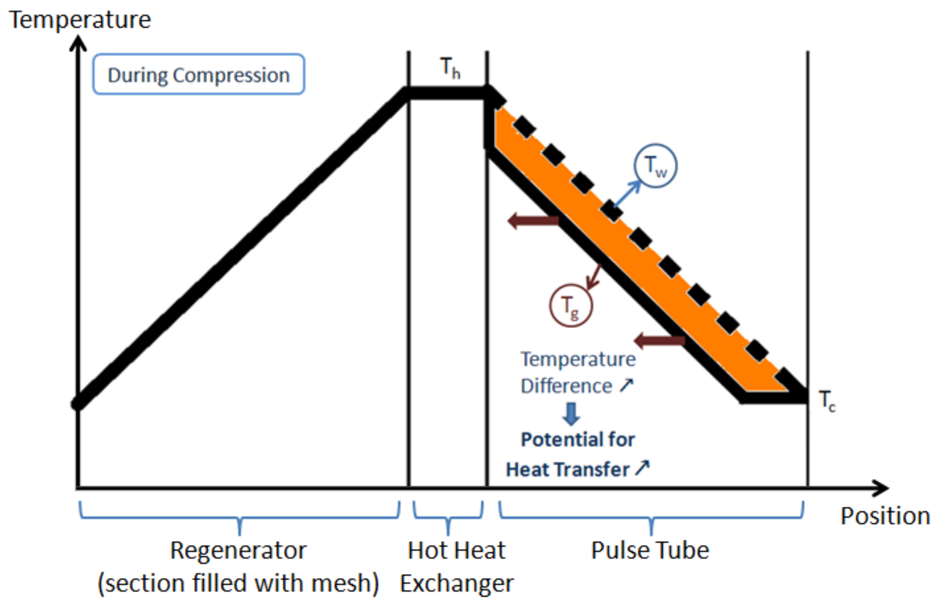

Figure 6.10: Temperature profile shift during compression.

Through these considerations, Organ explains the thermal lag effect in his engine [24]. In the time between expansion and compression strokes, the difference in temperature between pulse tube and gas is highest. During these dwell periods, overall pressure and temperature is then lowered or raised through heat exchange over time with the pulse tube. Consequently, expansion happens at a higher pressure than compression and work can be delivered.

For this system to function, it is important to see that the pulse tube should have restricted heat transfer capacity. If the rate of heat transfer is too high, the gas that enters it will immediately adopt its temperature and the dephasing is lost. If the rate is too low, the gas will not be able to exchange heat with the pulse tube wall during the dwell times. The means to have indicated work is now lost and the engine cannot produce work. Organ observed this optimal heat transfer capacity in the pulse tube from both experiments and simulations [24]. For this, he varied hydraulic radius of the pulse tube while keeping free-flow-area and volume constant.

Comments on the dephasing of Organ's engine The concept of the thermal lag effect as proposed in section 6.1, can be linked to Organ's explanations. He connects the idea of the time delay between the movement of the gas and heat exchange to the functioning of the pulse tube.

A remark has to be made about the functioning of the heater and cooler.

- Tailer states that the gas exchanges heat with the heater and cooler during the dwell times <u>at bottom and top dead centre</u> [22].
- Organ states that the gas exchanges heat with the *pulse tube* during the dwell times at bottom and top dead centre. The *heater and cooler* only exchange heat with the gas <u>during compression and expansion</u>. During expansion, the heater adds heat to the gas to keep it isothermal. During compression, the same thing happens with the cooler drawing heat from the gas [24].

So once the pressure level is raised or lowered, the heater delivers heat to the gas during the expansion and the cooler draws heat during compression. Considering both steps in Organ's process, it is questionable if indeed the pulse tube creates the essential effect that drives the engine. Referring back to West's statements about the essence of the thermal lag concept[20], Organ's engine demonstrates the same principle in which the cooler and heater exchange heat *at the right time.*

It is also interesting to think about the losses that occur during the cycle. It was discussed in section 6.1 that losses take place when the gas exchanges heat at the wrong time. This is when it is cooled during expansion or heated during compression. In Organ's engine, this happens when gas leaves the pulse tube: If, during expansion, gas leaves the pulse tube and enters the cooler, the gas dumps heat immediately due to the high heat transfer rate of the cooler. If, during compression, gas leaves the pulse tube and enters the heater, the gas immediately takes in heat from the heater. These losses are inevitable however, as there will always be some gas flowing out of the pulse tube.

These losses are minimised in Organ's engine. As the temperature profile is shifted towards the cooler along the expansion stroke, gas is pushed into the cooler and the temperature of the gas at the cooler entrance increases steadily. At the beginning, the difference in temperature between gas and cooler is zero. Towards the end of the stroke, this temperature difference has become high enough to enable heat loss to the cooler. Cooling thus picks up at the end of expansion. By then, most of the expansion work has already been delivered. During the compression stroke the same thing happens. It is only towards the end of the compression stroke that the temperature difference between the heater and the incoming gas is maximised, with the resulting losses.

Assumably, there is an optimum in pulse tube length. On one hand, it has to be short and the temperature gradient steep enough to create a significant temperature difference and thus a thermal lag effect as Organ describes it. On the other, the pulse tube has to be long enough to keep gas for a longer time in the pulse tube during strokes. This way, more cold gas is kept from reaching the heater during compression and hot gas from reaching the cooler during expansion, limiting the losses.

Organ calls the mesh at the end of the heater his 'regenerator'. This section does not behave as a regenerator, however. It provides a thermal capacity in the heater so temperature fluctuations are minimised and it adds heat transfer area. With the increased heat transfer area, isothermal gas behaviour is obtained.

6.4 Discussion

From the previous paragraphs it can be understood that both engines work on the thermal lag effect, but harness it in an different way. Organ claims that Tailer's TLE works on the pulse tube principle, even though its configuration is different [24]. This statement cannot be ruled out completely as the interface between the heater and the cooler, which spans the temperature difference, might act as a pulse tube.

Organ acknowledges that with varying the hydraulic radius of his pulse tube section, with free-flow-area and volume kept constant, flow resistance is varied as well [24]. This flow resistance is placed in the part of the engine were gas speeds are the highest. The induced flow losses will inevitably decrease engine efficiency. Also, even though the pulse tube creates a way to implement the thermal lag effect, it also increases dead space. This decreases potential for power output as the temperature interface is spread out. If Organ's engine would work on the principle that West and Tailer stated, the presence of the pulse tube would thus decrease the engine's performance. Furthermore, because the cylinder walls of Organ's engine are not cooled, the circulating flow that is induced when the gas is being compressed is not used effectively. In comparison to Tailer, he loses this inherent advantage.

Tailer's opinion on having a section between heater and cooler with a mesh is the following. The mesh will sit at a mean temperature of the cycle and function as a regenerator. During expansion, when hot gas is expanded out of the heater, the gas dumps heat into the mesh. This reduces expansion work. During compression, the cooled gas receives heat from the mesh when it flows through the passage. This increases compression work. Thus, adding heat transfer capacity in the passage between heater and cooler reduces the work output [22]. According to Tailer, the effect of a regenerator inside a TLE is not beneficial for its power output, in contrast to classical Stirling engines.

One must take note, however, that a regenerator in the section between heater and cooler could increase efficiency. If part of the working gas dumps heat in the cooler during expansion or receives heat in the heater during compression, this appears as losses to the engine. If a regenerator were designed, so that during expansion the gas does not dump the heat into the cooler but in the regenerator, energy is kept inside the system. During compression, the heat that it would receive in the heater is then recovered from the regenerator. This would thus increase efficiency. In similar pulse tube engines, this positive effect has already been observed experimentally [28].

The previous two paragraphs show that when designing the heat transfer capacity of the section between heater and cooler, a compromise must be made between the two discussed effects. Organ made exactly this observation when varying the hydraulic radius of his 'pulse tube', but attributed it to his theory of the pulse tube mechanism driving the engine. To draw definite conclusions whether Organ's pulse tube is really the driving mechanism of the engine or functions as a regenerator to minimise the losses, further experimental research is necessary.

Tailer and Organ have attempted to explain the behaviour of their engine. However, both of them lack the appropriate experimental data to back up their claims. It has become clear that there are different ways to implement a thermal lag effect. To optimise engine performance, it is important to fully understand the driving phenomena of the TLE. It cannot be ruled out that both interpretations of the thermal lag effect are present in a single configuration. For future research, it would be interesting to explore the different concepts that were discussed, in order to identify which TLE configuration renders maximum power output and efficiency.

Part II

Test Rig Design

Chapter 7

Previously Built Engines

7.1 Introduction

Only two researchers have built thermal lag engine test rigs on which measurements could be performed, Peter Tailer and Allan Organ. Even if both are TLE's, they display subtle differences. In general we can divide both engines in the following aspects:

- Hot space where the working gas receives the heat input
- Cold space where the working gas is cooled down
- Thermal barrier or pulse tube, separating the hot from the cold part
- Piston cylinder
- Piston and its sealing method
- Drive mechanism

Both Tailer's and Organ's engine are described in the following sections, 7.2 and 7.3. The different aspects of the engine will be treated in the order given above.

7.2 Peter Tailer's engine

As stated earlier, Tailer built three working thermal lag engines [19][22]. On the first engine, however, no measurements could be performed as this prototype served solely as a proof of concept. Later on, Tailer constructed two new engines from which a power output could be measured. The first of the new engines was set up horizontally. It had a problem of excessive vibration and suffered heating difficulties. This experiment, however, helped him gain the experience to build an improved engine that was set up vertically. A scheme of the original engine configuration can be seen in figure 7.1.

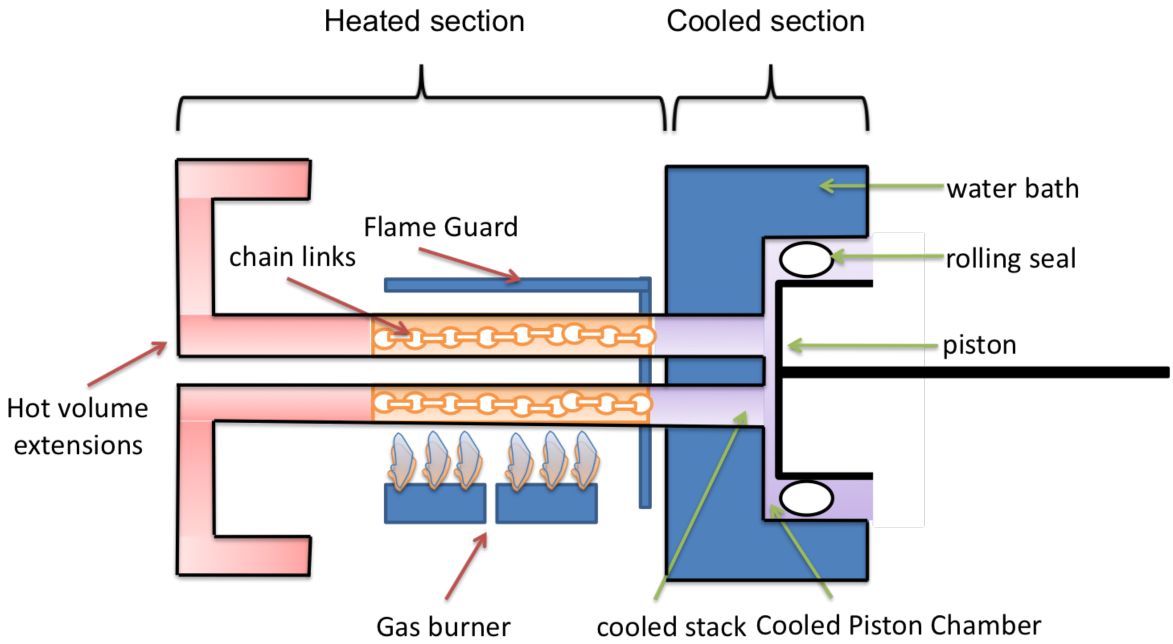

Figure 7.1: Peter Tailer's original engine configuration

The hot section of the horizontal engine consists of a long tube, which is heated with a gas burner from below. In the vertical engine the heated chamber is exposed to the gas burner through a flat plate, see figure 7.2. It provides a larger surface with the heat source, allowing the wall of the heated chamber to reach 630°C. Although the use of a gas burner is easy, it is impossible to measure the heat input. Consequently, Tailer could not calculate the efficiency of the engine. In both engines, hot volume can be varied. This not only influences the total engine volume, but also the ratio of hot to cold volume. In the horizontal engine the length of the hot tube could be varied. In the vertical engine, steel gaskets could be placed between the cover and top of the heated chamber to increase its volume.

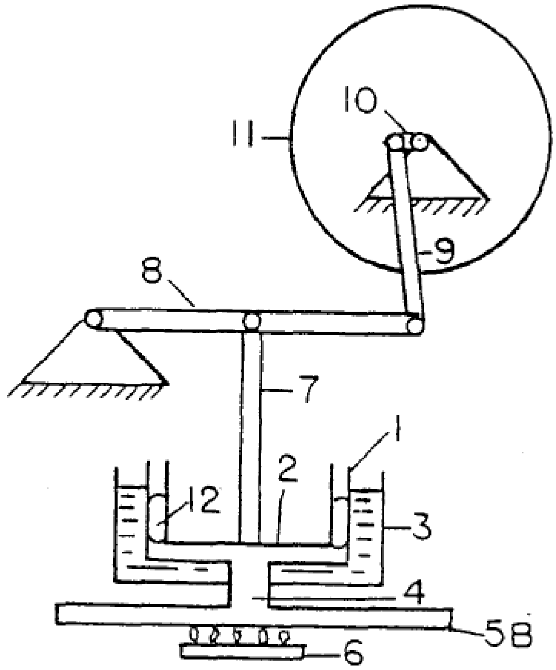

Figure 7.2: Peter Tailer's vertical engine configuration [22]

To improve heat transfer to the gas, Tailer experimented with simple chain links that were inserted randomly throughout the heated tubes. From the experiments, it was clear this improved the engine's performance [19]. Apart from the added heat transfer area, the chain links might also increase the heat transfer coefficient by inducing turbulent flow.

The cooled section of Tailer's engines is the piston cylinder itself. The horizontal engine is air cooled through fins that are welded onto the cylinder. The cylinder of the vertical engine is completely immersed in a cooling water bath. The head of the cylinder is also exposed to this water jacket. As a result, the gas in the piston chamber makes contact with the cold wall according to the piston motion. To assist cooling, Tailer added two elements in his vertical engine. First, a metal sheet was folded in a serpentine pattern and inserted into the channel that connects the heated chamber to the piston cylinder. Second, a wire mesh was placed in the top of the cylinder in front of the piston. Although this mesh added dead space, the improved cooling seemed to increase the engine performance considerably [22].

Between the heated and cooled part of the engine, there is a section where the gas does not exchange heat with the walls. Tailer sees no purpose to have this space in the engine. He states that it represents merely dead space that decreases the overall efficiency. Thus, he always tried to minimise this volume in his designs. It is impossible, however, to completely omit this section. A thermal barrier is needed between the hot and cold part of the engine.

Tailer installed a flame guard to shield the gas burner from the cooled cylinder. As a result, heat flow from the heater to the cooler through the engine's walls was reduced.

One of the toughest practical challenges of building these engines lies in the sealing of the piston inside the cylinder. In addition, the seal is of vital importance to the functioning of this engine. In 1991, Tailer et al. presented a solution for this problem: an internally pressurised annular rolling seal [17]. The seal consists of an elastomer vehicle inner tube that is fixed between a cylinder and a piston, see figure 7.3

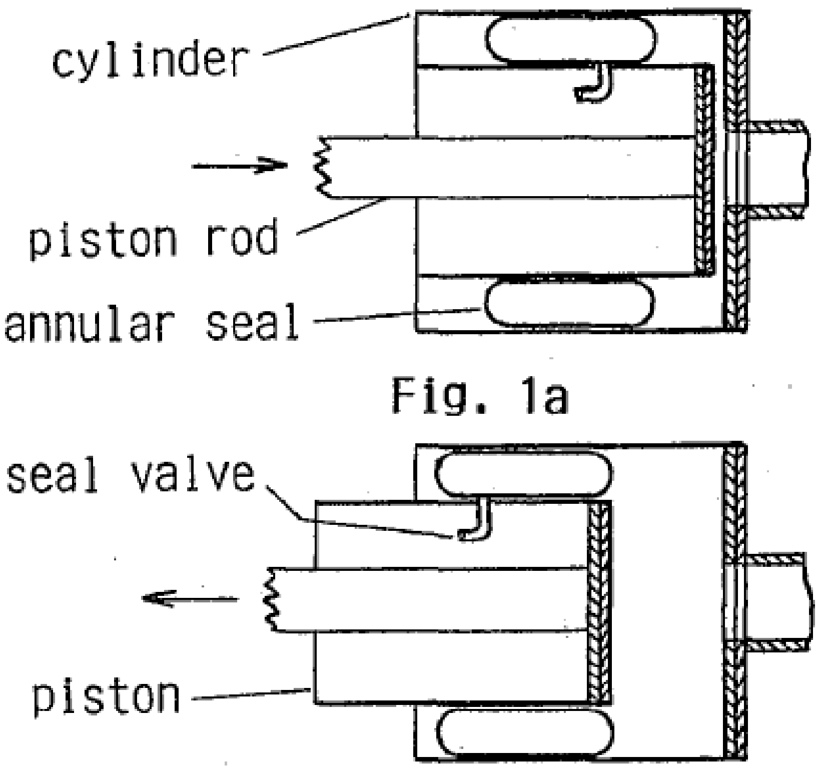

Figure 7.3: Internally pressurised annular rolling seal [17]

Good sealing is attained with little friction. Very crude tolerances on both piston and cylinder are sufficient. The only setback is the restriction on piston stroke length. Tailer's engines ran with a piston stroke of about 2 cm. To have enough displaced volume by the piston a large diameter of 15.9 cm was required. The cylinder measured 19 cm in diameter to harbour both the piston and the rolling seal. The dimensions of Tailer's horizontal engine are given in table 7.1.

Hot section		
Hot volume	m^3	0,00218
Tube heated area	m^2	0,07431
Tube air exposed area	m^2	0,19551
Flow area	m^2	0,00195
Cold section		
Fixed cold volume	m^3	0,00020
Chamber top area	m^2	0,00708
Chamber side area	m^2	0,00060
Tube wall area	m^2	0,02212
Piston head area	m^2	0,00632
Piston displacement	m	0,01900
Flow area	m^2	0,00195

Table 7.1: Dimensions of Tailer's horizontal engine.

To transfer the power output of the piston to a crankshaft, the piston shaft was connected to a pivoting link. There was no need for a crosshead or guidance of the piston shaft as considerable rocking of the piston was allowed because of the flexibility of the rolling seal. The connecting rod that drove the crankshaft was also attached to this pivoting link. A flywheel was mounted onto the crankshaft. Power output was measured with a 'Prony brake'.

7.3 Allan Organ's engine

Organ built his test rig expecting low indicated power. Thus, his top priority laid in eliminating mechanical friction. A schematic overview of the engine can be seen in figure 7.4.

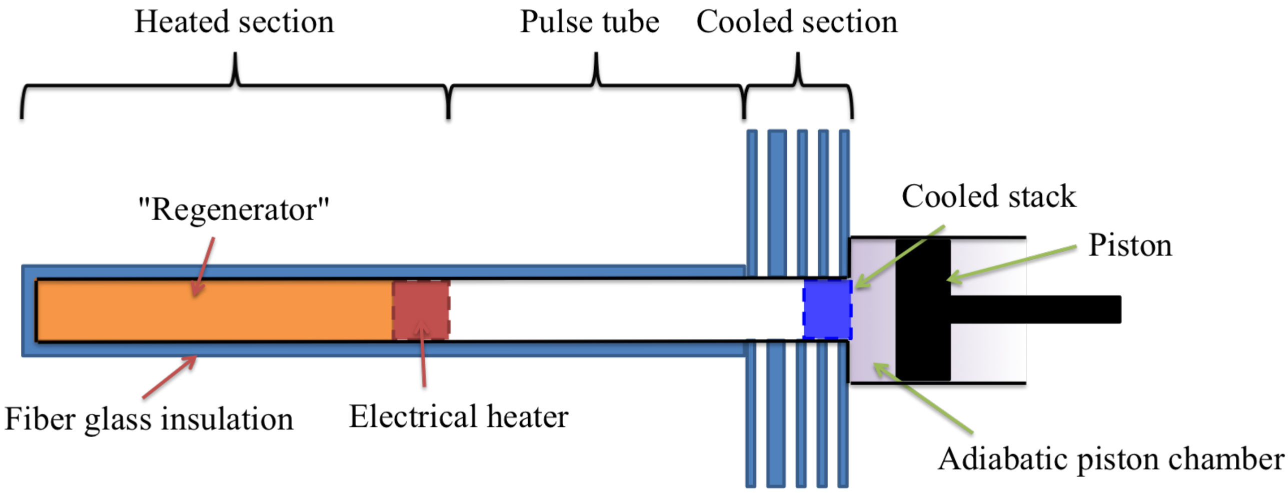

Figure 7.4: Allan Organ's pulse tube TLE

The heated section of Organ's engine is formed by a steel cylinder of approximately 3.5 cm in diameter. In his first experiments, a gas burner was used to provide heat input. Using a portable thermocouple, he could obtain an idea of the hot temperature: 480℃. In later experiments, the external heating method was replaced by an electrical resistance coil, inside the cylinder. This allowed input power to be set accurately. However, much heat was dissipated radially from the engine to the surroundings. Therefore, the heated section of the engine was covered by a standard glass fiber insulation of 25 mm thickness. This significantly increased the power input to the gas, but there was still no means of measuring heat input with much precision.

To further increase heat transfer in the hot section, Organ used a mesh in the space at the far end of the heater. He calls this space the regenerator. It consisted of a stack of *Retimet*^{TM} metal foam plugs accurately cut by a numerically-controlled water-jet machine. The grade of the metal foam plugs was very important. With a coarse mesh the engine ran, with a fine mesh it did not.

The configuration of Organ's cold section is slightly different from Tailer's. The piston cylinder is assumed adiabatic and the cooler is placed in front of the cylinder head. Unlike Tailer's engine, the cold heat transfer area does not change because of the piston's motion. The cold heat exchanger was air cooled on the outside with radial fins.

In contrast to Tailer's design, Organ adresses great importance to the section between the cold and the hot heat exchanger. According to him, this part does not only serve as a thermal barrier, but plays a vital role in the functioning of a TLE. The reason for this has been

discussed in much greater detail in the physics section 6.3 of the literature review. Organ made it possible in his design to insert different 'pulse tube' sections (a term borrowed from 'pulse tube cryocoolers'), which are made out of steel.. Unfortunately, it is not specified how this was implemented. The hydraulic radius ($= \frac{free-flow\ area}{wetted\ perimeter}$) of the pulse tube section was varied while volume and free-flow area were kept constant. Actually, this means that the heat exchange area between the gas and the pulse tube was changed.
One must notice that, according to Organ [24], this pulse tube is not heated nor cooled externally, and thus it only exchanges heat with the gas. Organ further states that the hydraulic radius of the pulse tube is critical, deriving this statement from both simulations and experiments. When it is too big or too small, the engine does not run. The pulse tube also creates a wider gap between heater and cooler. This helps to create a thermal barrier.

The piston and cylinder were bought in an Airpot^{TM} piston-cylinder set, which has a carbon piston running in a pyrex tube. Low friction was achieved but inevitably some air leakage was present. No further efforts are mentioned in eliminating the leakage. The piston had a diameter of 3.2 cm and the engine ran at a stroke of 2.47 cm. The piston cylinder was bolted to the cold heat exchanger and crankcase with O-rings in between to provide sealing.

The crankshaft was driven by a drive shaft that connected the piston directly to the crank arm. This of course gave rise to sideway pressures on the piston inside the cylinder. A simple friction dynamometer and a tachometer were used to measure torque and speed. With these devices effective power output was calculated.

Chapter 8

Requirements for Experimental Test Rig

8.1 Outset

From the discussion in section 6.4 of Tailer's and Organ's view on the underlying physics of the TLE, it has become clear that there are multiple ways to create the thermal lag effect. These engines have subtle differences in configuration. Organ uses a pulse tube and a cooler placed in front of an adiabatic cylinder. Tailer's piston cylinder itself functions as the cold heat exchanger, which changes heat transfer area according to the piston motion. To capture both effects in an experimental rig, it is necessary that it can adopt both of these configurations in order to perform all the experiments Tailer and Organ performed. Therefore, the rig must incorporate the different sections of both engines. Each section has its own requirements, which will now be discussed.

8.2 Hot heat exchanger

The hot heat exchanger provides the heat input that is required to drive the engine. The rate of heat transfer needs to be high to allow isothermal gas behaviour in the heater. The two main design parameters of this heat exchanger, power input and temperature, need to be controlled. Previous experimental results described in literature show that the efficiencies of these engines can be as low as 0.5% [24] [28]. To have at least a measurable power output at the crankshaft, which also incorporates mechanical losses, maximum heat input is designed to be 1 kW. In selecting the hot operating temperature, there is a compromise to be made between the thermodynamic efficiency of the engine and manufacturability. For example, it was anticipated that sealing the engine at high temperatures would be very difficult. To seal threads that need to be disassembled in a non-destructive manner, modern adhesives are available up to 300℃. Also, with a hot temperature of 300°C = 573.15 K and a standard atmosphere temperature of 20°C = 293.15 K, Carnot efficiency is already at 48.85%. Reaching higher Carnot efficiency will require an even higher increase in temperature. As these types of engines are aimed to be produced as economically as possible and use low grade energy, the hot temperature in this engine design was set at 300°C.

The hot heat exchanger design needs to incorporate a way to vary hot volume. This should be done with as little reduction of heat transfer area as possible. To have isothermal gas behaviour, the product UA of the overall heat transfer coefficient 'U' and the heat transfer area 'A' should be considerably high. U is predominantly influenced by the convection coefficients of the gas inside the engine. These coefficients are very difficult to predict as they are function of gas velocity, temperature and pressure and none of these have been determined experimentally. Therefore, to have a sufficiently high UA, it must be possible to increase the heat transfer area A. This can be done by placing inserts in the engine, as Tailer and Organ have done. The design must thus allow the placement of different types of inserts.

8.3 Cold heat exchanger

Tailer and Organ have dissimilar cold heat exchanger designs. The difference lies is the positioning of the cooler. To be able to mimic both situations, the test rig must be able to cool the gas in front of the piston as well as at the piston cylinder walls. If the engine's heat input is 1 kW, then our cooler must be able to cool 1 kW as well. In one of his experiments, Tailer placed a wire mesh in the piston head and saw an improvement in power output [22]. The design must incorporate a way of doing this too.

8.4 Thermal barrier - pulse tube

Tailer and Organ have different opinions about the function of the adiabatic section between hot and cold heat exchanger. Tailer minimises this volume as it increases dead space. For Organ, this 'pulse tube section' is of fundamental importance to the functioning of the engine. Thus, the design of the test rig should make it possible to change this piece. Hydraulic radius, volume, length, free-flow-area need to be variable. This section also needs to function as a thermal barrier between the hot and the cold section. If the thermal resistance of the barrier is too low, heat from the heater flows straight into the cooler, bypassing the working gas. This would mean an increased loss in available power input.

8.5 Piston, seal and cylinder

As discussed above, the cylinder walls need to act as the cold heat transfer area. This area varies according to the piston's motion. As we expect low power outputs, friction of the piston and the cylinder must be minimised. In Tailer's first engine, piston and cylinder diameter were respectively 15.9 cm and 19 cm with a stroke of 1.9 cm. Organ's engine had a piston and cylinder diameter of 3.2 cm with a stroke of 2.47 cm. Thus, the ratio of stroke to piston diameter is about 0.119 for Tailer and 0.772 for Organ. The design of the test rig should thus be able to carry out short and long strokes. This will influence the piston sealing method. The piston seal should minimise leakage and friction, but allow a long stroke.

8.6 Drive mechanism

The drive mechanism of the engine transfers piston work to a crankshaft. The crankshaft angle needs to be measured to know engine volume and speed. A flywheel is necessary to buffer energy received during expansion to deliver compression work. The design must incorporate a means to drive the crankshaft to get the engine running and a means to deliver brake power when it is providing work output. This mechanical work output needs to be measured as well, to allow the calculation of a mechanical efficiency.

8.7 Insulation

Having a hot section of the engine at 300°C will create significant heat losses to the surrounding atmosphere, which limits heat input to the gas. Therefore a thermal insulation covering both hot and cold parts of the engine is indispensable. To obtain correct energy balances, design must incorporate a way to measure, or at least have an indication of the occurring heat losses.

8.8 Instrumentation

The parameters to be measured within the scope of the thesis are the energy balance and internal pressure versus volume diagram of a working TLE. To accomplish this, measurements must be performed inside the engine simultaneously. To acquire the energy balances, power input and outputs must be measured. From the pV-diagram indicated work and power of the cycle can be derived. The design must include ways to measure the following energy flows:

- Heat Input
- Heat output (cooling power)
- Heat losses to surroundings
- Heat loss from heater to cooler

It is also important to include some safety measures in the engine design. A component can always fail during operation, which can lead to serious damage. Control of the temperature distribution throughout the engine is necessary.

Chapter 9

Experimental Test Rig Design

9.1 Introduction

In the previous chapter, design requirements have been set for the test rig. In this chapter, the final design to meet the requirements is explained in great detail. Design is based on the requirements that were derived from the in depth analysis of the underlying physics and the previously built engines in literature. A great effort has been made to be able to manufacture every part of the engine in our own lab at Ghent University. The different engine sections will now be discussed in the same order as in the previous chapters. Overviews of the test rig are shown in figures 9.1 and 9.2. An overview of the different sections, and where to find them in this chapter, is given in figure 9.3.

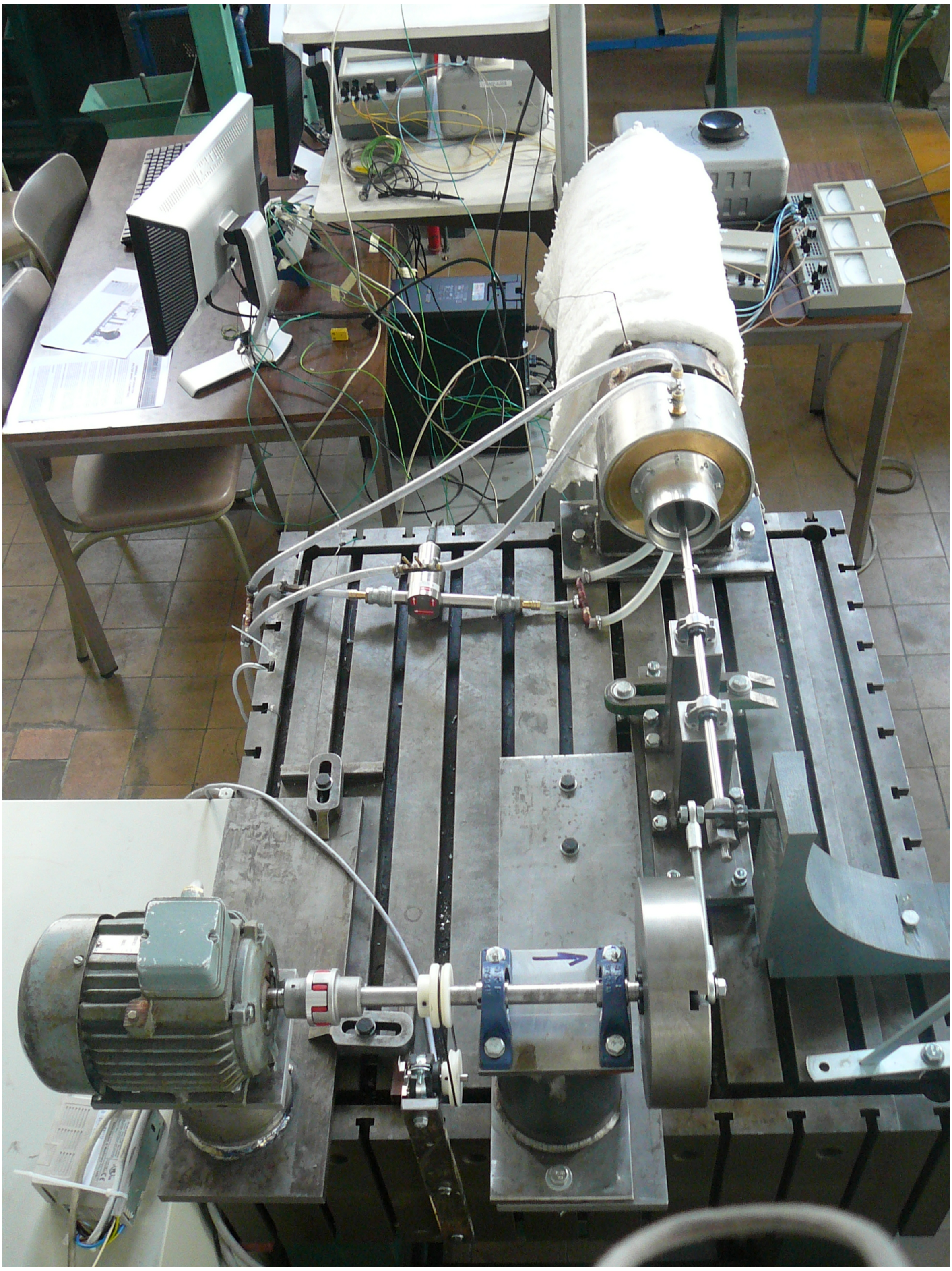

Figure 9.1: Overview of the test rig.

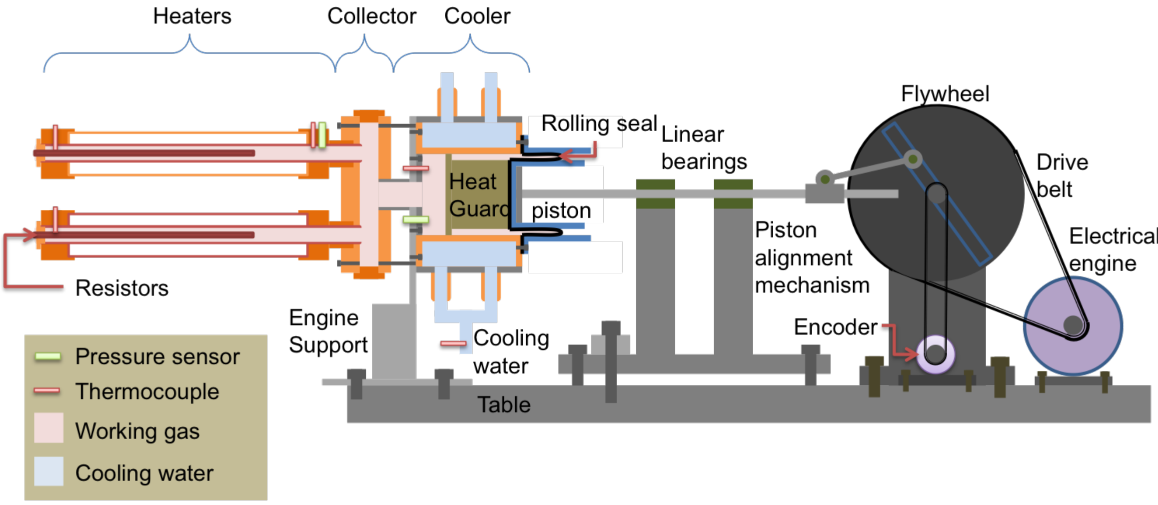

Figure 9.2: Schematic representation of the test rig.

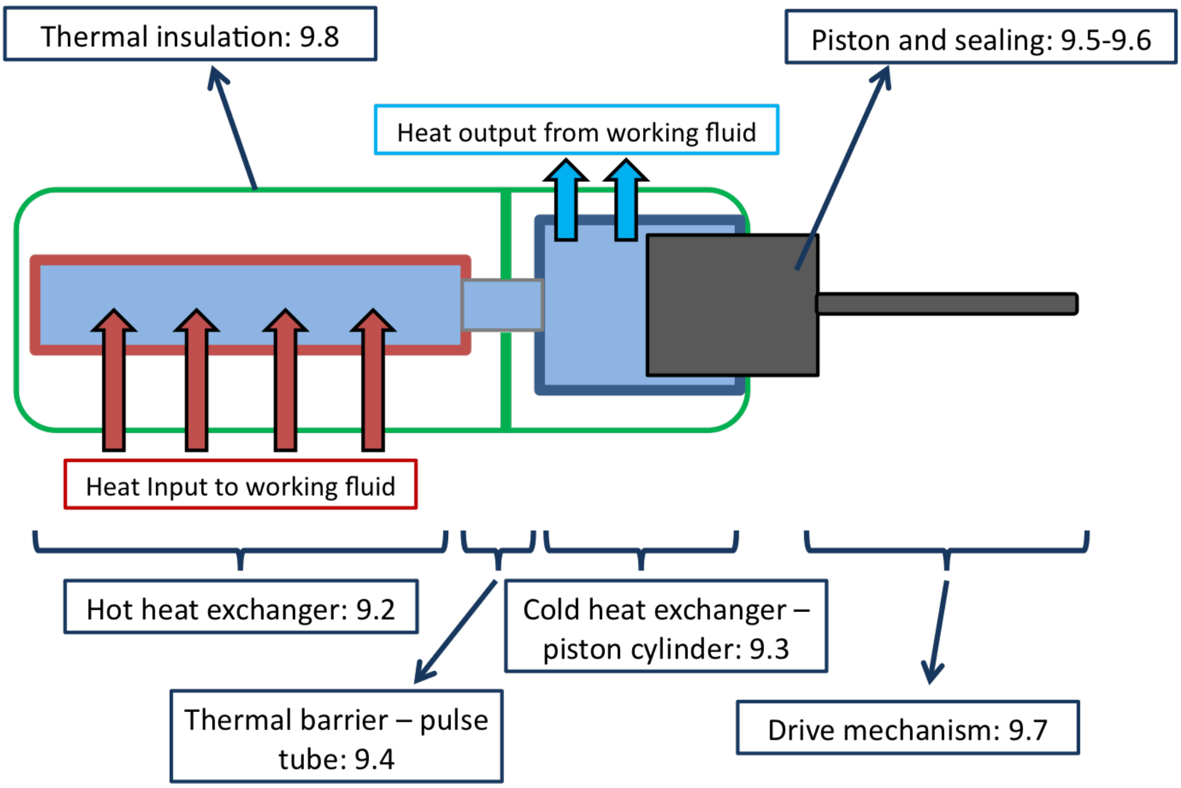

Figure 9.3: Overview of the different test rig components and where to find detailed descriptions in this chapter.

9.2 Hot heat exchanger

A heat source with a controllable heat input is provided by electrical resistors. The electrical power that feeds the resistors equals the heat input in the engine. Thermocouples are put on the resistors, to monitor its temperature. If a certain maximum temperature is reached, input power must be lowered or shut down. Electrical resistors are found on the market in many forms and are easily mounted in the rig. The only problem is to maintain a constant hot temperature. In the engine, heat input to the gas varies during the cycle. This will affect the temperature of the resistor. When suddenly heat is drawn out of the resistor into the gas, resistor temperature will drop instantly. These fluctuations are not desirable. This problem is solved by adding thermal inertia. This inertia acts as a thermal buffer between resistor and internal gas, so temperature fluctuations are minimised. To provide thermal inertia, the design incorporates an oil bath in which the resistors are immersed. The thermal oil that is used is 'Therminol 66'[1].

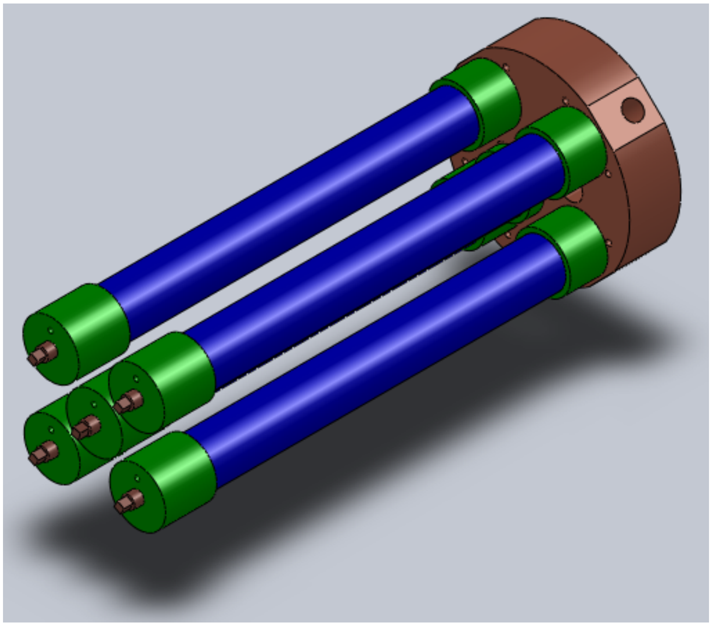

Figure 9.4: General overview of the heater tubes and collector.

The use of multiple tubes is opted in which the internal gas is heated. The tubes are screwed into a collector piece which leads the gas from the tubes into the adiabatic section, as seen in figure 9.4. This modular approach allows great flexibility as one or more tubes can be taken off. The use of multiple tubes also increases heat transfer area. This is beneficial to obtain quasi isothermal gas behaviour. An oil bath is formed by an annular space around the gas tubes. The resistors are bars with a diameter of 8 mm and a length of 350 mm that can be

[1]Therminol 66: http://www.therminol.com/pages/products/eu/66.asp

threaded into the side flanges of the annular space. Each of the five resistors can provide a heat input of 200 W. Inner and outer tubes have a mean diameter of respectively 21 mm and 48 mm and a thickness of respectively 1 mm and 2 mm. The resistors and inner tubes are thus both surrounded by the thermal oil. This configuration can be seen in figure 9.5. Hence, the oil acts as a heat transfer medium and thermal inertia. The maximum temperature swing of the oil during the cycle relative to the mean temperature of 300°C is 0.17%, see appendix B.

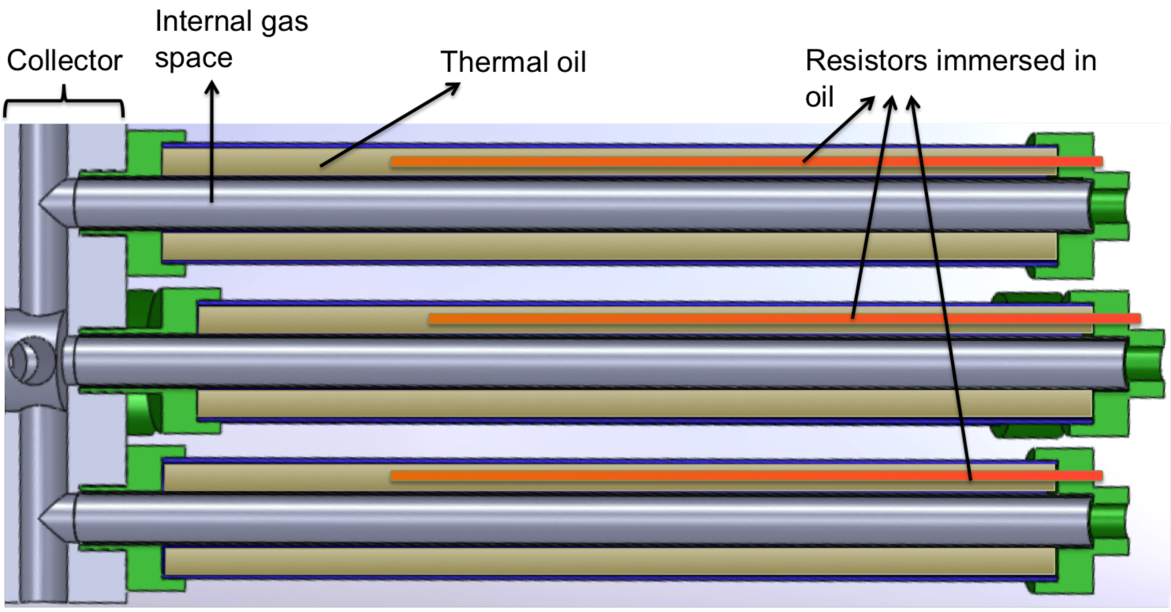

Figure 9.5: Heater tube: designed configuration

In this configuration, the working gas receives heat from the wall at a quasi-uniform temperature, as the thermal oil transfers the easily from the resistor wall to the inner tube. The flanges at both ends of the tubes are designed to fix the position of inner and outer tubes. At the collector side, the flanges also provide the thread to fasten the heater tubes onto the collector. At the open end, they provide an opening with threaded caps from where inserts can be introduced in the inner tubes. This can be done either to decrease the heated volume or add heat transfer area. In the latter case, the inserts must have good contact with the walls. The flanges are designed to provide sufficient space to instrument the heater tubes with thermocouples and pressure sensors. Every flange, close the collector or on the outside, can be instrumented with a pressure sensor and some thermocouples. This can be done to measure wall temperatures of the inner tube, oil temperature or gas pressure. All parts of the hot heat exchanger are made of brass as it has high thermal conductivity. The different parts of a single heater tube are soldered together with silver, except the caps at the open end of the heater to be able to introduce different sets of inserts.

If the annular space would be a hermetically sealed volume, the pressure would rise at elevated temperatures because the oil is hindered in its thermal expansion. The expected pressure rise is calculated to be 114.66 MPa. The calculation can be found in appendix A. As this is unacceptable for the thin copper tubes with a thickness of 2 mm, the oil must be allowed to expand. A solution to the problem is to provide an expansion tank. The volume increase of the oil is then buffered by an air volume that is being compressed. The pressure rise of the air in the expansion tank must be limited to be able to contain it safely. Calculations for the minimum required air volume can also be found in appendix A. The expansion tank consists of a steel cylinder, as this geometry minimises stress concentrations. Two square plates are welded to form top and bottom. A threaded tap at the top provides a way to insert the oil. The annular spaces of the heater tubes are connected to the tank through small tubes, which congregate before entering. Before entering the tank, the oil tube forms a U shape downwards. This forms a thermal inversion to prevent hot oil from circulating in the tank due to density changes. A drawing of the expansion tank and the connecting tubes can be seen in figure 9.6. The inside diameter and length of the tank are 15 and 30 cm. This gives a total volume of 5.125 liter. Referring to the calculations of appendix A, this gives us a p_{end} of 2.545 bar.

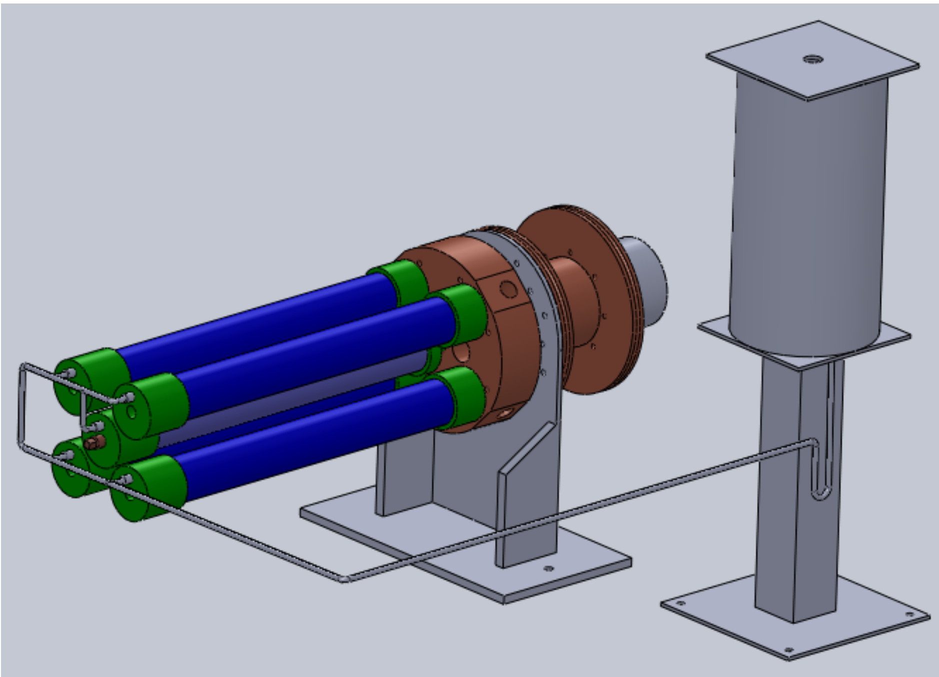

Figure 9.6: Overview of the oil expansion tank and connections to the heater tubes

To lead the working gas from the five tubes into the adiabatic section a piece called the collector is machined. It is a thick copper disk with channels that connect the inner heater tubes to a central hole leading to the piston cylinder. The main purpose of the piece is to provide a modular heater, where different heater tubes can be added or left out. In total, five heater tubes are arranged in an X-configuration on the disk. Channels are drilled from the perimeter of the disc to meet in the centre. Parallel to the axis of the disc, holes are drilled to connect with these channels. From construction, the channels are open at the perimeter. This provides an easy access for additional instrumentation or a tap to pressurise the engine with a compressor. The rest of the holes have to be sealed off. There are two axial blind holes in the collector. They provide enough space for a thermocouple and pressure transducer to be installed in the cylinder head. This way, measurements are taken directly in piston cylinder. The collector can be seen in figure 9.7.

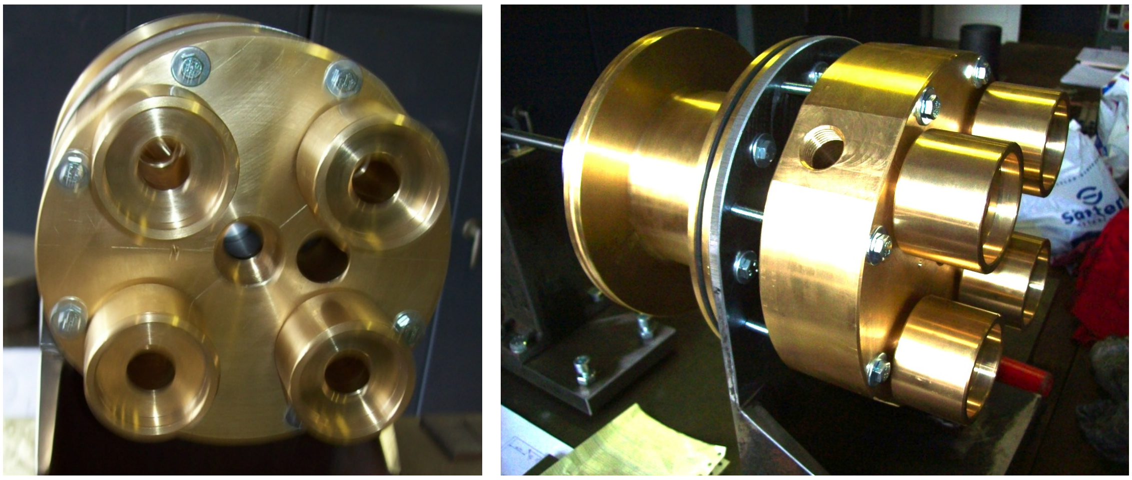

(a) (b)

Figure 9.7: Collector

What was actually built Due to construction delays the main goals of the project were put at risk and changes to the configuration were made. These changes shortened manufacturing time. The oil bath and reservoir were omitted. Another heater design was devised, inspired by Allan Organ's heating method [24]. The resistors were inserted directly into the inner tubes. The construction time was shortened drastically but heat transfer area was reduced by a factor 3. However, as modelling had evolved since the time of the initial design, it had become clear that to make the engine run, a heat transfer area of 2 m^2 was needed. The heat transfer area of the original design would thus have been insufficient as well. It now seemed that inserts to increase heat transfer area were necessary anyhow.

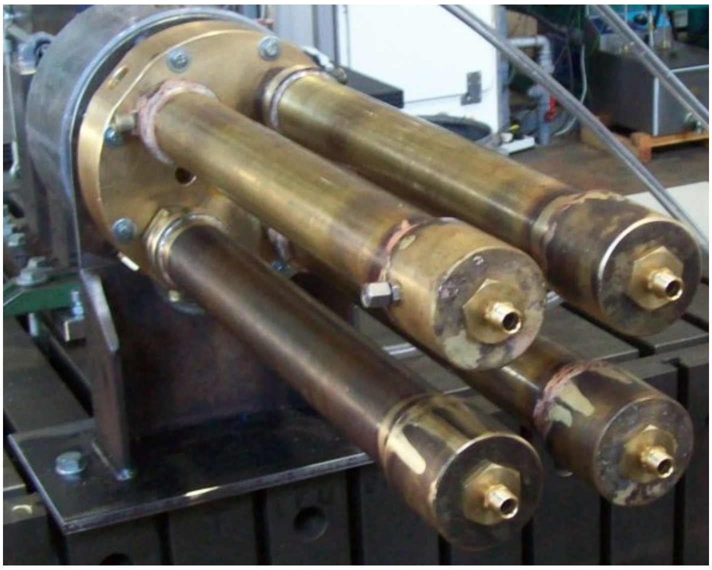

Figure 9.8: The actual implementation with resistors suspended in air

The resistor connection pieces were screwed into the caps that seal off the inner tubes, see figure 9.8. At first, this was sealed with Loctite. Later on, as observed from experiments (see section 10), this solution suffered excessive leakage. As the deadline of the project was closeby, the decision was made to insert a steel wire mesh[2] to increase heat transfer area. The resistors' holders and caps where then soldered onto the flanges, see fig 9.9.

Figure 9.9: The caps of the heater tubes were soldered shut to prevent leakage.

This was a drastic decision as the flexibilty that had been designed into the rig was lost. The heat source temperature fluctuation increased as well, as the thermal inertia provided by the

[2]Bekaert Stainless Steel Wire Fiber Web

oil was omitted. The negative consequences were compensated by the fact that experiments could be performed before the project deadline.

The first experiment, see section 10, revealed that by placing the resistors in the air at the back of the heater tubes heating was not sufficient. The collector was not able to heat up above 85℃ and heat input to the gas was a mere 20 W. An improvement was made by wrapping additional electrical resistors around the beginning of the heater tubes, close to the collector. To do this, the outer tube, which would have formed the oil bath, had to be cut open, see figure 9.10. This allowed the collector temperature to rise to 136.85℃.

Figure 9.10: The outer tubes were cut open to increase heat input. Additional resistor wires were tightly wrapped around the inner tubes at the side of the collector.

9.3 Cold heat exchanger - piston cylinder

The basic configuration of the cold heat exchanger resembles that of Tailer's engine. This means that the cylinder walls are being cooled and that the reciprocating piston varies heat transfer area by (un-)covering them. The cooling is provided by using a water jacket. It consists of an aluminium mantle that slides over the flanges of the cylinder. Sealing is assured by O-rings that are placed in grooves, which are cut in the flanges. To have absolutely no leakage, additional plumbing silicone is used. The cylinder is made of brass because of its good conduction properties.

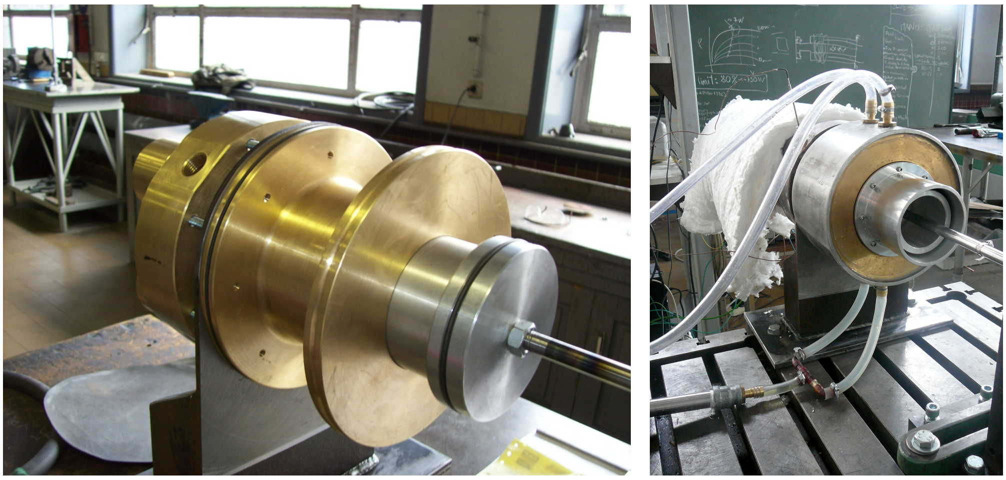

(a) Brass cylinder with grooved flanges to form a water jacket

(b) Finished water jacket

Figure 9.11: Cold heat exchanger - Piston cylinder

An external cooler can be set to a fixed inlet temperature in the range of -5℃ to 40℃. It pumps the cooling fluid through the water jacket in a closed circuit. The water jacket has two inlets and two outlets. A thermocouple and flow meter are installed in the return tube of the closed cooling circuit. This gives control over heat output and cold heat exchanger temperature. The major difference with Tailer's engine is that this design allows longer strokes. It is possible to put fins or a mesh in contact with the cylinder walls in front of the piston head and have the piston motion start behind the insert. If UA with the insert is high enough, Organ's cooler is adopted. It is not a problem that the cylinder walls that are (un-)covered by the piston motion are still cooled. If the rate of heat transfer is high enough, gas that flows through the insert will be at a low enough temperature. The cooled walls behind the insert will then not exchange a significant amount of heat with the gas. To adopt Tailer's cold heat exchanger, nothing is placed in front of the piston and piston motion starts from the cylinder head. Both configurations of the rig can be seen in figure 9.12.

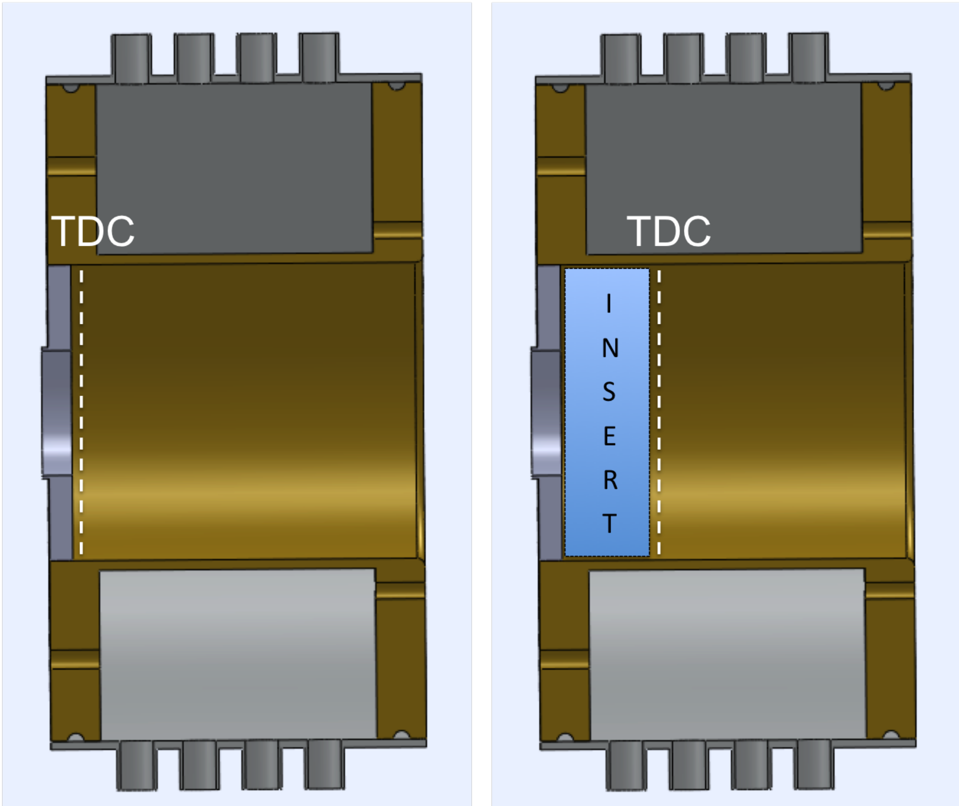

(a) Tailer's cooler configuration (b) Organ's cooler configuration

Figure 9.12: Cold heat exchanger - Piston cylinder

It was not possible to design the cold heat exchanger through heat transfer calculations. The limiting factor to the heat transfer lies in the convection of the gas inside the cylinder. There is, however, no experimental data available about the nature of this convection coefficient. The external cooler has a maximum cooling capacity of 3 kW. As the rig requirements were set at a maximum cooling capacity of 1 kW, this cold heat exchanger is more than sufficient for the application.

The cooling circuit is also used to cool the pressure sensors that are positioned in the hot section or that come in contact with hot gas. The circuit is tapped before and after the water jacket to redirect cooling fluid to the sensors and back to the external cooler, see figure 9.13.

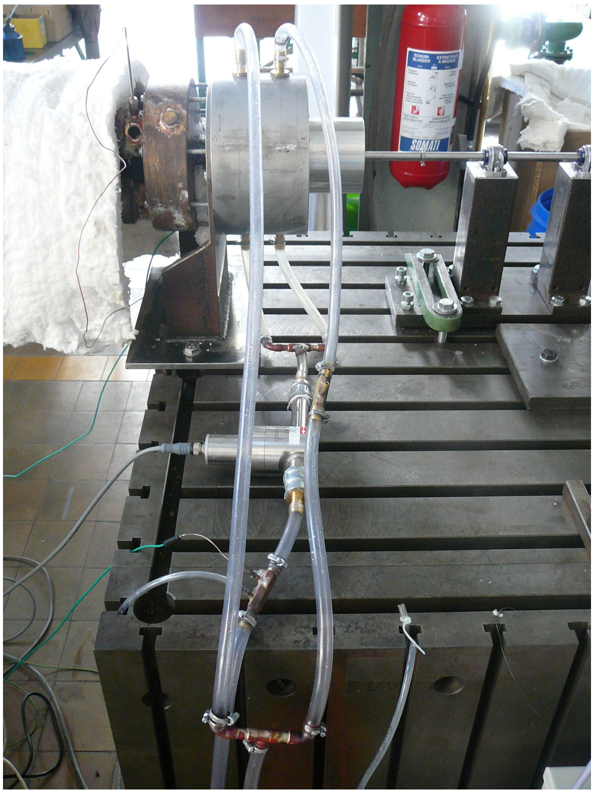

Figure 9.13: External cooling circuit for the water jacket and the pressure sensors.

The piston cylinder is bolted onto a steel engine support that is fixed onto the table, see figure 9.14. A small alignment disk with a ridge that fits into the central hole of the support, is bolted onto the support. This disk is circular with a outer diameter equal to the cylinder diameter. The cylinder is slid over this disk and bolted onto the support. This assures proper alignment of the cylinder relative to the table and the central hole in the engine support. The disk also provides space to screw the sensors into the cylinder head, as the engine support is too thin. The contact surface between the cylinder and the collector is sealed with common plumbing silicone.

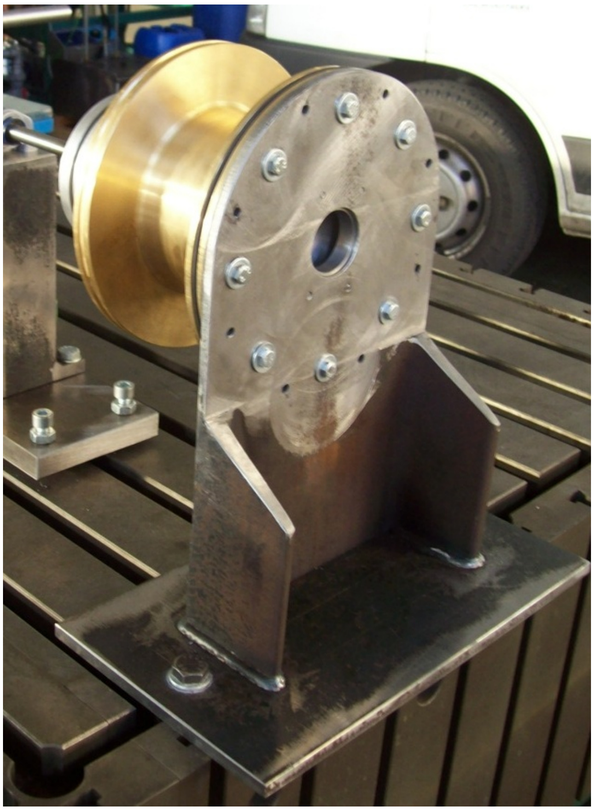

Figure 9.14: Engine support with cylinder attached.

9.4 Thermal barrier - pulse tube

The collector and the piston cylinder are connected by a steel duct. This junction piece has a double function. On one side, it separates the hot from the cold section by leaving an air gap between the collector and the piston cylinder. This creates space to place an insulation material between the hot and the cold part of the engine. On the other, it is an important aspect in changing the engine configuration. The duct can be taken out and replaced by another, changing length, hydraulic radius, free-flow-area, etc., see figure 9.15. It is also possible to place inserts in this section. This allows performing experiments to validate both Tailer's and Organ's claims.

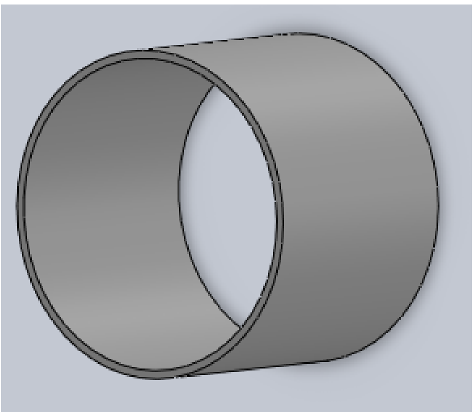

(a) Standard junction piece

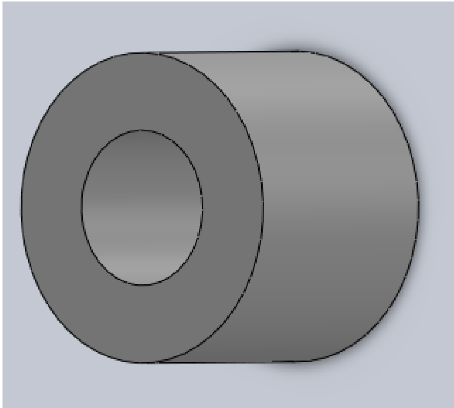

(b) Restricted junction piece

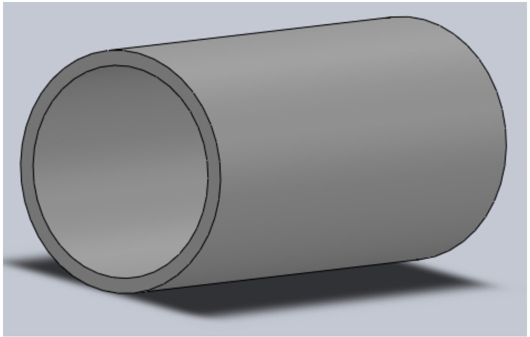

(c) Standard pulse tube

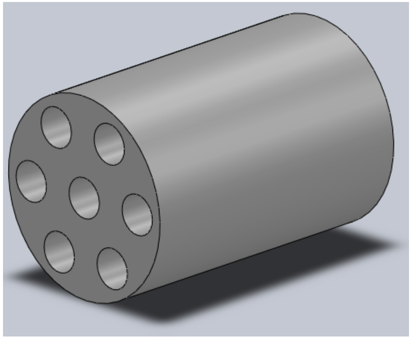

(d) Pulse tube with smaller hydraulic radius

Figure 9.15: Different connecting sections can be used to adopt either Tailer's TLE or Organ's pulse tube TLE.

Long bolts are used to clamp the junction piece in between of the collector and cylinder. These bolts go through blind holes in the collector, bridge the air gap and screw into the engine support, see figure 9.16.

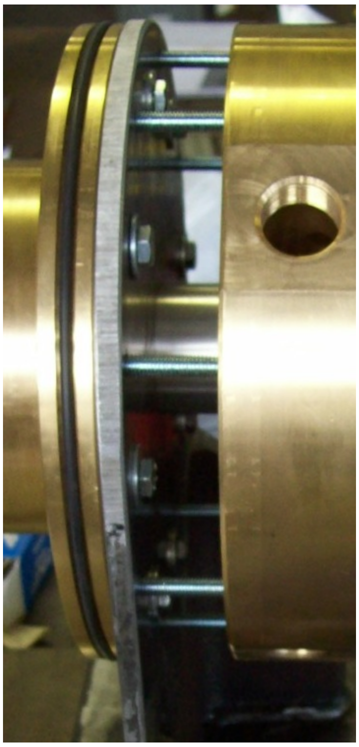

Figure 9.16: Air gap between the hot and cold sections with the junction piece in the middle.

The contact surfaces of the duct with the cylinder and collector are sealed with high temperature resistant Loctite Blue Silicone RTV. The duct is made of steel because of its lower thermal conductivity compared to other metals such as aluminium, copper or brass. The first ring that is used had a length, internal and external diameter of respectively 2.5 cm, 3.8 cm and 4.2 cm. An indication of the maximum heat loss that flows from heater to cooler through this ring can be calculated. Maximum heat loss would occur if the collector and cooler stand at a temperature of respectively 300℃ and 20℃. The thermal conductivity of steel is then evaluated at the average between these two temperatures, 160℃: 48.672 W/mK. The thermal resistance of the steel ring then becomes:

$$R_{ring} = \frac{l}{k_{steel} \times A} = \frac{0.025\ m}{48.672\ W/mK \times \frac{\pi(0.042^2 - 0.038^2)\ m^2}{4}} = 2.0437\ K/W \tag{9.1}$$

The heat loss then becomes:

$$Q_{ring} = \frac{\Delta T}{R_{ring}} = \frac{300°C - 20°C}{2.0437\ K/W} = 137\ W \tag{9.2}$$

This is about 10% of the heat input. For structural reasons, it can not be made thinner however. Therefore, this heat loss must be accepted.

9.5 Piston and piston sealing

For the design of the piston and piston sealing, three options have been investigated.

1. A piston/cylinder combination with very low tolerances and high precision surface finish. No additional sealing method is applied.

2. High precision surface finish and piston or rod sealing with rubber O-rings.

3. A piston with crude tolerances and low precision surface finish adapted to harbor a rolling diaphragm seal.

In first instance, an aluminium piston was designed to fit the brass cylinder with a 25 micron clearance in order to provide sufficient compression and a low leakage rate, see figure 9.17. The cylinder is made of brass because of its high conductivity coefficient, as discussed in the paragraph concerning the cold heat exchanger. The piston, however, is made of aluminium for two reasons. Aluminium is light and it is compatible with brass in terms of sliding friction. Consequently, the piston will not grip in the cylinder due to misalignment and any damage due to contact will be inflicted on the piston and not on the cylinder. Now, because the piston is made of a different material than the cylinder, it is important to know how the radial clearance changes under working conditions (piston head at 120°C). The calculation in appendix F indicates a clearance of 40 micron in a working state. Subsequently, a first test was performed on the rig with a gas flame in direct contact with the inner tubes. After an adequate heating time, the piston was first driven, then left free piston. Although the clearance under working conditions does not differ much from the design value, the compression and sealing proved insufficient. A high leakage rate was observed as well as the absence of gas spring behaviour. Also, the low tolerance piston proved difficult to align and suffered from high friction in the case of misalignment.

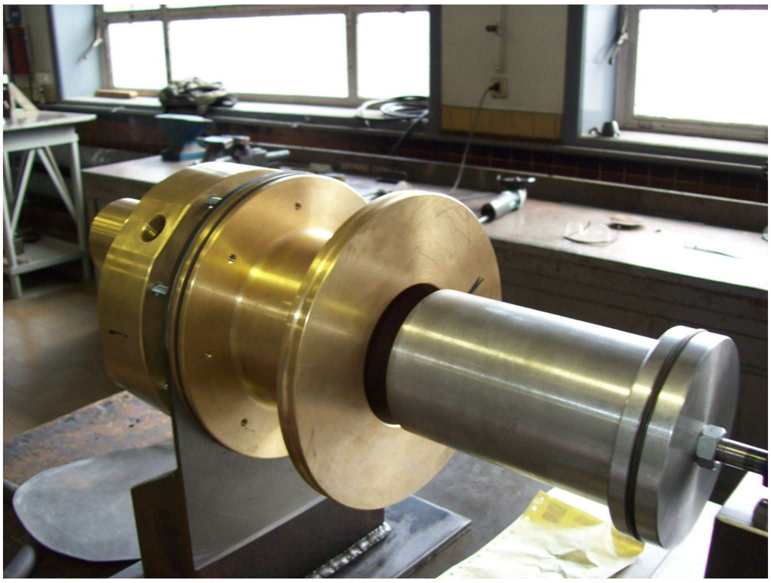

Figure 9.17: First piston: accurately machined to very low tolerances.

In the next step, the option of sealing the piston with a lubricated rubber O-ring was investigated. An O-ring can either be accommodated in a groove on the piston or the cylinder. In the latter case, this type of sealing is referred to as rod sealing. The use of an O-ring can reduce the leakage rate to an acceptable level, but can never eliminate it completely. Also, the rubbing of a ring against the piston or cylinder wall induces excessive wear if lubrication is insufficient. This would greatly increase the initially acceptable leakage rate. And last, the running friction between the O-ring and the wall induces high mechanical losses, even with sufficient lubrication. The calculation in appendix C results in 50 W as an indication of the order of magnitude of the frictional loss. From the disadvantages cited, it can be concluded that the option of an O-ring piston sealing is unsuitable for the application.

In a third step, the use of a rolling diaphragm seal was investigated. A rolling diaphragm seal is made from the combination of an elastomer and a fiber fabric. It allows to hermetically seal the piston while maintaining low friction. Additionally, the implementation of a rolling diaphragm seal allows more liberal machining tolerances, which significantly reduces hardware costs. They are commonly used in applications such as air pressure actuators, process control valves and pressure switches amongst others. With the highest regards to the Marsh-Bellofram corporation, a 'top hat' seal was obtained. This 'top hat' configuration is fit for our application as it allows long strokes, see figure 9.18.

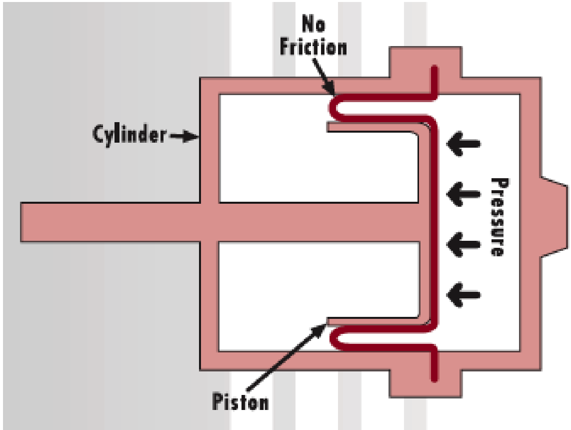

Figure 9.18: Rolling diaphragm seal installed in cylinder.

Although it is advised to keep speed levels under 1 Hz to garantee long life, this seal is the best possible solution that could be obtained in short term. From figure 9.18 it can be understood how a rolling seal works. The pressure in the piston chamber presses the seal against the cylinder wall and piston body. When the piston moves up- or downward, the seal rolls further onto the piston body or cylinder wall and back. Friction is always low, as there is no relative movement between the seal and the walls.

To install the seal, it is first rolled onto the piston body and fixed on the piston head with a curved lip retainer that is bolted on top, as seen in figure 9.19. Once it is fixed, the seal is rolled back upward to form a 180° convolution. The last is step is then to fix the pre-moulded edges between flanges of the cylinder. This piston/cylinder combination can only be used with a single pressure side. If the pressure at the other side becomes higher, or the pressure side is in vacuum, the convolution collapses and the seal is blocked. If, however, a slight over-pressure is maintained at all times, the seal will always be pressed against the walls. With careful installment, proper alignment and good contact of the seal with the walls, the seal provides no leakage and low friction.

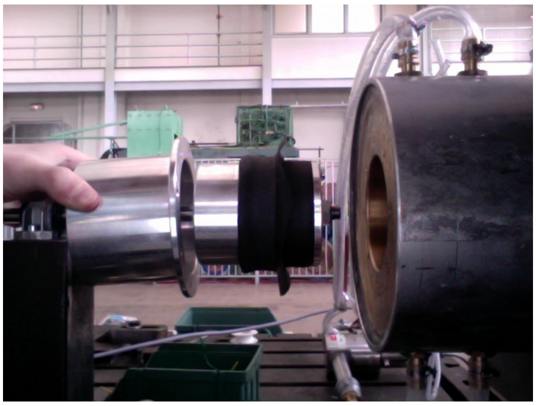

(a) Seal is rolled over the piston body and fixed by the curved lip retainer. Convolution is formed.

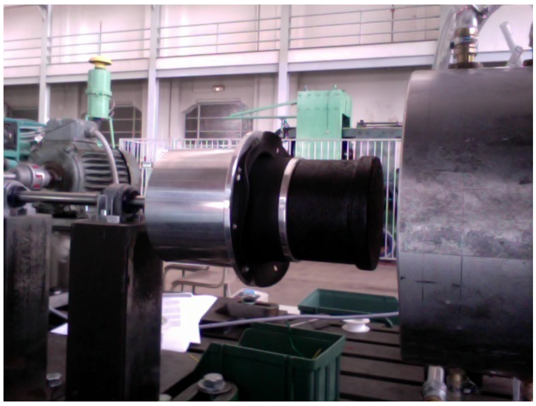

(b) Heat guard is attached to piston head.

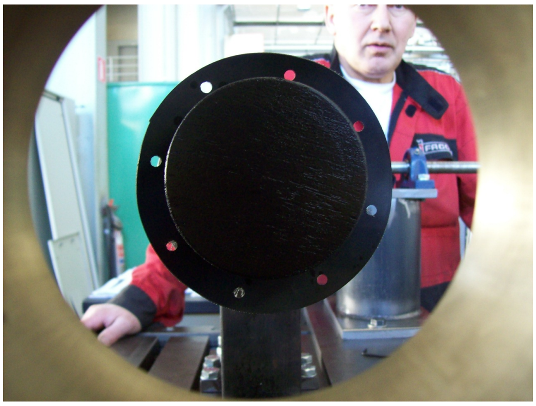

(c)

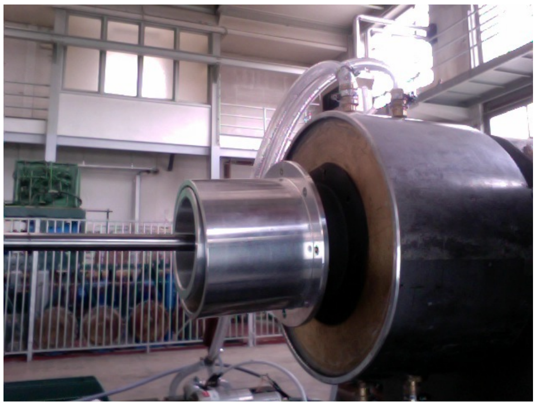

(d) Pre-moulded edges are clamped between the piston cylinder and additional flange.

Figure 9.19: Installation procedure of the rolling diaphragm seal.

In the Bellofram manual[3], it is advised - in terms of proper functioning and wear - to use the rolling seal in down stroke rather than up stroke and to avoid the stroke extremes, see figure 9.20. That is why the cylinder and piston designs were adapted to divide piston stroke lengths equally over the up and down stroke of the seal. To achieve this, a flange was added to prolong the cylinder, support the seal and to provide a means of clamping it against the cylinder.

[3] Marsh Bellofram Rolling Diaphragm Seal manual: http://www.marshbellofram.com/Diaphragm/PDF/designmanual.pdf

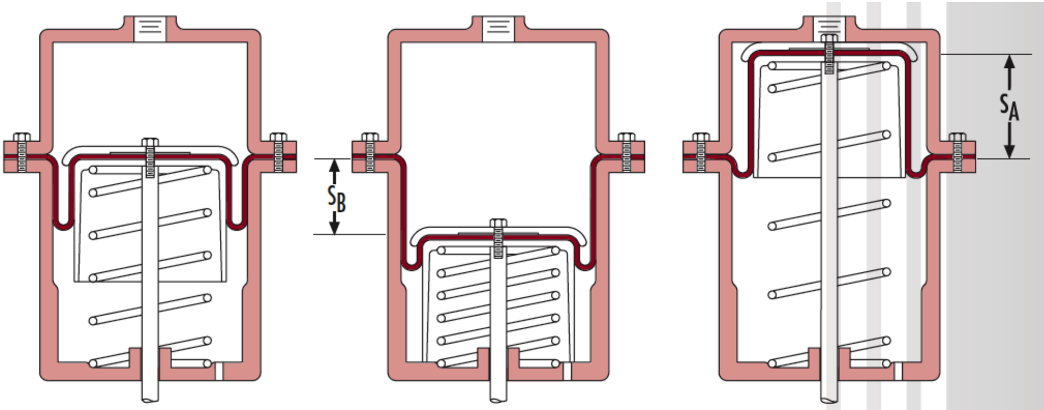

Figure 9.20: Representation of neutral plane (left), down (middle) and up (right) strokes.

The top hat seal, however, has a limited up and down stroke of 7.5 cm. As the cylinder is 10 cm long, this causes a significant increase in dead space. That is why a wooden piece is placed on top of the piston to prolong it. This piece also acts as a heat guard for the seal. It was treated with heat resistant varnish to make it resistant against hot air flowing into the piston chamber. The entire piston set can be seen in figures 9.19 and 9.21

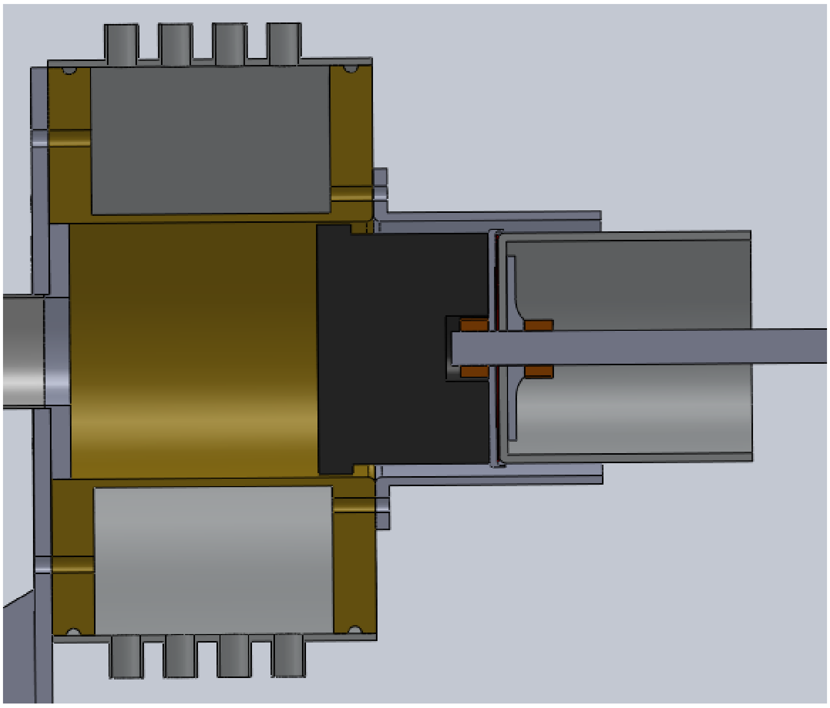

Figure 9.21: Section view of the piston and cylinder design adapted to install a rolling seal.

9.6 Sealing the engine

At the cylinder and piston side, a perfect seal was obtained thanks to the rolling diaphragm seal. At the hot side of the engine, all threaded connections needed to be sealed. Detecting the leaks was done by pressurising the engine with a compressor and spraying the threads with a leak detection soap. The pressure sensors were sealed with copper rings that are pressed between the sensor and wall. The remaining threads were sealed with teflon tape. Even in cold condition, this was insufficient. Consequently, a Loctite threadlocker that was available in the lab was used. In cold condition, sufficient sealing was obtained: a leakage rate of 0.2 bar/h was observed. In the hot state (300°C), all threaded connections leaked again. A new product was selected: Loctite 266[4]. This product is made especially for high temperature applications. The first set of experiments were performed with this sealant. Although the engine sealing proved to be sufficient to do the experiments, the sealant had degraded significantly after the test. The ongoing problems led to the solution of soldering all the threaded connections with silver for the last experiment. Even then, a perfect seal was not attained. It was however not possible to detect the leaks as the tap to pressurise the engine could not be screwed onto the rig anymore.

9.7 Drive mechanism

The piston is connected to a driving mechanism in order to deliver work to a flywheel that can be connected to a load application. In first instance, however, the test engine will be driven by an electrical engine. Overviews of the driving mechanism are shown in figures 9.22 and 9.23.

[4]Loctite 266: http://tds.loctite.com/tds5/docs/266-EN.pdf

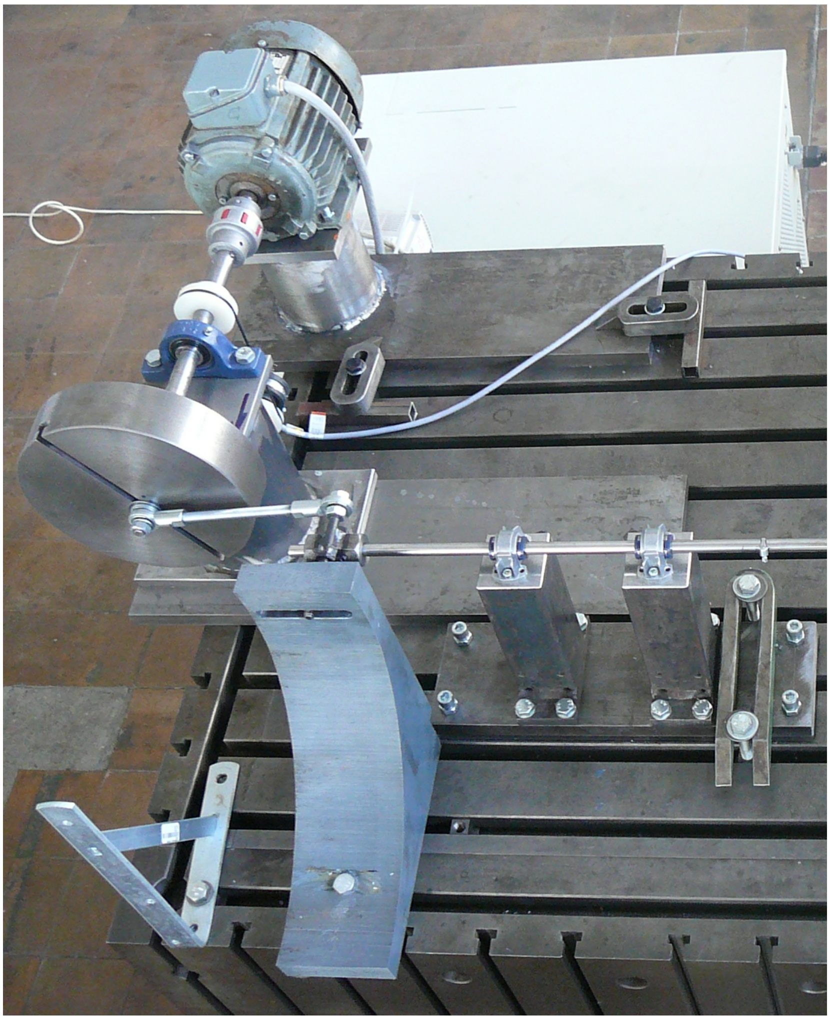

Figure 9.22: Overview of the driving mechanism.

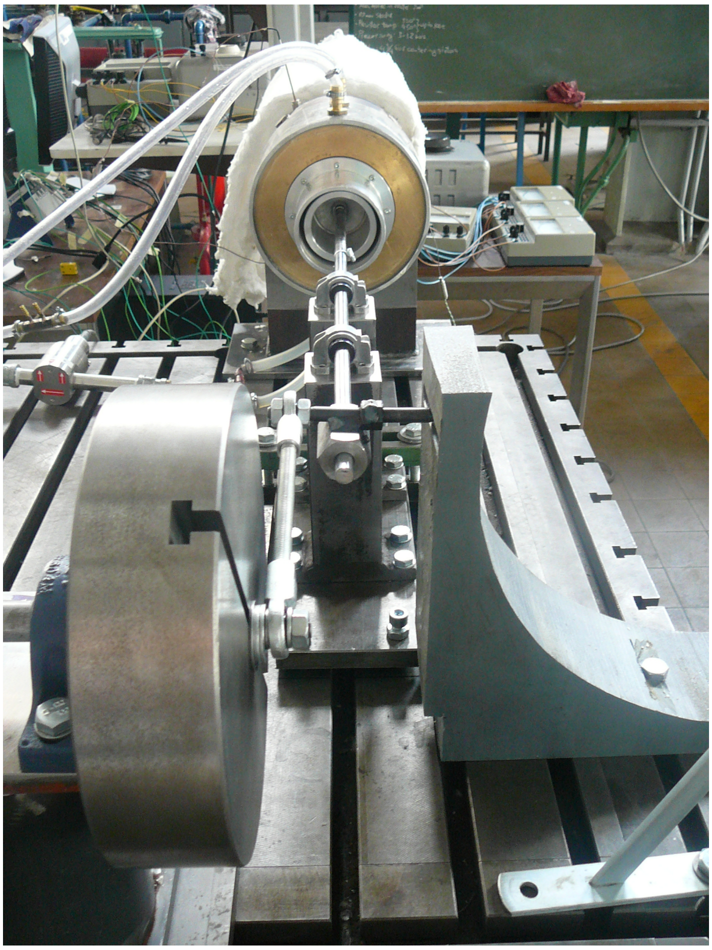

Figure 9.23: Overview of the linear guidance mechanism and connection to the flywheel.

Again, it is important for the well functioning of the rolling seal to properly align the piston with the cylinder shaft. That is why the piston needs to be accurately positioned and fixed onto the piston rod and the rod itself needs to be guided in its linear motion. The piston is hollow and has a blind hole in the middle of its head through which the piston rod extends. The rod is made of hardened stainless steel and is carefully threaded at one end. The piston is attached to the rod by two nuts at either side. Because the threads of mass produced nuts have a very poor finish, a tailored solution is necessary to align the piston with the rod. A disc is screwed onto the rod at the ambient side of the piston. The threads on both the rod and the disc need to be accurately machined in order to maintain a right angle between the rod and the disc. The piston head is then tightened against the large contact surface of the disc to assure a right angle between the rod axis and the piston head, see figures 9.24 and 9.25.

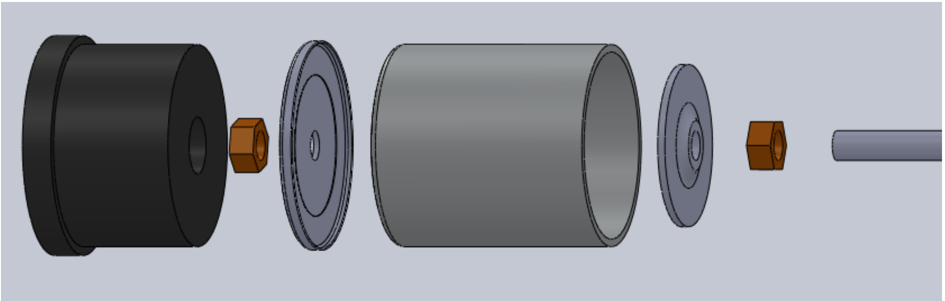

Figure 9.24: The piston is aligned with the piston rod with the use of a carefully machined disc.

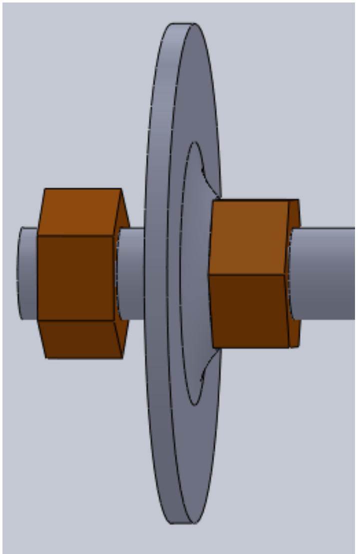

Figure 9.25: The piston is aligned with the piston rod with the use of a carefully machined disc.

The rod itself is guided linearly by two SKF linear ball bearings[5], which are mounted onto a stand, see figure 9.26. The stand is supported by four bolts that can be manipulated to adjust the height of the bearings. This way the piston shaft can be aligned in all directions. Once the desired height is reached, each bolt can be locked by a nut. To align the piston with the cylinder, the low tolerance piston is mounted onto the rod first. The use of the accurately machined piston head allows a far more precise alignment than could be reached with the piston adjusted to the rolling seal. When satisfactory alignment is acquired, the stand is clamped onto the table.

[5]SKF linear ball bearings: SKF LUHR 12

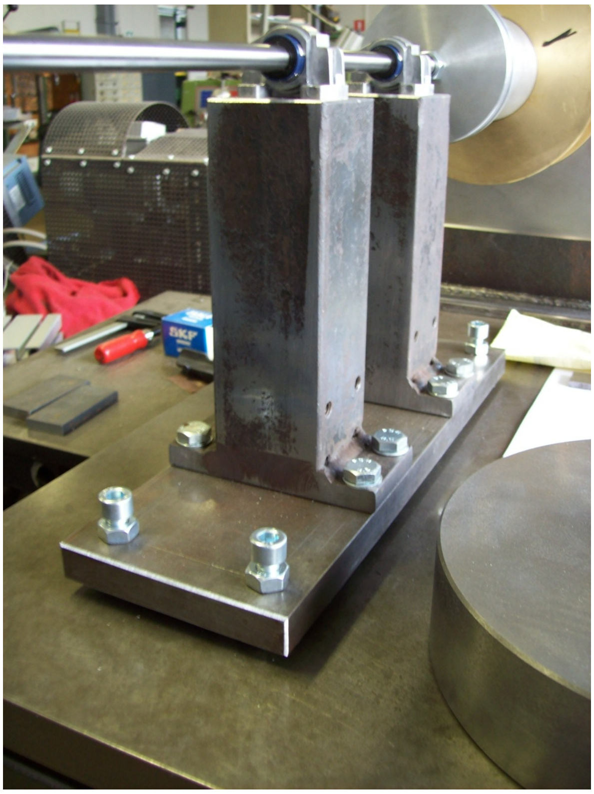

Figure 9.26: Alignment and linear guidance is provided by linear ball bearings mounted on top of an adjustable stand.

The piston rod is connected to the driving shaft, as can be seen in figure 9.27. The position of the connection point is varied using a sliding block that can be fixed onto the rod with two small bolts. It is necessary to vary this position when piston stroke is changed in order to maintain the same amount of dead space at top dead centre.

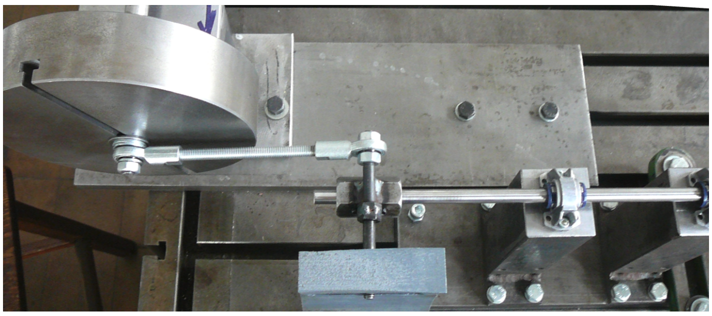

Figure 9.27: An adjustable connection point between piston rod and drive shaft allows variable piston strokes.

The drive shaft is attached to a flywheel with a moment of inertia of 0.0993 $kg\ m^2$. This flywheel has a T-slot over the entire diameter in which the other end of the drive shaft can be attached with a bolt, see figure 9.28. This allows the piston stroke to be varied over a continuous range of 20 cm. The stroke, however, is limited by the rolling seal to a maximum of 14 cm. The flywheel is fixed onto a crankshaft which is supported by two radial ball bearings. For a load calculation and expected bearing life, refer to appendix **??**. The flywheel is attached to the crankshaft with a hub shaft connection[6].

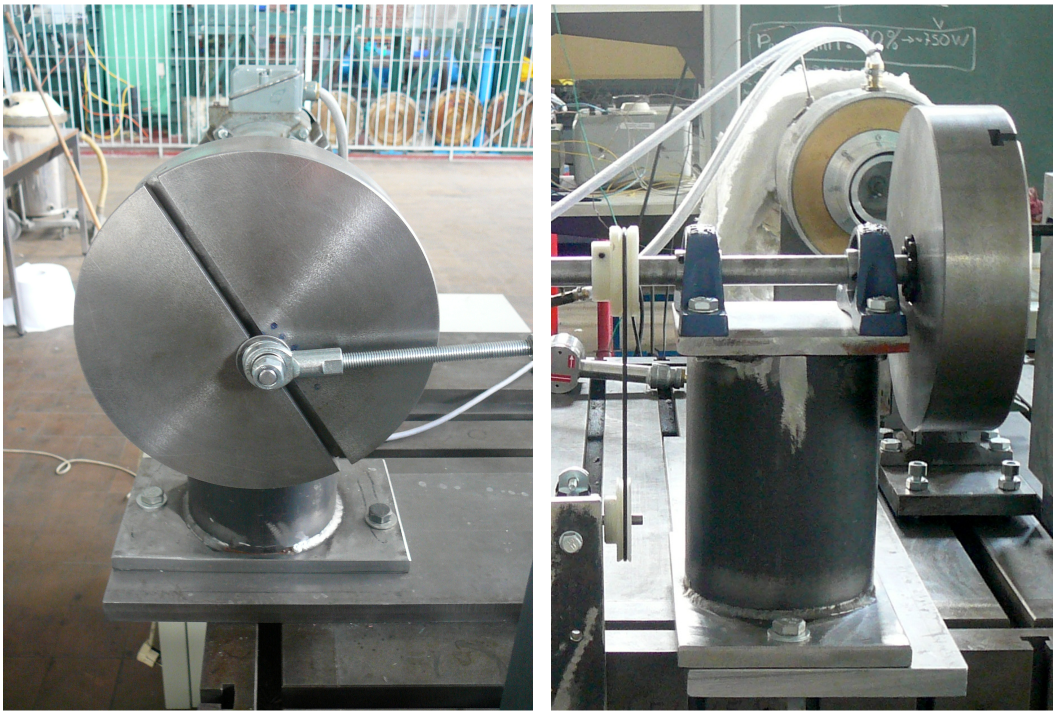

(a) The flywheel with a T-slot provides variable stroke length.

(b) Flywheel and crankshaft are supported by radial ball bearings.

Figure 9.28: Flywheel and radial bearings.

The test engine is driven by a three phase electrical engine with a power output of 750 W, see figure 9.29(a). The engine is mounted onto a stand and coupled to the crank shaft by a standard Rotex^{TM} coupling. Engine frequency is controlled with a T-Verter frequency controller, see figure 9.29(b). Evidently, power output drops significantly with lower frequencies. This might pose a problem when attempting to drive the engine at extremely low frequencies.

[6]Ringfeder Locking Assembly RfN 7012 20x47: http://www.ringfeder.com/

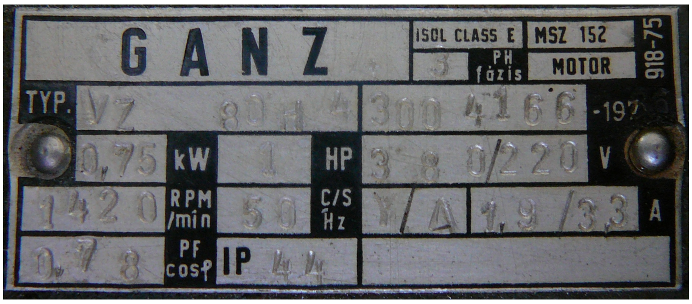

(a) A three phase electrical motor is used to drive the engine in dynamic experiments.

(b) Frequency controller for the electrical engine to perform driven tests.

Figure 9.29: The test engine is driven by a frequency controlled three phase electrical engine.

9.8 Insulation

To minimise heat losses to the surroundings an insulation is provided around the hot part of the engine. A simple rectangular box, made of wood, is placed. It extends over the heater tubes, collector and junction piece. Inside the wooden box, a insulation layer with a 10cm thickness is glued. The insulation material used is Rockwool Rockfit 431. This allows an easy method of obtaining an indication of the heat loss. Each wall has two thermocouples attached to it. One on the inside of the insulation layer and one on the outside. During operation of the engine, all these temperatures are registered. The heat loss through each wall can then be calculated approximately with the following formula:

$$Q_{wall} = \frac{T_{in} - T_{out}}{\frac{wall\ thickness}{k_{rockwool} \times A_{wall}}} \tag{9.3}$$

By summation of all the heat losses through the different walls, a total heat loss to the surroundings can be calculated. This will always be an approximation because of the following reasons:

- A uniform temperature is assumed at both internal and external surface of the wall.
- Corner effects are not considered.

Before building the insulation box, it was necessary to do a preliminary calculation to check if the insulation would be sufficient to minimise heat losses. This is done in appendix D. The resulting heat loss is 52 W. Compared to the total heat input of 1 kW, this represents 5.2%. This is acceptable for the application. Heat transfer between cooler and surroundings is minimised in the following way: Cooling fluid temperature is set at atmospheric temperature and an insulation layer is wrapped around the cylinder. As the temperature gap over this insulation layer is only in the order of a few degrees, this heat loss can be neglected.

What was actually built Due to construction delays, another insulation method was devised. The heater tubes and collector were wrapped directly with an insulation material, see figures 9.30 and 9.31. During the different experiments, the thickness layer was about 10 cm. Heat losses were calculated through convection correlations or through the conduction formula applicable to cylindrical geometries. For the details of these calculations, see chapter 10.

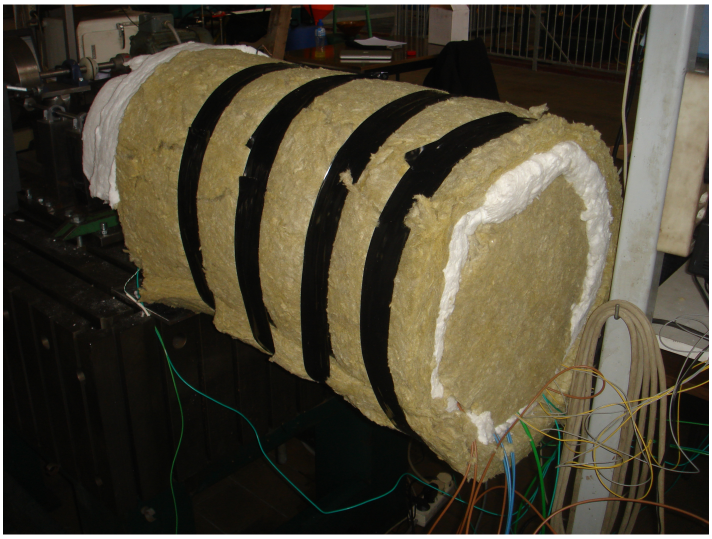

Figure 9.30: Insulation for the second set of experiments

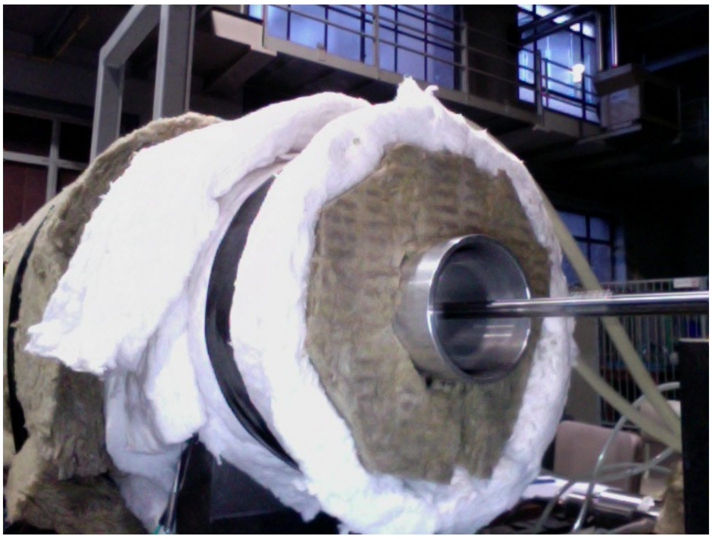

Figure 9.31: Insulation around the water jacket and the rolling seal flange for the second set of experiments.

9.9 Instrumentation

To conduct experiments, several measurements need to be performed. These include pressure, temperature, mass flow, frequency and crank angle. Below is an overview of the instrumentation implemented in the rig.

Table 9.1: Instrumentation general overview

Entity	**Sensor**
Temperature	thermocouple, infrared
Pressure	piezo-electric transducer
Frequency	incremental encoder
Crank angle	incremental encoder
Mass flow	incremental encoder
Electric power input	Wattmeter

9.9.1 Thermocouple

Two types of thermocouples are used in the rig. The first type are K-type Thermocoax thermocouples that are used to perform mean or 'slow' temperature readings. Two thermocouples are positioned at the far end of the heater tubes to monitor resistor temperature. Another one is positioned at the water outlet of the cooling circuit. Cooling fluid temperature and mass flow provide the information to calculate the heat output through the cooler.

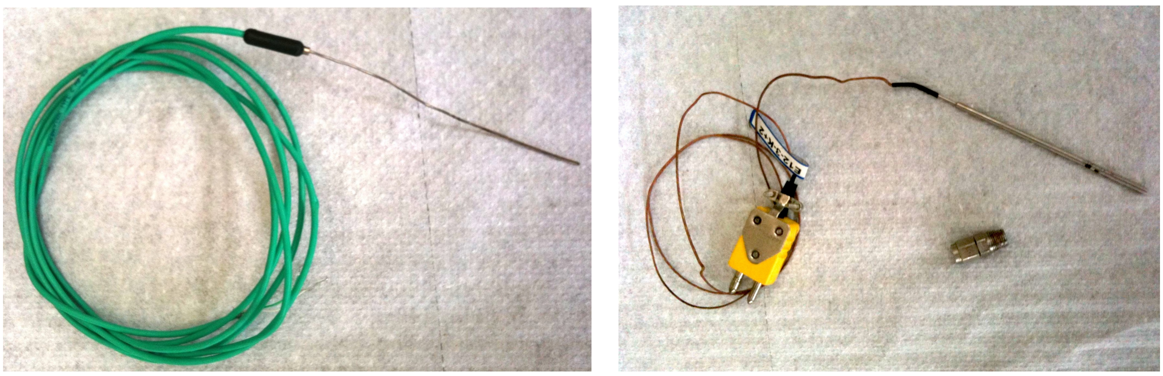

(a) Thermocoax K-type thermocouple (b) Nanmac Eroding Ribbon K-type thermocouple

Figure 9.32: Temperature measurements

The second type of thermocouples are K-type Nanmac Eroding Ribbon thermocouples, which were purchased to perform fast gas temperature measurements. High reaction speeds are required in order to record the temperature cycles at different parts of the engine and to expose the thermal lag effect. Two fast thermocouples are placed on the rig. One of the thermocouples is placed in the cylinder head, the other in the flange of one of the heater tubes. It was uncertain if gas temperature could actually be measured instead of wall temperature. Both thermocouples therefore extended at least 5 mm from the walls. Experience showed, however, that there was no reaction of the fast thermocouples throughout a cycle. A small experiment shed more light on the problem. The Nanmac thermocouples were compared with the more standard Thermocoax thermocouples by submitting both sensors to gas flame pulses simultaneously. The experiment revealed a far superior behaviour of the latter. A fast and accurate response of the Nanmac thermocouple was observed, but only over a temperature range of a few degrees. High temperature differences are not picked up because of the high thermal inertia of the sensor. This, of course, compromises the Nanmac sensors for evaluating the gas temperature cycles. They might be used however to measure the form of the temperature function. This could be interesting as they could show at which point in time the gas temperature in heater and cooler changes. This could reveal the thermal lag effect.

When steady state is reached, a complete temperature profile is to be recorded. This allows the identification of the different heat flows in the engine. Thermocouples give information about the inside of the engine. The temperatures on the outside surfaces are measured optical temperature reader, see fig. 9.33. These readings can, however, only be used as an indication as the measurement is highly dependent of the type of surface (form, roughness, ...) the reader is pointed at.

Figure 9.33: Scanny infrared optical temperature reader

9.9.2 Pressure transducers

Pressure is measured with Kistler piezo-electric pressure transducers. These sensors convert pressure into an electrical charge. This electrical charge is then amplified by a Kistler Charge Amplifier and sent to the data acquisition unit.

Position	**Brand/N°**	**Type**	**SN**	**Calibration factor**$[\frac{pC}{bar}]$
Cylinder	Kistler	701A	639871	81
Heater	AVL	16QP100c	1077	157.21

Table 9.2

Two pressure sensors are implemented in the rig, see table 9.2. One is positioned in the cylinder head, the other in the flange of one of the heater tubes.

Figure 9.34: Kistler 701A and AVL 16QP100c piezo-electric pressure transducers

The sensors cannot withstand high temperatures over a long period of time. Both sensors are therefore connected to the cooling circuit of the piston cylinder. The bypass at the water outlet is placed downstream thermocouple to avoid a systematic error in the heat loss calculations.

Both sensors can only be used to measure relative pressures. A reference is needed to obtain absolute pressures. The absolute pressure sensor from the lab, however, could not be used as there is no means of cooling it. From the experiments we have observed that we never obtained a perfectly sealed engine. The smallest pressure during the cycle was therefore set at ambient pressure.

9.9.3 Encoder

An incremental encoder is linked to the crankshaft by a rubber belt (O-ring) transmission with a 1:1 ratio. It generates two kinds of pulses on parallel output lines to measure frequency (1 pulse/rev) and crank angle (1000 pulses/rev). To identify absolute crank angles, a reference point should be set. For that reason, the frequency pulse was accurately calibrated to coincide with top dead centre of the piston. Experience has learned that the slip of the transmission is to high to ensure a fixed reference point. The crank angle measurement can be related to a volume function. In combination with the pressure measurements, a pV-diagram can be obtained from which indicated power output can be calculated.

Figure 9.35: Transmission between the crankshaft and the encoder.

9.9.4 Cooling power

The flow meter generates pulses to measure mass flow of the cooling liquid (1870 pulses per litre). It is placed in the cooling circuit, downstream of the water jacket outlet but upstream of the bypass that cools the pressure sensors. The inlet water temperature can be set by the external cooler. In the returning flow, another thermocouple was installed. The temperatures of the cooling fluid and the mass flow measurement enable calculation of the amount of heat that is drawn from the engine.

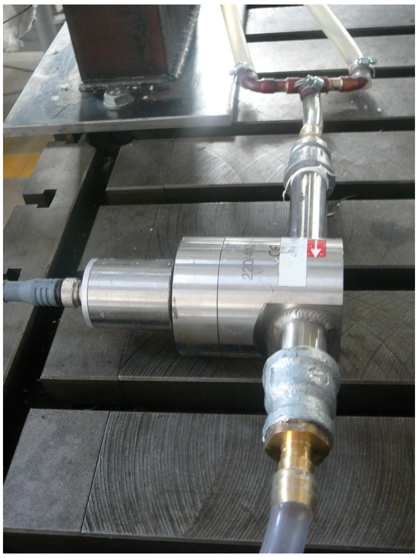

Figure 9.36: The mass flow encoder is installed upstream of the cooling bypass in the return tube.

9.9.5 Resistor control

Heat input is provided by electrical resistors that are connected in parallel to a transformer. Voltage is set manually and heat input is measured by a Watt-meter. On two of the resistors, a thermocouple (Thermocoax) is installed. It provides a monitor to control the resistor temperature. The second thermocouple is redundant.

For the second set of experiments, four additional resistor wires were wrapped around the inner tubes at the collector side. The power input of these extra resistors was controlled by a transformer and measured by volt and ampere meters, see figure 9.37. The resistor wires were connected in parallel. Voltage was measured over the connection points. To measure current, four ampere meters were each connected in one of the parallel resistor wire circuits. Electrical power input was easily calculated by multiplying the product of voltage and mean current by four.

Figure 9.37: Electrical power input of the extra resistor wires is calculated from voltage and current readings.

9.9.6 Data acquisition

The rig is equipped with a variety of sensors. A data acquisition unit[7] was purchased to acquire and preprocess the incoming signals before sending them to the PC 'simultaneously'. Each type of signal is sent to its appropriate module. For an overview of the CompactDAQ modules, see table 9.3 and figure 9.38.

Table 9.3: CompactDAQ modules

To be measured	**Calibration/range**	**Type**
Pressure	$-10 \rightarrow +10\ V$	NI 9205
Temperature	$41 \left[\frac{\mu V}{K}\right]$	NI 9213
Frequency	$1\ \frac{pulse}{revolution}$	NI 9401
Crank angle	$1000\ \frac{pulses}{revolution}$	NI 9401
Mass flow	$1870\ \frac{pulses}{litre}$	NI 9401

After the signals are digitalised by the CompactDAQ, they are read into the PC with a LabVIEW program. The DAQ Assistant modules in the LabVIEW environment were used to perform time based measurements every 20 seconds at a sample rate of 100000 $\frac{samples}{s}$. The data is scaled, written to a text file and projected on the screen.

[7]National Instruments CompactDAQ NI9174

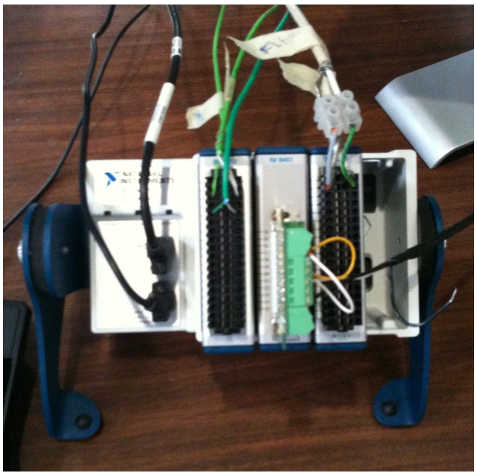

Figure 9.38: CompactDAQ

The sample rate is high in order to have accurate measurements of the cycles. Consequently, the raw data that is written to text files must be processed to allow easy handling of the final data set.

If the engine's frequency is f, there are:

$$X = \frac{100000 \frac{samples}{s}}{f \frac{cycles}{s} 1000 \frac{readings}{cycle}} \tag{9.4}$$

or $\frac{100}{f}$ samples taken for every crank angle in the cycle.

A program was written in MatLab to trim down the raw data to uniform text files. First, three complete cycles are selected from the raw data set based on the encoder pulse (1 pulse per revolution). Second, the X pressure measurements taken for each crank angle are averaged out. This produces a uniform text file containing three cycles divided in a thousand steps each. As automatic identification of maximum pressures (TDC reference) proved difficult to program in MatLab, further processing was done in Office Excel with a reference based on visual inspection. The MatLab code can be found in appendix G.

Part III

Experimental Work

Chapter 10

First Experiment

10.1 Introduction

After pre-experimental testing, all mechanical problems were dealt with and the rig was ready for the first experiments. The main structure that is followed to describe the experiments is:

- *Experimental design*: How is the experiment prepared? What is the setup of the rig? Which measurements are made and why?
- *Results and analysis*: What measurements were obtained? How is the data processed? What are the results?
- *Conclusions*: What can be concluded from the results? Recommendations for the next experiments?

10.2 Remarks and assumptions

10.2.1 Amount of heat transfer area

As results from the literature study, the gas in the heater should behave isothermally. A large heat transfer area is therefore needed. To have an indication of how large this needs to be, the ratio of heat transfer area to displaced volume is calculated for Tailer's and Organ's engine. The ratios are given in table 10.1.

Table 10.1: Ratio of hot heat exchange area to displaced volume.

Tailer	42.2 $\frac{cm^2}{cc}$
Organ	136.3 $\frac{cm^2}{cc}$
Test rig without mesh	1.56 $\frac{cm^2}{cc}$
Test rig with mesh	23.77 $\frac{cm^2}{cc}$

In the current configuration, with only the resistors in the heater tubes, this ratio is 1.56 cm^2 per cc displaced volume.

A steel wire mesh of Bekaert[1] was obtained. The previous considerations and the anticipated time shortage led to the choice of inserting it in the engine for the upcoming experiments. The mesh was delivered in the form of sheets of approximately 6 mm thickness. To help it achieve the mechanical stifness required to be insert it in the heater tubes around the resistors, the following solutions was devised: The mesh was laid onto a thin copper foil and rolled around a bar of 8 mm diameter, the same diameter as the resistors. The bar was then removed and the mesh was inserted in the heater tube. The opening created by the bar, allowed sliding the resistor in. The dimensions of the copper foil and mesh layer are 400 x 400 mm. This adds an additional heat transfer area of 1.21 m^2. The ratio of heat transfer area to displacement volume is now 23.77 cmm^2 per cc of displaced volume.

10.2.2 Cooling power

In our original design, cooling power of the engine would be calculated by measuring water inlet and outlet temperature (T_{in} and T_{out}) and mass flow of the coolant $\dot{m}_{coolant}$. The cooling power would then be calculated from:

$$Q_{out} = \dot{m}_{coolant} \times c_{p,water} \times (T_{out} - T_{in}) \tag{10.1}$$

The cooling water circuit in our experimental rig is driven by a 3 kW integrated cooler that was available in the lab. Even when this cooler was set to provide its minimum mass flow, no temperature difference between water inlet and outlet could be observed during the experiments. The energy balance of the entire engine was thus impossible to obtain. This problem was solved by insulating the hot from the cold section. This way an energy balance of only the hot section could be obtained. The experimental method is explained in more detail in section 10.3.

10.2.3 Driving the engine

Even when the rig was expected to work as an engine and drive another device, an electrical engine was used to drive the piston. This was necessary as it was not sure if the engine would provide a work output under all working conditions. Also, in the cases where the rig behaves as an engine, it is not sure whether it provides enough work to overcome external friction originating from the piston seal, bearings, etc. In those cases the electrical engine only helps to overcome friction losses. The fact that another engine drives the rig creates no problem to observe the work output that the rig delivers. By calculating the indicated work output from the pV-diagram, it can be seen if the rig behaved as an engine or heat pump.

[1]Beckaert Stainless Steel Wire Fiber Web

10.2.4 Problems encountered with TDC referencing

The encoder was selected for two reasons.

- Record absolute crank angle (incremental): 1000 pulses per revolution.
- Provide a reference for TDC: 1 pulse per revolution.

With the use of an oscilloscope, the reference pulse was calibrated to coincide with TDC. The transmission from the crank shaft to the encoder shaft was provided by a belt mechanism. This transmission suffered from slip. The order of magnitude of the slip was low enough to record absolute crank angle with sufficient precision, but the error stacks up over every cycle. It was clear that the TDC reference point was lost at the end of each experiment. Therefore, an assumption was made in order to relate absolute crank angle to the volume function. For every cycle, TDC was referenced to the maximum pressure. This assumption, however, proved difficult to implement in MatLab code so the data processing was performed in two steps. First, the raw data was trimmed down to an averaged out set of three cycles. Then, the first maximum was identified visually and referenced as TDC.

The assumption of identifying maximum pressure with TDC makes sense for the kind of cycles that are being analysed. Because there is no distinct pressure peak, as in internal combustion cycles, it is reasonable to assume that maximum pressure will occur at TDC, when volume is smallest. To have an idea of the uncertainty that this assumption entails, the pV-diagram of the cycle at 7 Hz with an 8 cm stroke is plotted three times in figure 10.1. Apart from the original diagram, two others are plotted with an offset of one degree crank angle in both directions. Notice that this pV-diagram was obtained in the second experiment and it is discussed in section 11.3. There is no significant change in the shape of the cycle to interfere with the interpretation that is given.

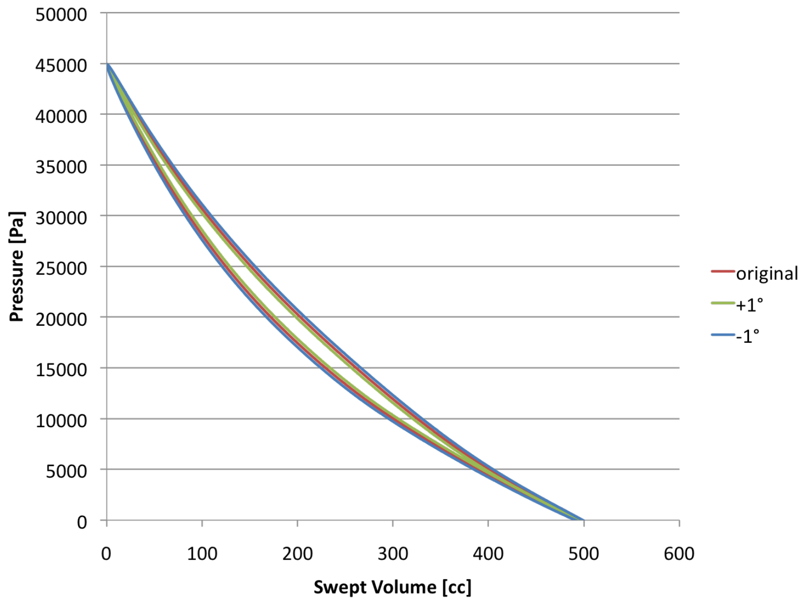

Figure 10.1: Three pV-diagrams of the cycle at 7 Hz with an 8 cm stroke to illustrate the effect of 1° crank angle offset.

10.3 Experimental design

Goals of this experiment The first goal of this experiment was to obtain an insight in the temperature profile and heat fluxes throughout the engine. The second objective was to drive the engine and obtain a first pV-diagram.

Current status of the rig The hot heat exchanger, consisting of heater tubes and collector, was wrapped with a ceramic fiber[2] insulation material. The thickness of this layer was 7.5 cm. The same insulation material was also inserted between the heater tubes and between collector and cylinder to provide a thermal barrier. All the threads were now sealed with the high temperature threadlocker[3], which however had not yet been tested. To have an idea of the absolute pressure of the engine, and an indication of the leakage, the manometer was left screwed in the collector. As discussed in section 10.2.1, the steel wire mesh was inserted in the heater tubes. A representation of the setup can be seen in figure 10.2.

[2] ThermalCeramics Refractory Ceramic Fibre: Cerablanket 128 kg/m^3 - http://www.thermalceramics.com/
[3] Loctite 266: http://tds.loctite.com/tds5/docs/266-EN.pdf

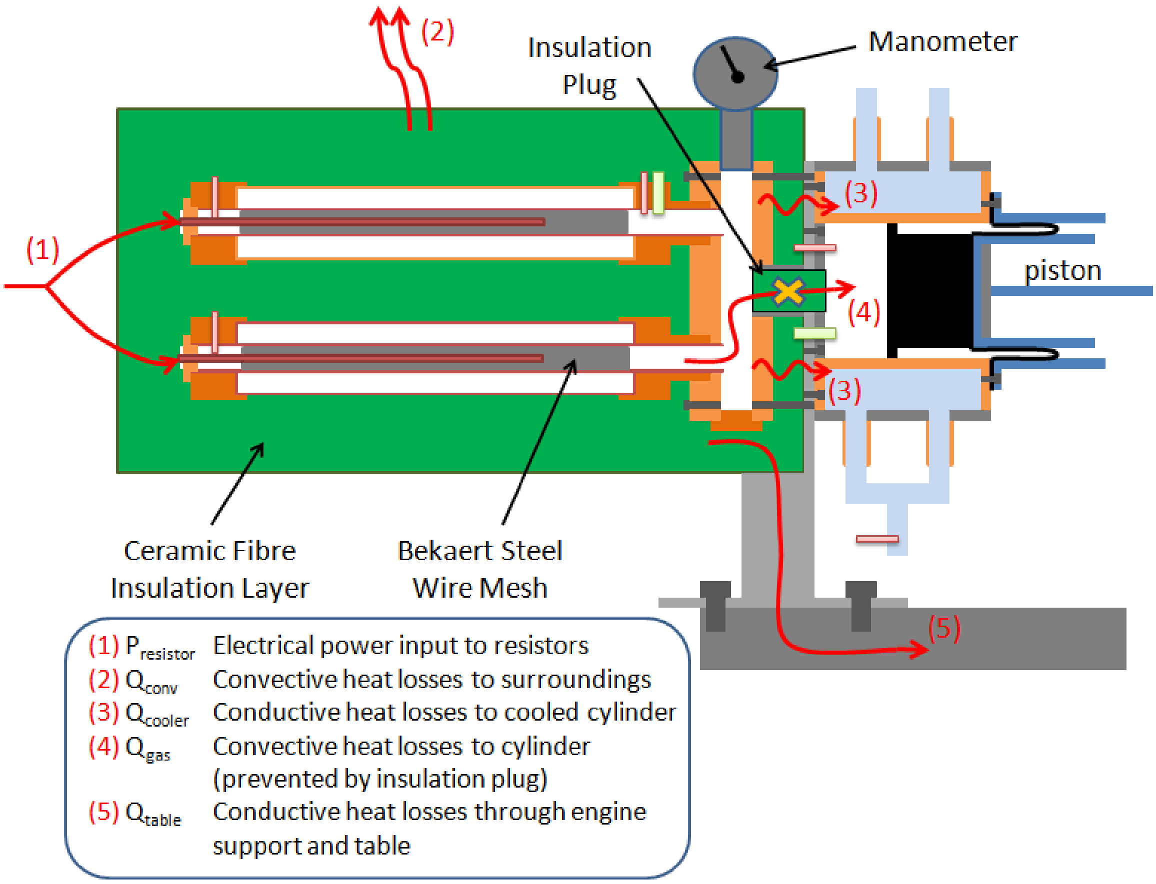

Figure 10.2: Experimental setup and energy fluxes

Experimental method As discussed in section 10.2.2, the setup does not allow the determination of cooling power. To obtain an energy balance of the engine and have an indication of the heat input to the internal gas, a different solution was devised. Basically, the hot section was insulated from the cold section allowing the accurate determination of the energy balance of the hot section alone. To achieve this, the convective heat transfer through the working gas to the cooler, which was impossible to measure or calculate, had to be blocked. This was done by inserting an insulation plug at the entrance of the cylinder, which obstructed the gas path to the cylinder. The piston was set at TDC to prevent the plug from being blown into the cylinder during the warm up of the engine. Heat transfer from the hot to the cold section was now completely conductive and could be accurately calculated by measuring the temperature difference across the interface. The energy fluxes that exist in the engine and needed to be determined are also shown in figure 10.2. The electrical power input to the resistors was known directly from a Watt meter. An indication of the remaining energy fluxes could be calculated by measuring the appropriate temperatures throughout the engine, which can be seen in figure 10.3. These temperatures were measured using an infrared thermometer.

To reach the temperatures between the cylinder and collector that are covered by insulation material, an insulation piece was made that could be taken out. This way, during operation, this piece could be removed quickly to measure the needed temperatures. The infrared thermometer is accurate up to 1°C. One must also be aware that these measurements were highly dependable of the surface form and roughness. The results must thus merely be seen as an indication of the true temperatures.

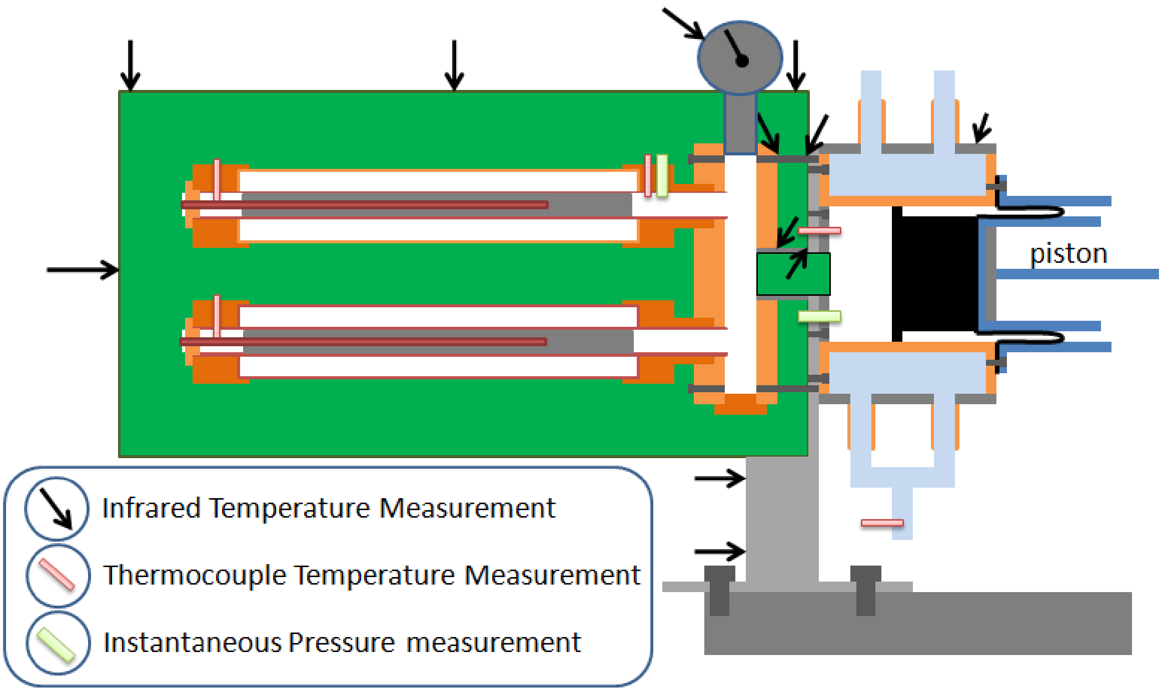

Figure 10.3: Temperature measurements that were performed

After determining the static energy fluxes, the insulation plug was removed and the piston driven. As the gas path provided an additional heat transfer branch, see figure 10.4, an additional heat input was needed to keep resistor temperatures at 300°C. By assuming that all energy fluxes determined in static state stayed the same, this additional heat input can be attributed to the working gas flow in the engine.

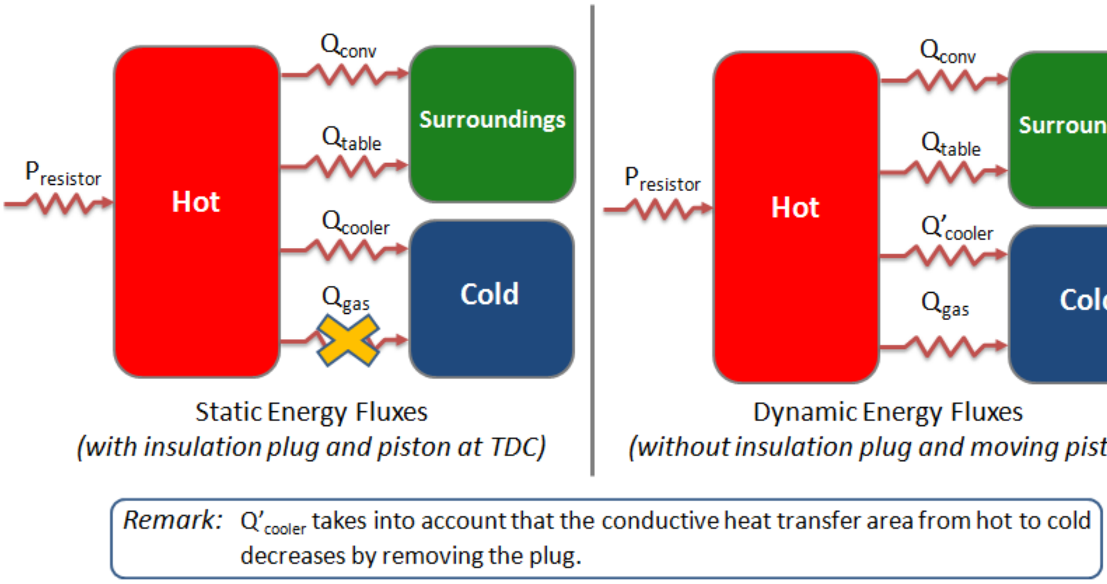

Figure 10.4: Experimental Setup and Energy Fluxes

During the first dynamic test, pressure and crank angle readings were performed. This allowed determining the pV-diagrams of the thermodynamic cycle. The piston stroke and cooling circuit temperature were set at respectively 5.5 cm and 15°C. Two engine frequencies were evaluated: 5 Hz and 3.2 Hz. In each of the two working states, heat input to the resistors was adjusted so that the resistor temperature did not exceed 300°C.

10.4 Energy balance: results and analysis

Warm up to steady state The warm up started with a power input of 500 W. To retain the structural strength of the Loctite threadlocker, the highest temperature of the engine was kept beneath 300°C. Therefore, attention was given to both thermocouples that registered the resistor temperatures. As soon as they rose above 300°C, power input was reduced. The temperatures throughout the engine were measured every 20 seconds to be able to control if steady state had been obtained. After 3.5 hours, the thermocouple close to the collector was only about 75°C and still rising slowly. To speed up the process, some of the insulation under the collector was removed and the collector was heated up with a gas burner. As soon as the collector reached 100°C, the gas burner was removed and the insulation restored. It was observed that collector temperature dropped down and then oscillated for a while around steady state, 85°C. At that point, the electrical power input was 130 W. Now, all temperature measurements shown in figure 10.3 were performed. With those temperatures, the occurring energy fluxes described in figure 10.2 were determined. These calculations can be seen in the following sections.

10.4.1 Convective heat losses to the surroundings Q_{conv}

This is the convective heat lost to the atmosphere. The heater, wrapped with an insulation layer, formed a cylindrical shape with a diameter of 0.28 m and a length of 0.655 m. Both radial and axial heat losses occured, see figure 10.5. The manometer was screwed in the collector and could not be covered by the insulation. This created an additional convective heat loss to the atmosphere.

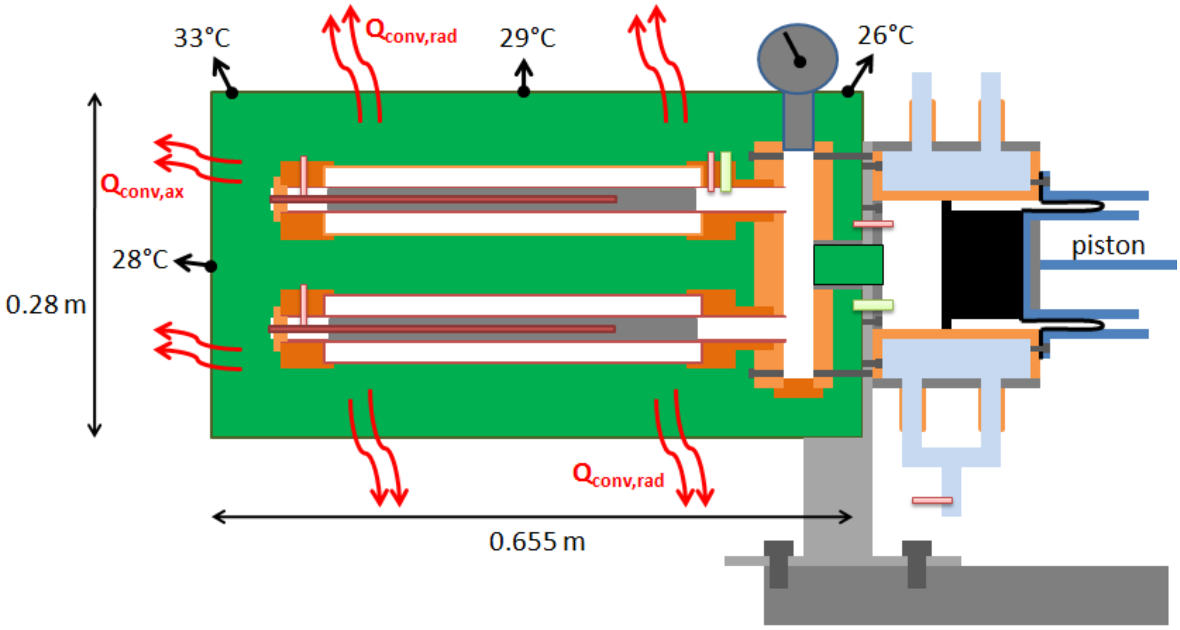

Figure 10.5: Convective heat Losses

$Q_{conv,rad}$ The radial convective heat losses were calculated with the correlation of Churchill and Chu for 'natural convection from a horizontal cylinder', which is applicable over the range $10^{-5} < Ra_D < 10^{12}$ [29]:

$$Nu_D = \left(0.60 + \frac{0.387\ Ra_D^{1/6})}{\left[1 + (0.559/Pr)^{9/16}\right]^{8/27}}\right)^2 = \frac{h \times D}{k_f} \tag{10.2}$$

For this correlation, fluidum properties should be evaluated at the film temperature $T_f = (T_s + T_\infty)/2$. T_∞ was equal to 25°C, the atmospheric temperature during the experiment. There was a temperature gradient on the cylindrical surface along its axis. The whole surface was assumed to stand at the mean temperature: $T_s = (33°C + 26°C)/2 = 29.5°C$. Therefore air properties were evaluated at $T_f = (29.5°C + 25°C)/2 = 27.25°C$:

- Expansion coefficient $\beta = 3.3466 \times 10^{-3}\ /K$
- Kinematic viscosity $\nu = 15.784 \times 10^{-6}\ m^2/s$

- Thermal conductivity $k_f = 0.026208\ W/mK$
- Prandtl number $Pr = 0.71228$

The diameter of the cylinder D = 0.28 m. This gives a Rayleigh number of:

$$\begin{aligned} Ra_D &= Gr_D \times Pr \\ &= \frac{g\ \beta\ (T_s - T_\infty)\ D^3}{\nu^2} \times Pr \\ &= 0.92721 \times 10^7 \end{aligned} \tag{10.3}$$

This lies within the applicable range of the used correlation. The correlation gives a a Nusselt number $Nu_D = 27.645$ and a convection coefficient $h = 2.588\ W/m^2$. The resulting radial heat loss becomes:

$$\begin{aligned} Q_{conv,rad} &= h \times A \times (T_s - T_\infty) \\ &= 2.588\ W/m^2K \times (\pi\ 0.28\ m\ 0.655\ m) \times (29.5°C - 25°C) \\ &= 6.71\ W \end{aligned} \tag{10.4}$$

$Q_{conv,ax}$ The axial convective heat losses were calculated with the correlation of Churchill and Chu for natural convection from a vertical plate [29]:

$$Nu_L = \left(0.825 + \frac{0.387\ Ra_L^{1/6})}{\left[1 + (0.429/Pr)^{9/16}\right]^{8/27}}\right)^2 = \frac{h \times L}{k_f} \tag{10.5}$$

The whole surface was assumed to stand at a uniform temperature of 28℃. Air properties must thus be evaluated at $T_f = (25°C + 28°C)/2 = 26.5°C$:

- Expansion Coefficient $\beta = 3.3553 \times 10^{-3}\ /K$
- Kinematic Viscosity $\nu = 15.715 \times 10^{-6}\ m^2/s$
- Thermal Conductivity $k_f = 0.026155\ W/mK$
- Prandtl Number $Pr = 0.71235$

The height of the vertical plate L is set equal to the cylinder diameter D. The Rayleigh number becomes:

$$\begin{aligned} Ra_L &= Gr_L \times Pr \\ &= \frac{g\ \beta\ (T_s - T_\infty)\ L^3}{\nu^2} \times Pr \\ &= 0.62478 \times 10^7 \end{aligned} \tag{10.6}$$

The correlation gives a Nusselt number $Nu_L = 27.341$ and a convection coefficient $h = 2.554\ W/m^2$. The resulting axial heat loss becomes:

$$\begin{aligned} Q_{conv,ax} &= h \times A \times (T_s - T_\infty) \\ &= 2.588\ W/m^2K \times \left(\frac{\pi\ (0.28\ m)^2}{4} \right) \times (28°C - 25°C) \\ &= 0.47\ W \end{aligned} \tag{10.7}$$

$Q_{manometer}$ The manometer has the shape of a short horizontal cylinder. Therefore, the convective losses could be estimated by using the same correlations that were used for $Q_{conv,rad}$ and $Q_{conv,ax}$. The diameter and length of the manometer were respectively 10 cm and 4.5 cm. Its temperature during the experiment was 52°C. The air properties, needed for the correlations, must thus be evaluated at $T_f = (52°C + 25°C)/2 = 38.5°C$:

- Expansion coefficient $\beta = 3.2173 \times 10^{-3}\ /K$
- Kinematic viscosity $\nu = 16.831 \times 10^{-6}\ m^2/s$
- Thermal conductivity $k_f = 0.026995\ W/mK$
- Prandtl number $Pr = 0.71108$

The same calculations as above could be used. The radial heat loss was 1.86 W and the axial heat loss was 1.16 W. This gives a total convective heat loss from the manometer of (the factor 2 accounts for the two end surfaces):

$$Q_{conv,mano} = 1.86\ W + 2 \times 1.16\ W = 4.18\ W \tag{10.8}$$

Total convective heat losses to surrounding atmosphere The total convective heat losses to the surroundings thus were:

$$\begin{aligned} Q_{conv} &= Q_{conv,rad} + Q_{conv,ax} + Q_{conv,mano} \\ &= 6.71\ W + 0.472\ W + 4.18\ W \\ &= 11.36\ W \end{aligned} \tag{10.9}$$

10.4.2 Conductive heat losses to the cooled cylinder Q_{cooler}

With the insulation plug inserted at the entrance of the cylinder, all heat losses from collector to cooled cylinder were conductive. The gap between collector and cylinder is 2.5 cm. Heat could pass through the insulation material, the steel ring that leads to the cylinder and through the 8 steel bolts that hold collector and cylinder together, see figure 10.6.

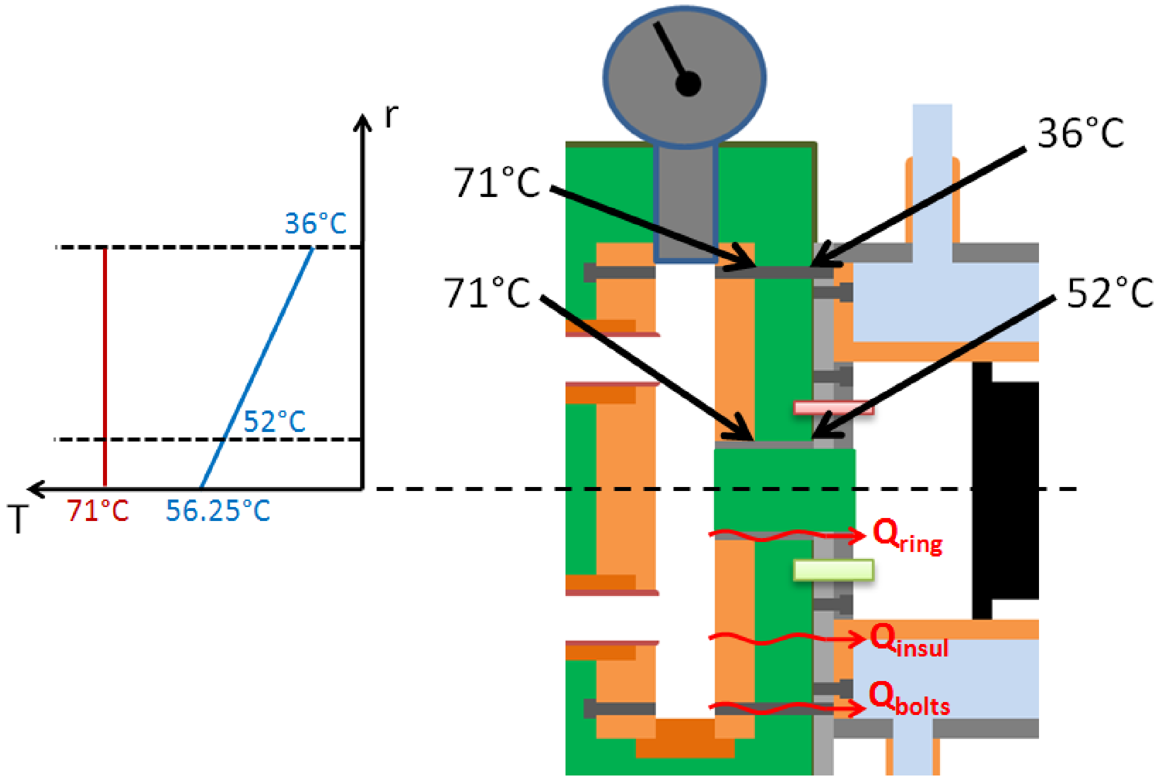

Figure 10.6: Conductive heat losses to cooled cylinder

Q_{insul} Apart from the ring and bolts, the entire gap between collector and cylinder was filled with the ceramic fiber insulation material. This has a thermal conductivity of 0.06 W/mK. The temperature of the collector was uniform, $T_{collector} = 71°C$. For the cylinder, a linear temperature profile was assumed in the radial direction, see figure 10.6. Thus:

- $T_{collector} = 71°C$
- $T_{cylinder}(r) = 52°C - 202.53°C/m \times r$
- $R_{thermal}(r) = \frac{l}{k_{insul} \times A} = \frac{0.025\ m}{0.06\ W/mK \times 2\ \pi\ r\ dr}$

With these considerations, Q_{insul} could be calculated:

$$\begin{aligned} Q_{insul} &= \int_0^R \frac{T_{collector} - T_{cylinder}(r)}{R_{thermal}(r)} \\ &= \int_0^{0.1\ m} \frac{71°C - 52°C + 202.53°C/m \times r}{\frac{0.025\ m}{0.06\ W/mK}} 2\ \pi\ r\ dr \\ &= 2.13\ W \end{aligned} \tag{10.10}$$

In this calculation, the area of the insulation was slightly overestimated as the area of the bolts and ring was included as well.

Q_{ring} The steel ring had an inner and outer diameter of respectively 3.8 cm and 4.2 cm. The length is the same as the gap between collector and cylinder: 2.5 cm. The temperature difference over the ring was 71°C - 52°C = 19°C. The thermal conductivity of steel, evaluated at the mean temperature of 61.5°C, was 51.95 W/mK. The heat loss through the ring was thus:

$$\begin{aligned} Q_{ring} &= \frac{\Delta T}{R_{ring}} \\ &= \frac{71°C - 52°C}{\frac{0.025\ m}{51.95\ W/mK \times \pi (0.042^2 - 0.038^2) m^2/4}} \\ &= 9.92\ W \end{aligned} \tag{10.11}$$

Q_{bolts} There are 8 M8 bolts which are made out of steel. The temperature difference over the bolts was 71°C - 36°C = 35°C. The thermal conductivity of these steel bolts, evaluated at the mean temperature of 54°C, was 52.20 W/mK. The heat loss through the bolts was thus:

$$\begin{aligned} Q_{bolts} &= \frac{\Delta T}{R_{bolts}} \\ &= \frac{71°C - 36°C}{\frac{0.025\ m}{52.20\ W/mK \times 8 \times \pi (0.008\ m)^2/4}} \\ &= 29.39\ W \end{aligned} \tag{10.12}$$

Total conductive heat losses to cooled cylinder The summation of these three losses forms Q_{cooler}:

$$\begin{aligned} Q_{cooler} &= Q_{insul} + Q_{ring} + Q_{bolts} \\ &= 2.13\ W + 9.92\ W + 29.39\ W \\ &= 41.44\ W \end{aligned} \tag{10.13}$$

10.4.3 Conductive heat losses through table Q_{table}

The conductive heat loss to the table passes through the engine support. Two temperatures were measured to obtain an indication of this heat loss, see figure 10.7. As both temperature readings gave approximately the same value, it could be concluded that no significant heat was lost through the table. This result makes sense as the engine support is fixed to the cooled cylinder. The heat was therefore rather drawn into the cooler than through the table.

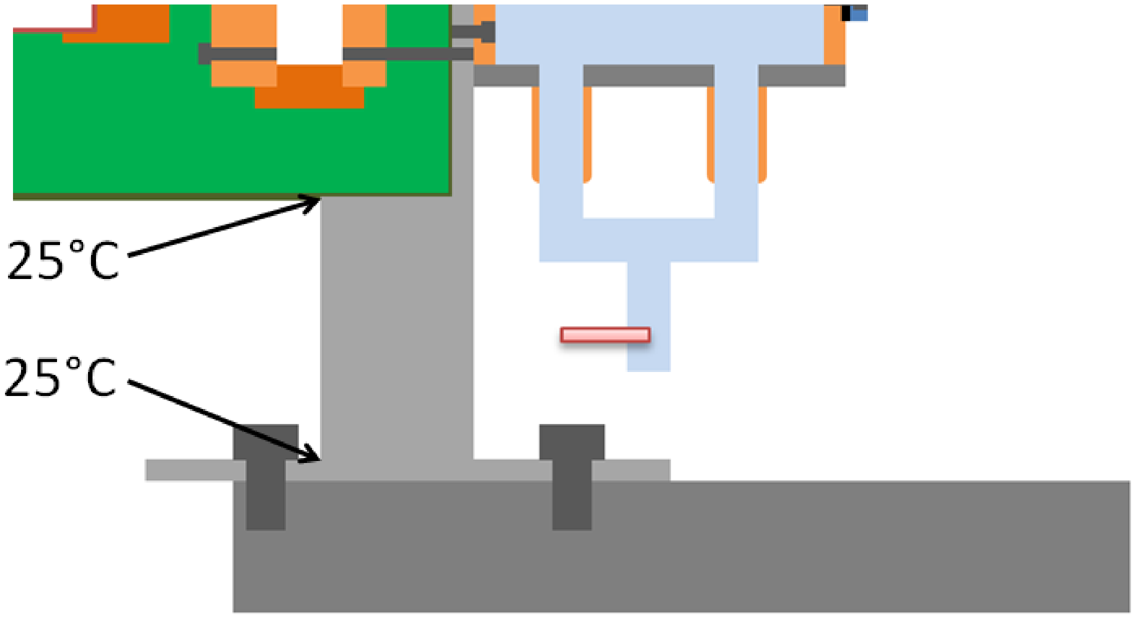

Figure 10.7: Conductive heat losses to table

Static energy balance From the previous sections, the total energy balance of the hot section could be written:

$$P_{resistor} = Q_{conv} + Q_{cooler} + Q_{table} + Q_{closure} \tag{10.14}$$

$$130\ W = 11.36\ W + 41.44\ W + 0\ W + Q_{closure} \tag{10.15}$$

This means that $Q_{closure} = 77.2\ W$. In the ideal case $Q_{closure}$ should only include the heat carried away by the cooling circuit of the pressure sensors, as this was the only heat loss that is not accounted for. It seems unlikely, however, that such a great amount of heat was carried away by the cooling of the sensors. There are several possible reasons why $Q_{closure}$ is so large:

- There were gaps in the insulation through which additional heat was lost.
- The temperature readings were very different from the true temperatures because of the accuracy of the infrared thermocouple.
- The correlations to estimate the convective heat losses are not perfect. There is always an error compared to the real heat loss.

10.4.4 Dynamic tests

After achieving steady state, the insulation plug at the cylinder entrance was removed and the engine was driven with a 5.5 cm stroke at 3.2 Hz and 5 Hz. To keep the resistor temperatures at 300°C an additional heat input to the resistors was required. Heat input could go up from 130 W to 150 W. After waiting some time to achieve steady state, the measured temperatures were checked again. They did not differ much from our initial readings. This verified our assumption that the energy fluxes in a static state stayed approximately the same when the engine was driven. Referring to figure 10.4, the energy balance of the hot section becomes:

$$P_{resistor} = Q_{conv} + Q'_{cooler} + Q_{table} + Q_{closure} + Q_{gas} \tag{10.16}$$

$$150\ W = 11.36\ W + Q'_{cooler} + 0\ W + 77.2\ W + Q_{gas} \tag{10.17}$$

The conductive heat losses to the cooler have decreased as the area was reduced by removal of the plug. The integral of equation (10.10), could be re-used but with adjusted integration borders. The integration should start at the outside diameter of the steel ring.

$$\begin{aligned} Q'_{insul} &= \int_{r_{ring}}^{R} \frac{T_{collector} - T_{cylinder}(r)}{R_{thermal}(r)} \\ &= \int_{0.021\ m}^{0.1\ m} \frac{71°C - 52°C + 202.53°C/m \times r}{\frac{0.025\ m}{0.06\ W/mK}} 2\ \pi\ r\ dr \\ &= 2.07\ W \end{aligned} \tag{10.18}$$

This means that:

$$\begin{aligned} Q'_{cooler} &= Q_{insul} + Q_{ring} + Q_{bolts} \\ &= 2.07\ W + 9.92\ W + 29.39\ W \\ &= 41.38\ W \end{aligned} \tag{10.19}$$

From equation 10.16, the heat that left the heater through the gas path could be calculated:

$$\begin{aligned} Q_{gas} &= 150\ W - 11.36\ W - 41.38\ W - 0\ W - 77.2\ W \\ &= 20.06\ W \end{aligned} \tag{10.20}$$

As is evident from previous considerations, this value is an indication of the heat input that was delivered to the gas during the dynamic testing. During the two working situations, pV-diagrams were obtained as well. These will be discussed in the following sections.

10.5 pV-diagrams: results and analysis

10.5.1 5 Hz

Remark: The pressures shown on the pV-diagrams are relative. As the engine was leaking during the tests, it was assumed that the lowest pressure during the cycle is equal to atmospheric pressure.

A pV-diagram of the cycle at 5 Hz with a 5.5 cm stroke is shown in figure 10.8. Expansion curves are always presented in red, compression curves in blue. Looking at top dead centre

(TDC), it can be seen that the expansion curve maps the compression curve (a). This indicates that the heater had an insufficient rate of heat transfer. The cycle is going too fast to allow the heater to deliver heat to the gas. If the heater were fast enough, pressure would rise at TDC, lifting the expansion line over the compression line and thus opening up the cycle.

At the end of the expansion, the curve tends to bend downward (b). Cooling has increased towards bottom dead centre (BDC), making pressure drop. At the beginning of the compression stroke, cooling continues due to the thermal inertia of the gas. As cooling becomes maximised after BDC, the trend of lowered pressure carries on along the compression line, creating a 'belly' that opens up the cycle (c). Compression occurs at a lower mean pressure than expansion.

This pV-diagram represents a motor cycle, because the compression line is drawn sufficiently beneath the expansion line due to cooling. It has an indicated work output of 0.06 J. At 5 Hz the indicated power output is of 0.309 W with an error of 0.232 W. For a more in-depth error analysis, see appendix E. The high error value should be put into context. The error on the cycles will always be of the same order of magnitude because of the accuracy of the sensors. Once the cycles start producing more work, the error will become small relative to the calculated work and power. To decrease the error at this stage, more accurate pressure sensors and an encoder of higher precision should be used.

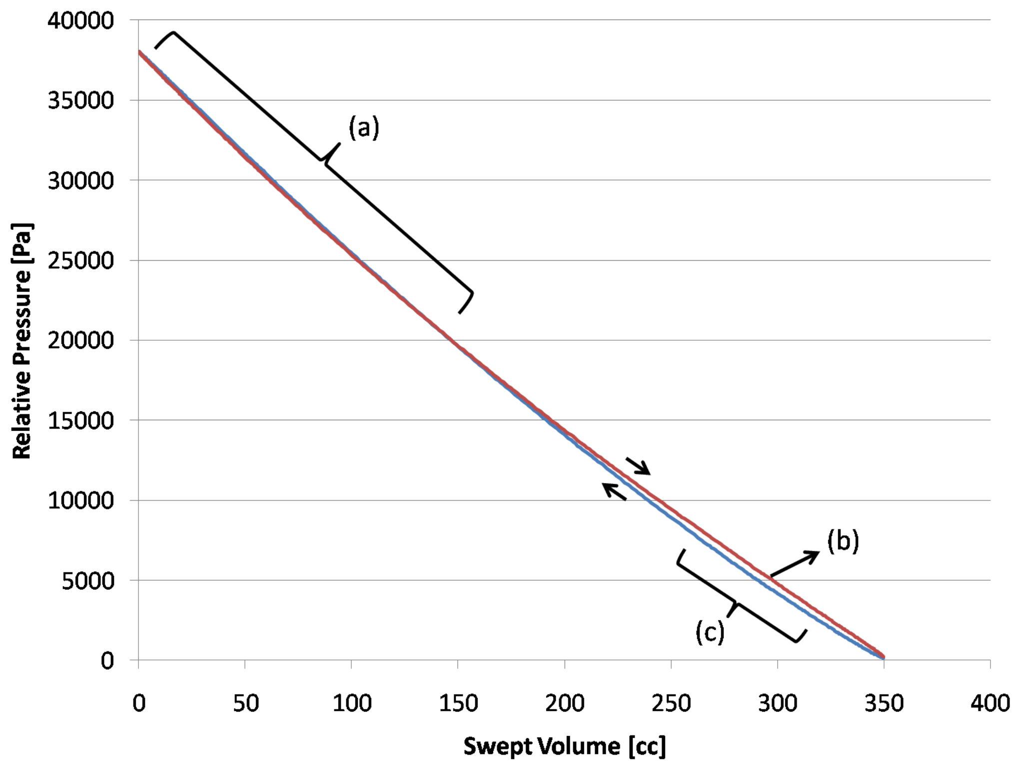

Figure 10.8: pV-diagram of the cycle at 5 Hz, 5.5 cm stroke and 15℃ cooler temperature (red = expansion, blue = compression)

10.5.2 3.2 Hz

When frequency was reduced to 3.2 Hz, it is evident that heater and cooler had more time to exchange heat with the gas. However, the limited flywheel inertia had an influence as well. Crankshaft speed was higher during expansion than during compression. This effect is more pronounced at lower frequencies as the kinetic energy buffer, provided by the flywheel, is smaller. This can be seen by comparing figure 10.10(a) and 10.10(b) in which expansion and compression are respectively marked as red and blue. In the 3.2 Hz cycle compression is given more time relative to expansion than in the 5 Hz cycle. We can thus conclude that at a lower frequency, the heat exchangers have more time to exchange heat with the gas, but this effect is stronger for compression than for expansion.

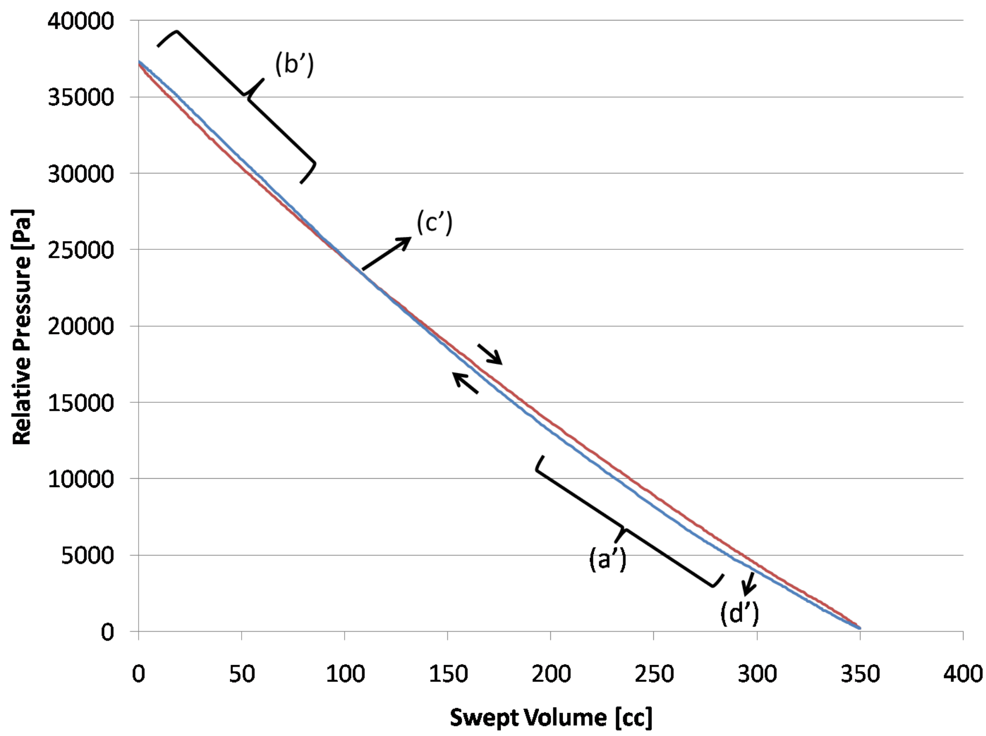

Figure 10.9: pV-diagram of the cycle at 3.2 Hz, 5.5 cm stroke and 15°C cooler temperature

The pV-diagram at 3.2 Hz is shown in figure 10.9. The same cooling effect is observed. Because the cycle is going slower than in the previous case, there is more time to cool the gas and the belly of the compression line opens up more (a'). More time is given for the gas to cool down, but also to heat up. Toward the end of the compression stroke, the gas is already heating up and pressure rises. As is discussed above, the expansion stroke that follows happens faster. The heater cannot heat the gas fast enough to compensate the pressure drop resulting from the increasing volume. As a result, the expansion line drops below that of compression after TDC (b'). This effect could already be observed to a lesser extent in the 5 Hz cycle when looking at the compression and expansion line in greater detail, see figure 10.8.

Further along the expansion stroke heat input improves again when gas pressure and thus temperature drops, increasing the temperature difference between heater and gas. This gives the expansion a more isothermal character. Furthermore, cooling has not yet increased significantly. As a result, the expansion line crosses the compression line and a butterfly shaped cycle is created (c'). Because the area within the loop at BDC is greater than that at TDC, the cycle has a net work output.

This pV-diagram still represents a motor cycle. It has an indicated work output of 0.071 J. At 3.2 Hz the indicated power output is of 0.227 W with an error of 0.186 W.

It is interesting to examine the belly of the compression line more carefully. At BDC, there is already some cooling as a pressure drop can be observed. However, an inflection point can be distinguished at a certain distance from BDC from where the cycle starts opening up significantly (d'). This indicates that the most intense cooling happens at this point during compression, rather than at BDC. Neither Tailer, West or Organ have predicted or anticipated this cooling behaviour. They all state that the major pressure drop of the gas, due to cooling, happens *during the dwell time at* BDC. This observation, however, seems consistent with our suggestion of increased cooling during compression of the gas, see section 6.2. Due to the mass inertia of the gas and and the piston re-compressing the gas, flow vortices are induced, see figures 6.5(a), 6.5(b) and 6.5(c). This leads to higher gas velocities at the cylinder walls and cylinder head which increases the convection coefficients during compression.

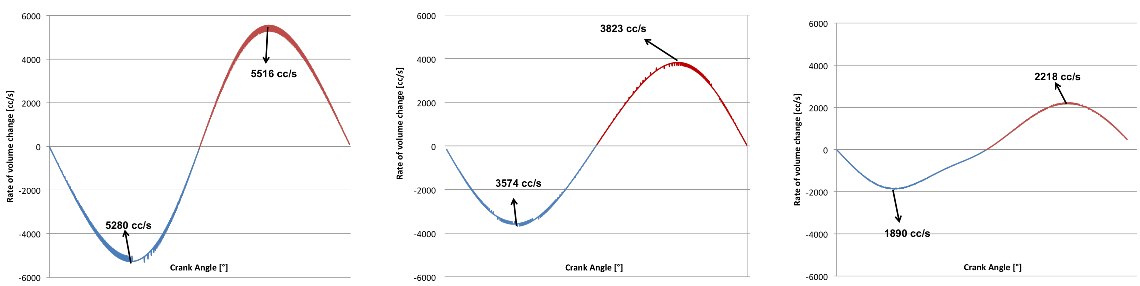

(a) 5 Hz (b) 3.2 Hz (c) 1.5 Hz

Figure 10.10: Rates of volume change at 5, 3.2 and 1.5 Hz

10.5.3 1.5 Hz

The pV-diagram at 1.5 Hz is shown in figure 10.11. At such a low frequency, the cooler's impact on the cycle becomes very important, as it gets even more time to exchange heat with the gas. At the same time, almost the exact same expansion curve is observed as before, see figure 10.12. Even though the heater gets additional time as well, its heat transfer capacity is not sufficient relative to the cooler to have an influence.

Furthermore, the additional time given to compression relative to expansion is even more pronounced at this frequency. This can be seen by comparing the plots in figures 10.10(a), 10.10(b) and 10.10(c). In these graphs, the rate of volume change is plotted against crank angle. The ratio of the maximum rate of volume change during expansion to that during compression is shown in table 10.2 for the different cycles. As can be seen, this ratio increases more than lineary with decreasing frequency. This effect will have favoured the cooling during compression even more. The pV-diagram at 1.5 Hz still represents a motor cycle. It has an

Table 10.2: Comparison of the relative rates of volume change: ratio of maximum volume change during compression to expansion (absolute).

Frequency [Hz]	**Ratio [%]**
5	95.7
3.2	93.4
1.5	85.2

indicated work output of 0.525 J. At 1.5 Hz the indicated power output is of 0.778 W with an error of 0.244 W.

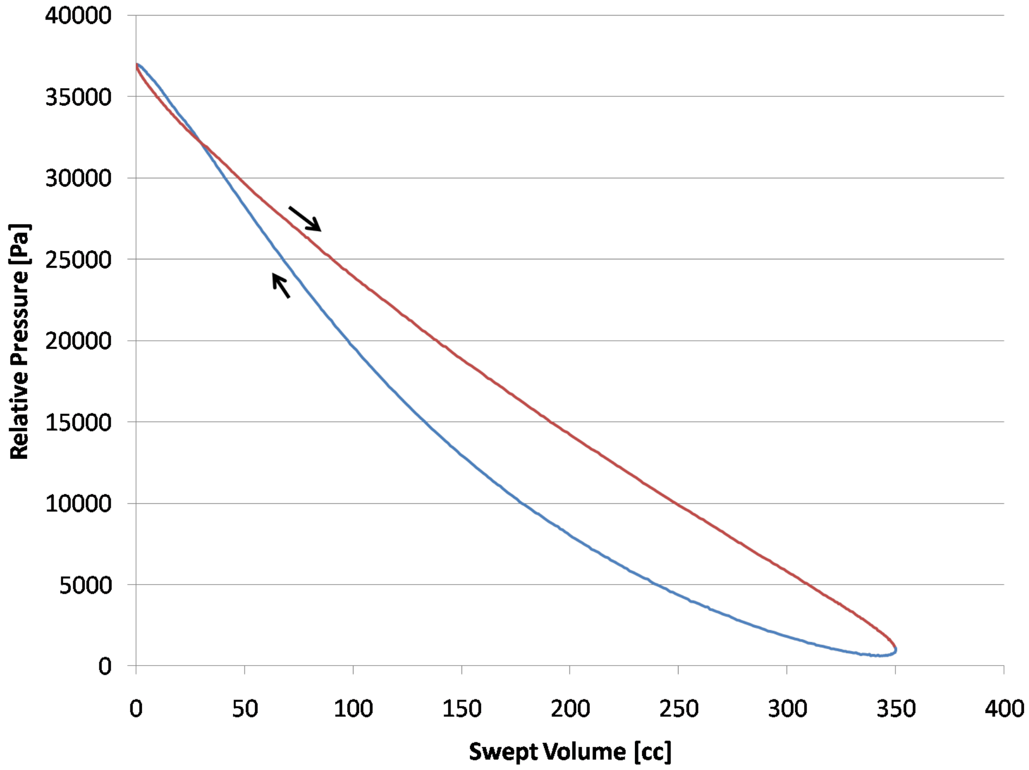

Figure 10.11: pV-diagram of the cycle at 1.5 Hz, 5.5 cm stroke and 15°C cooler temperature

In figure 10.12, the pV-diagrams of the previous three situations are plotted in the same graph. The comparison of the expansion and compression lines illustrates the dependency of the engine's performance on speed of operation relative to the rate of heat exchange in the heater and the cooler. The expansion lines all lie close together. This implies that the heater is insufficient. The compression lines, however, are strongly influenced by the engine frequency.

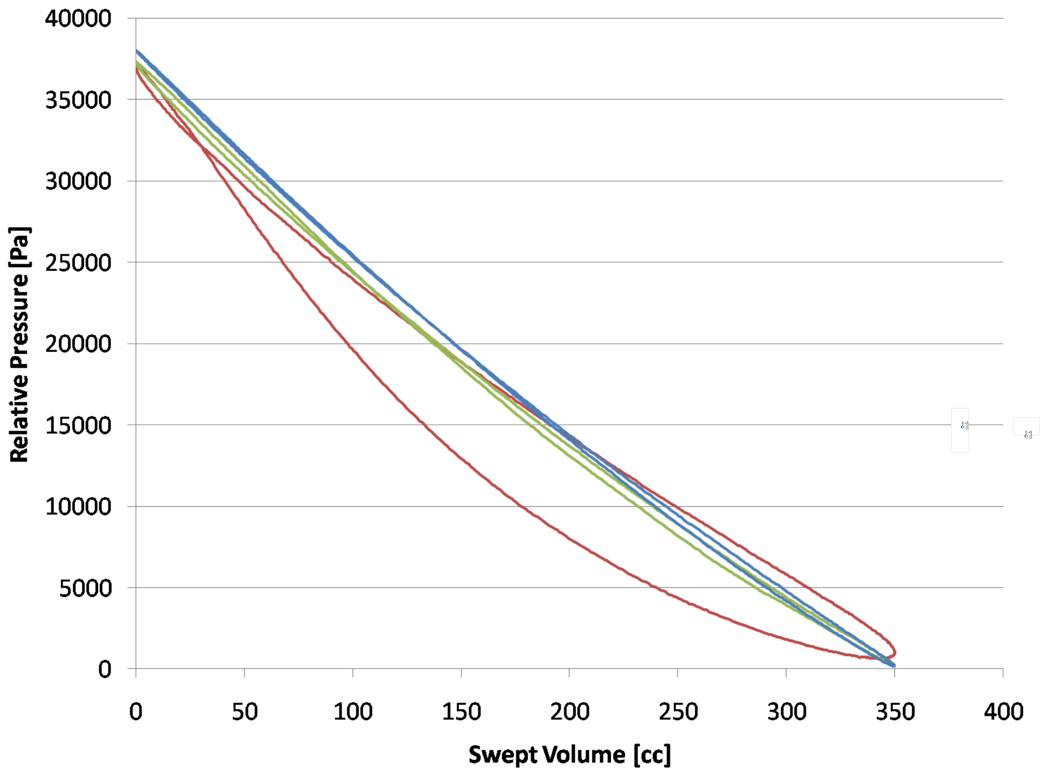

Figure 10.12: pV-diagrams of the three cycles

10.5.4 Overview: results of the first set of experiments

An overview of indicated work and power is given in table **??**. In figure 10.13 indicated power and work are plotted against engine frequency.

Table 10.3: Overview of indicated work and power of the cycles from the first set of experiments.

Stroke length	Frequency	Indicated work [J]	Indicated power [W]	Error
5.5	5	0.06	0.309	0.232
5.5	3.2	0.071	0.227	0.186
5.5	1.5	0.525	0.788	0.244

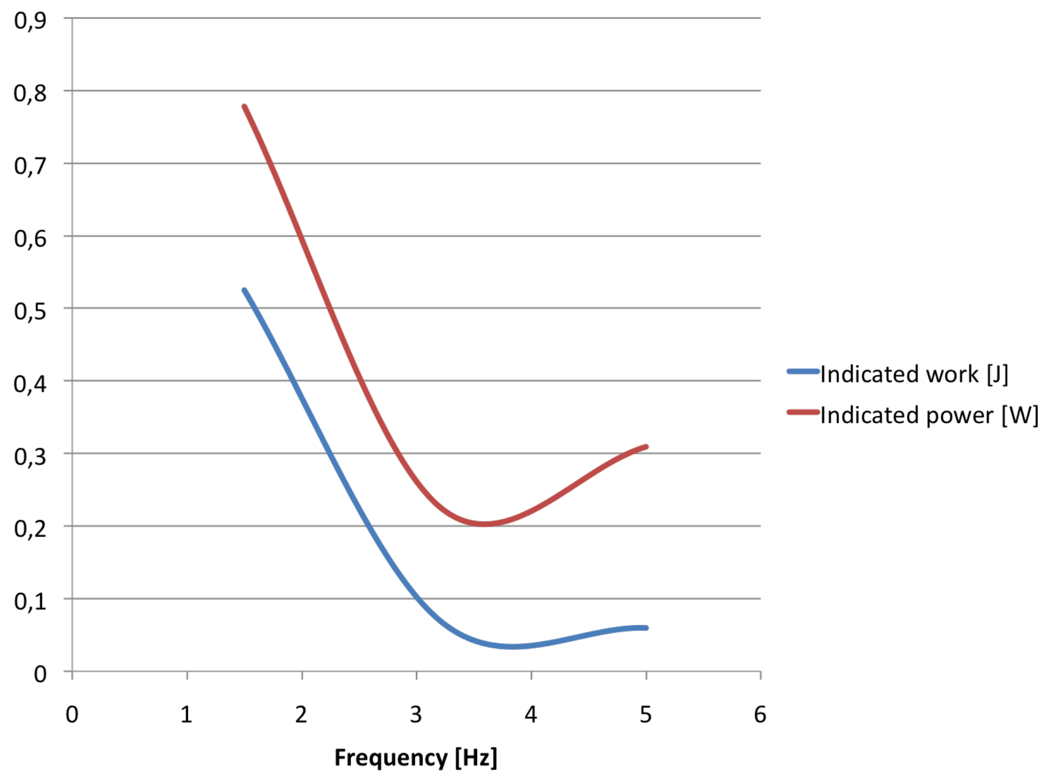

Figure 10.13: Indicated power and work - 5.5 cm stroke

Figure 10.13 shows indicated work and power versus engine frequency. Going from 5 Hz to 3.2 Hz, indicated work decreases. Both the heater and the cooler are given more time to exchange heat with the gas. At 5 Hz, heating is too insufficient to have an influence on the cycle. It is the cooling that creates a positive effect and work output is produced. At a lower frequency, this cooling effect is still present and even more pronounced because compression is given more time relative to expansion, as was discussed in section 10.5.2. Additionally, heating is now also given enough time to influence the cycle. The effect, however, is negative, as heating is improved mainly during compression. It thus compensates for the additional cooling effect. This results in a decreased work output. Going from 3.2 Hz to 1.5 Hz, there is a sharp increase in work output. By further slowing down the cycle, there is not only more time given to the heat exchangers; but the difference in time given to compression relative to expansion becomes very high, see table 10.2. Heating is still insufficient and continues to have only a modest influence. The cooling, however, has become very effective with the time given. The positive effect from the cooling has suddenly increased a lot more relative to the influence of the heater. This observation shows that to optimise a TLE, the engine speed must be adapted to the ratio of the heat transfer capacity of heater and cooler.

10.6 Conclusions

The static test showed that there was a significant error on the energy balance, represented by the large value of $Q_{closure}$. To improve the determination of the energy balance, the following improvements are proposed for the next set of experiments:

- Install the insulation with more care, so possible gaps are minimised.
- All temperature measurements should be performed with thermocouples instead of with the infrared thermometer.
- Heat losses should be calculated through conduction formulas, rather than with convection correlations.

The high temperature threadlocker, used to seal the threads provided sufficient sealing to perform the tests. After the experiment, however, when the engine was cold again, many of the threads leaked again. It seems that even for this threadlocker 300℃ lies at the limits of its working range.

Both energy balance and pV-diagrams have shown that the heat input to the gas was not sufficient. The collector temperature during the experiments only rose to about 85℃. In our original design, the hot source temperature was aimed to be 300℃. This is off course a result of the placement of the resistors directly inside the air. Temperature at the back of the heater tubes is 300℃, but there is a strong temperature drop through the thin walled copper tubes. In order to increase heat input to the gas, it seems necessary to increase collector temperature. This can be done by adding extra heating elements close to the collector.

Some interesting observations could be made from the experiments. First, an increased cooling rate was observed at a certain point *during* compression. This seems to confirm the suggestion made in the underlying physics section, that the convection coefficients in the cylinder increase because of an induced circulating air flow. This effect was not anticipated or predicted by any of the researchers studied in literature and could never have been observed without measuring inside the engine. Second, it became apparent that to optimise TLE performance, the engine speed needs to be adapted to the ratio of the heat transfer capacities of heater and cooler.

Even with the encountered problems, the pV-diagrams looked promising as both recorded cycles showed that the rig was working as an engine. Even though the heat input was not sufficient, the cooler ensured that the cycle still behaved as an engine. If the heater can be improved so the expansion line gets lifted above the compression line at TDC, work output will improve considerably.

Chapter 11

Second Experiment

11.1 Experimental design

Goals of this experiment The goals of these experiments are to determine an energy balance and pV-diagrams of the engine with a parameter sweep of piston stroke and frequency. The piston stroke range that is evaluated is [3 cm - 5 cm - 8 cm] and the frequency range is [1 Hz - 3 Hz - 5 Hz - 7 Hz]. The goal is to observe engine performance trends with varying engine speed and piston stroke.

Current Status of the Rig The rig did not differ much from the first experiment, as described in section 10.3. A few changes were made to improve the experiment, based on the suggestions made after the previous experiment, see section 10.6. To measure the heat losses through conduction, the insulation was installed differently. First, the heater tubes were wrapped with an insulation layer. This provided a cylindrical shape. Then, a thin copper foil was wrapped around it. Over this copper foil, a second insulation layer was wrapped with a known thickness. The temperature of the copper foil and of the outer insulation surface were measured. This gave the temperature difference across the insulation layer, with known dimensions and properties. Heat transfer through conduction could then be easily calculated. The same was done at the free end of the heater tubes to determine the axial heat losses. All temperature measurements were performed with thermocouples, see figure 11.1. As can be seen, the thermocouples were placed perpendicular to the expected heat flux lines. This minimised the influence of the heat flow through the thermocouple cases on the measured temperature. If a temperature was measured on an outside surface, the thermocouple was laid onto the surface and covered by a piece of insulation material. This reduced the influence of the surrounding air.

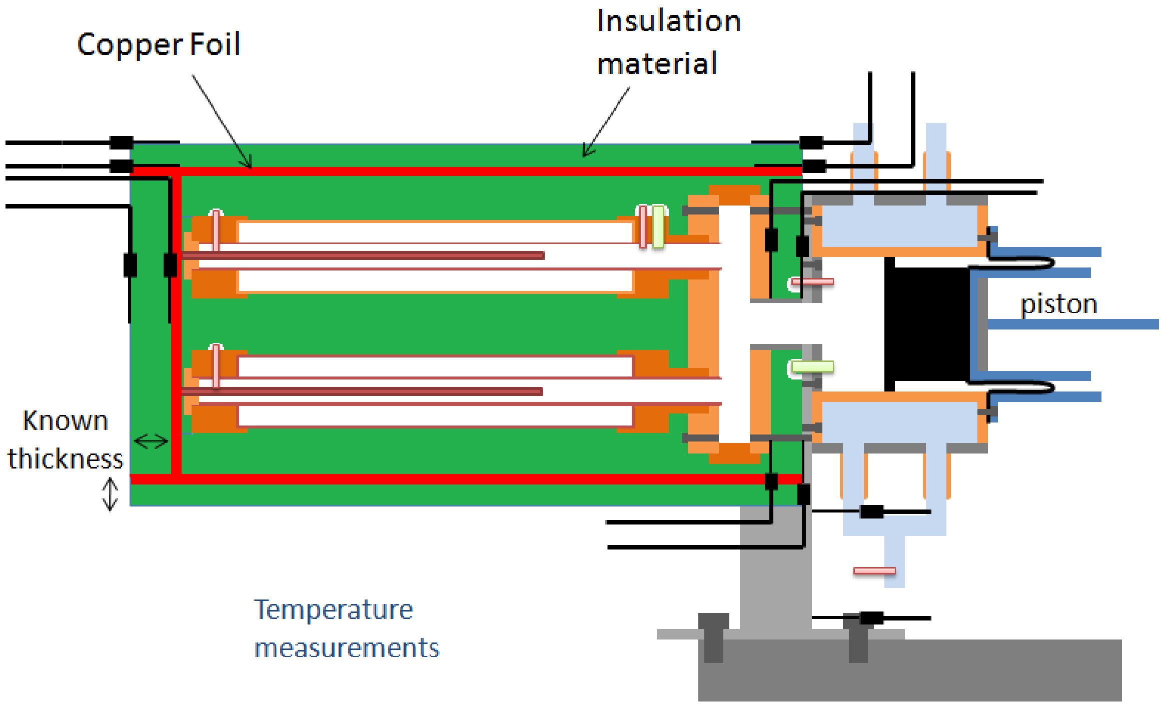

Figure 11.1: Thermocouple measurements

To increase heat input to the gas and achieve a higher temperature at the collector, additional wire resistors were wrapped around the inner tubes of the heater, see figure 11.2. They were able to provide an additional power input of 1 kW. An additional thermocouple was installed to measure the wire resistor's temperature. As it was not possible to get rid of the leakages with the sealants, all heater openings, on the collector and heater tubes, were closed by soldering them with silver. Observing the gas spring created by moving the piston, it could be observed that there were still some significant leaks. As no tap could be screwed into the collector anymore to pressurise the engine, it was impossible to detect the leaks.

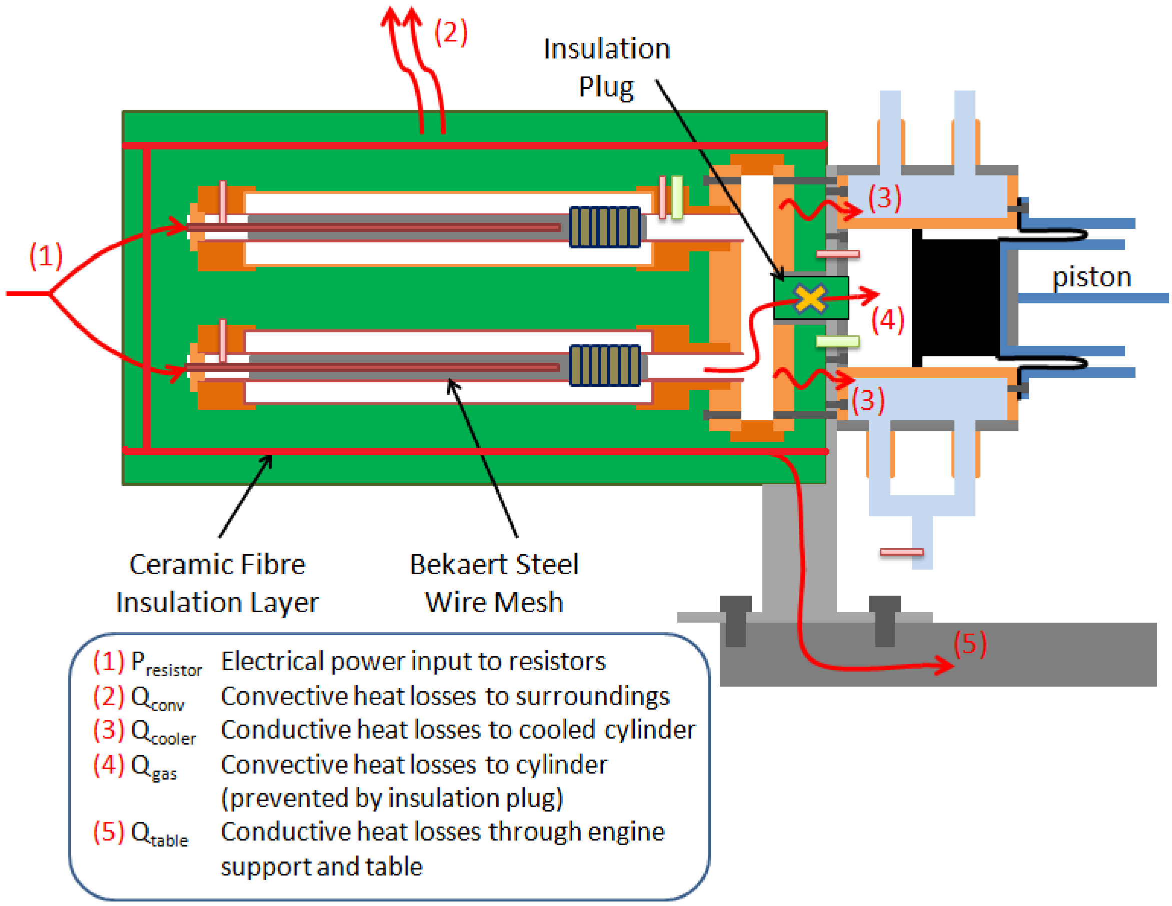

Figure 11.2: Rig setup and energy fluxes

Experimental method The method to determine the energy balance of the hot section did from that of the first experiment, as described in section 10.3. The only difference lied in the measurement of heat losses through conduction and all measurements being performed by thermocouples, as already stated in the previous paragraph. First the engine was heated up (with an insulation plug at the cylinder entrance) and temperatures were recorded every 20 seconds to be able to observe if steady state was obtained. When steady state was achieved, all temperature readings, shown in figure 11.1, were performed. This allowed the calculation of the energy fluxes, shown in figure 11.2. Then, the insulation plug was removed and the engine driven. Heat input was adjusted to prevent resistor temperature from exceeding 300°C during all experiments. The experiments started with an 8 cm stroke, varying frequency from 7 Hz to 1 Hz. Subsequently, the same procedure was run through for a stroke of 5 cm and 3 cm.

11.2 Energy balance: results and analysis

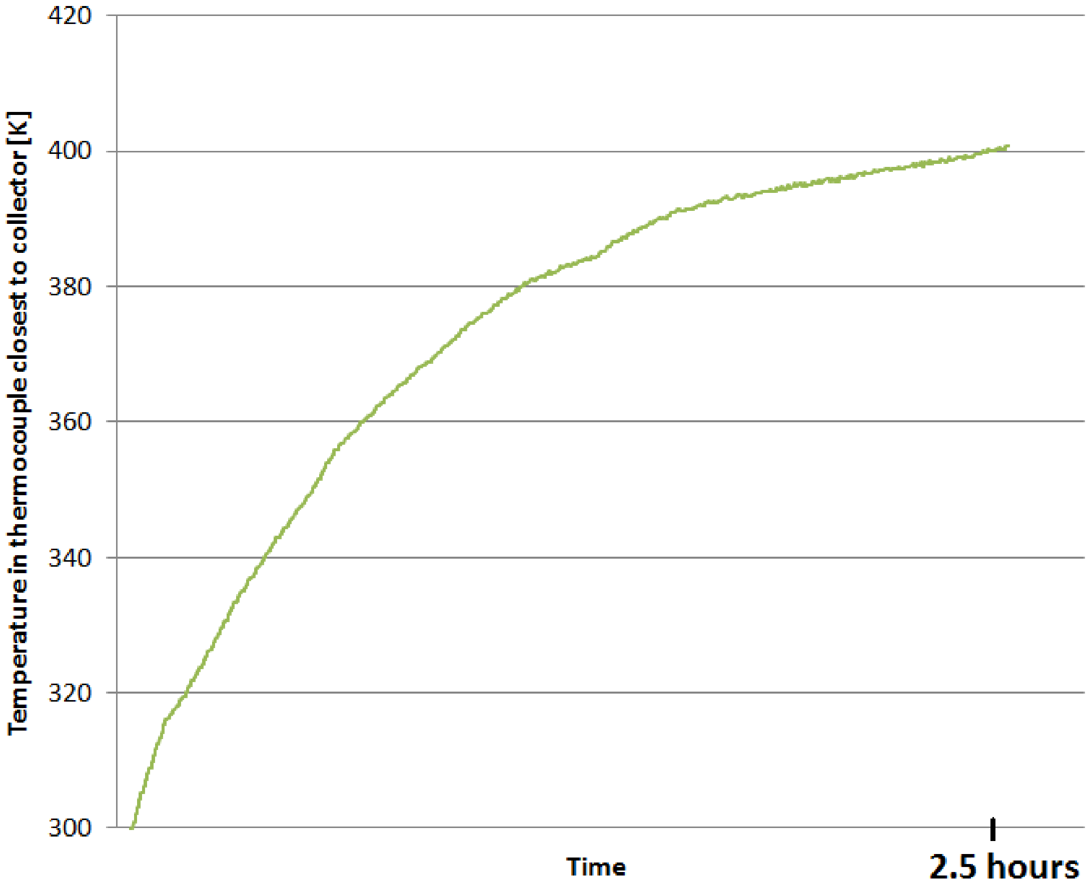

Figure 11.3: Warm up temperature profile of thermocouple in heater tube close to collector

Warm up to steady state Heat input started at 500 W and was reduced when resistor temperature reached 300℃. The prime focus laid on the thermocouple in the heater tube close to the collector. In the previous experiment, this temperature would only rise to about 85℃. The addition of the extra wire resistors should increase this. After 2.5 hours this temperature reached 126.85℃. As can be seen from figure 11.3, steady state was approximately achieved and temperature measurements throughout the engine could be performed. The results of these measurements can be seen in figure 11.4. Steady state heat input was 320 W.

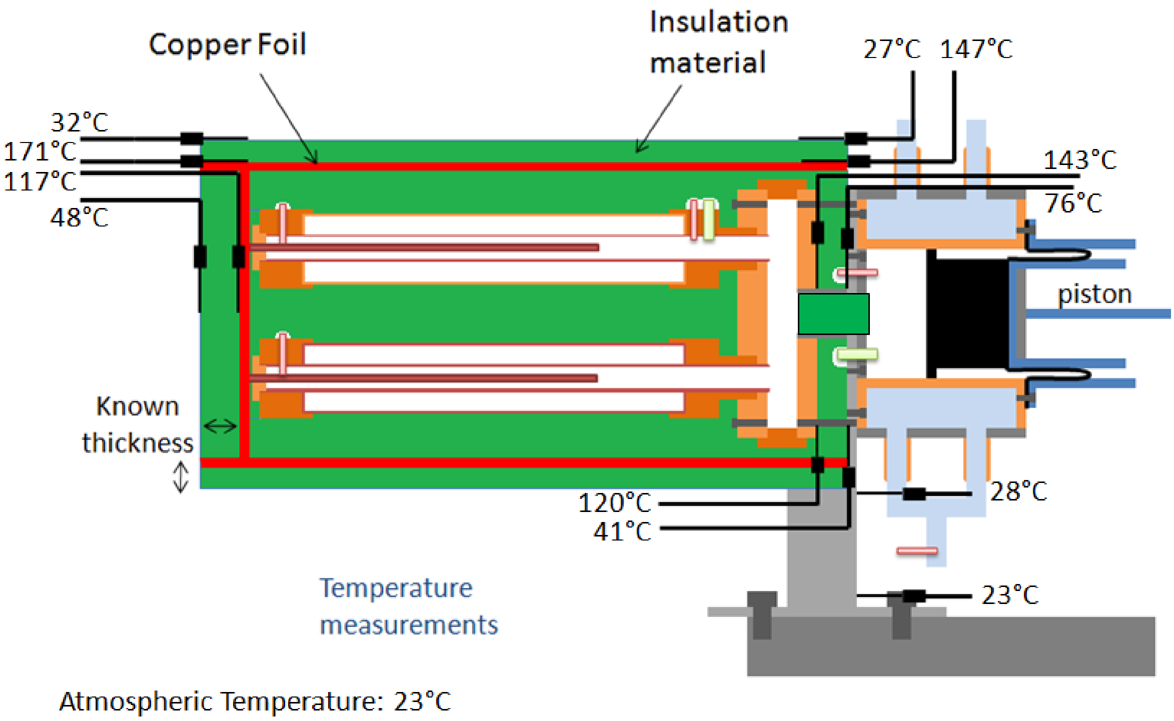

Figure 11.4: Temperature measurements throughout engine in steady state

With these temperatures, the energy fluxes of figure 11.2 were calculated. This is shown in the following sections. The calculations are very similar to those of the previous experiment, see section 10.4.

11.2.1 Heat losses to surroundings through insulation

Radial heat losses to surrounding $Q_{surr,rad}$ Between copper foil and atmosphere, a layer of ceramic fiber[1] and rockwool[2] was placed. The cylinder shaped by the copper foil has a diameter of 0.23 and a length of 0.655 m. The ceramic fiber layer has a thermal conductivity of 0.06 W/mK and a thickness of 2.5 cm. The rockwool layer has a conductivity of 0.036 W/mK and a thickness of 5 cm. The thermal resistance from inside to outside surface of these insulation layers, for an infinitesimal length dx, is:

$$R_{CF} = \frac{ln(0.28/0.23)}{2\ \pi\ dx \times 0.06\ W/mK} = \frac{1}{1.9165\ W/mK \times dx} \tag{11.1}$$

$$R_{RW} = \frac{ln(0.38/0.28)}{2\ \pi\ dx \times 0.036\ W/mK} = \frac{1}{0.7407\ W/mK \times dx} \tag{11.2}$$

The temperature difference across the insulation is not uniform. There is a temperature gradient in axial direction through the copper foil and along the outside surface, see figure

[1]ThermalCeramics Refractory Ceramic Fibre: Cerablanket 128 kg/m^3 - http://www.thermalceramics.com/
[2]Rockwool Rockfit 431 Adapt: http://www.rockwool.be/

11.4. The temperature profiles are assumed linear:

$$T_{copper}(x) = 147°C + 36.64\frac{°C}{m} \times x \tag{11.3}$$

$$T_{outside}(x) = 27°C + 7.63\frac{°C}{m} \times x \tag{11.4}$$

The total radial heat loss is then known through integration:

$$\begin{aligned} Q_{surr,rad} &= \int_0^L \frac{T_{copper}(x) - T_{outside}(x)}{R_{CF} + R_{RW}} \\ &= \int_0^{0.655\ m} \frac{T_{copper}(x) - T_{outside}(x)}{\frac{1}{1.9165\ W/mK} + \frac{1}{0.7407\ W/mK}} dx \\ &= 45.314\ W \end{aligned} \tag{11.5}$$

Axial heat losses to surrounding $Q_{surr,ax}$ The axial heat losses occur at the free end of the heater. Between the copper foil and atmosphere there was a layer of rockwool. This layer formed a rockwool disc with a diameter of 0.23 m, a thickness of 5 cm and a thermal conductivity of 0.036 W/mK. As can be seen in figure 11.4, the temperature difference across the disk was 117°C-48°C=69°C. Heat losses are thus calculated by:

$$\begin{aligned} Q_{surr,ax} &= \frac{k_{RW}\ A}{t} \times \Delta T \\ &= \frac{0.036\ W/mK\ \pi\ (0.23\ m)^2/4}{0.05\ m} \times (117°C - 48°C) \\ &= 2.064\ W \end{aligned} \tag{11.6}$$

Total heat losses to surroundings through Insulation

$$Q_{surr} = Q_{surr,rad} + Q_{surr,ax} = 45.314\ W + 2.064\ W = 47.38\ W \tag{11.7}$$

The heat losses to the surroundings in the previous experiment were calculated to be only 11.36 W, while the thickness of the insulation layer was similar. As measuring these losses through conduction is more accurate, we can conclude that the estimated losses were seriously underestimated. The imprecision of the infrared temperature readings are the most probable reason.

11.2.2 Conductive heat losses to the cooled cylinder Q_{cooler}

These calculations are exactly the same as in section 10.4.2. Only the temperatures were different, see figure 11.5. Therefore, the linear temperature profiles were different as well (notice that the collector did not have a uniform temperature, as opposed to the first experiments):

$$T_{collector} = 149.11°C - 291.14°C/m \times r \tag{11.8}$$

$$T_{cylinder} = 85.3°C - 443.04°C/m \times r \tag{11.9}$$

Integration in the same manner as in equation 10.10, gives us: $Q_{insul} = 5.57\ W$

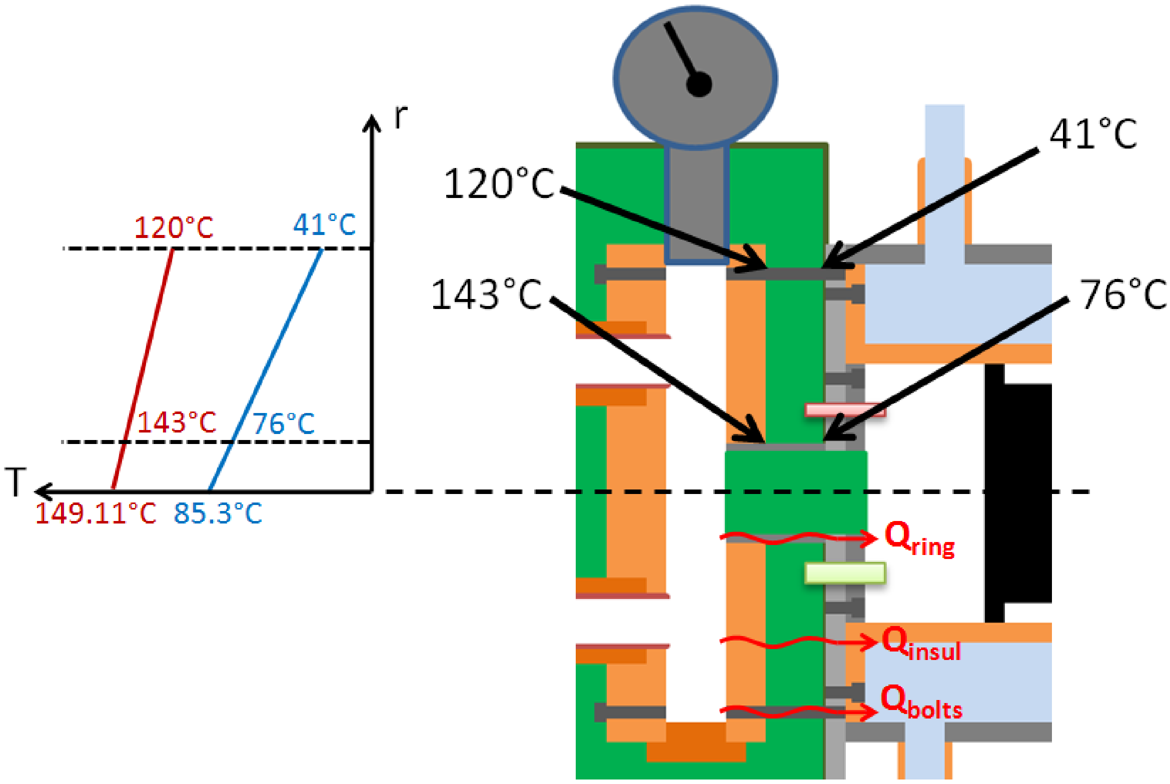

Figure 11.5: Conductive heat losses to cooled cylinder

The temperature difference across the ring was 143°C- 76°C= 67°C, which gives $Q_{ring} = 35\ W$. The temperature difference across the bolts was 120°C- 41°C= 79°C, which gives $Q_{bolts} = 66.08\ W$. The conductive heat loss from heater to cooled cylinder were thus:

$$\begin{aligned} Q_{cooler} &= Q_{insul} + Q_{ring} + Q_{bolts} \\ &= 5.574\ W + 35\ W + 66.08\ W \\ &= 106.65\ W \end{aligned} \tag{11.10}$$

11.2.3 Conductive heat losses through table Q_{table}

As opposed to the first experiment, a temperature difference along the engine support was observed, see figure 11.6. To calculate an estimation of the conductive heat losses, the engine support is viewed as a rectangular piece of steel. The dimensions are: height = 10 cm, width

= 20 cm, thickness = 0.5 cm. The loss is then:

$$\begin{aligned} Q_{table} &= \frac{k_{steel}\ A}{l} \times \Delta T \\ &= \frac{53.15\ W/mK\ 0.005\ m\ 0.20\ m}{0.10\ m} \times (28°C - 23°C) \\ &= 2.66\ W \end{aligned} \tag{11.11}$$

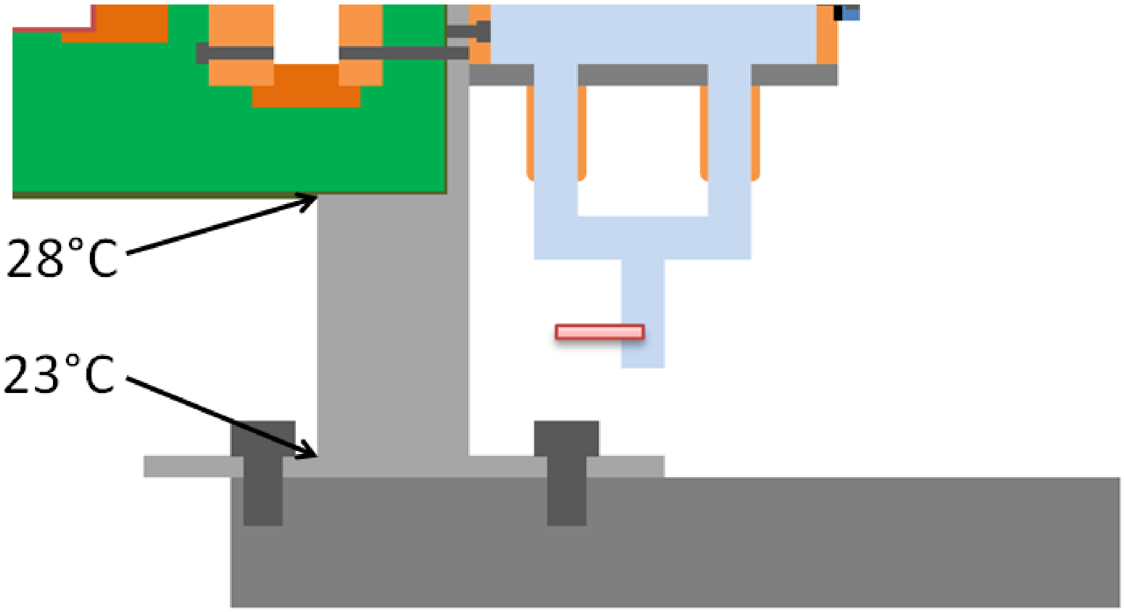

Figure 11.6: Temperatures at at engine support

11.2.4 Static energy balance

From the previous sections, the total energy balance of the hot section can be written:

$$P_{resistor} = Q_{surr} + Q_{cooler} + Q_{table} + Q_{closure} \tag{11.12}$$

$$320\ W = 47.38\ W + 106.65\ W + 2.66\ W + Q_{closure} \tag{11.13}$$

This means that $Q_{closure} = 163.31\ W$. In the ideal case $Q_{closure}$ should only include the heat carried away by the cooling circuit of the pressure sensors, as this is the only heat loss that is not accounted for. In this experiment, the value is even larger than in the first experiment, even though measures had been taken to perform the measuremens and calculations more accurately. There is a reason for this however: during warm up of the engine, one of the pressure sensor cooling circuits started leaking. As this was covered by insulation layers, it could not be observed immediately. As a result, the entire insulation below this leak became wet. This has reduced the proper functioning of that part of the insulation. Cooling fluid evaporated upon contact with the collector. These insulation problems can easily account for the major part of $Q_{closure}$.

The wet insulation also explains why the temperature of the collector did not rise above 145°C. Overviewing the situation and the measured temperatures, see figure 11.7, a higher collector temperature was expected. Due to the insulation problem, the heat could flow from the collector to the surroundings, cooling down the collector. The full potential of the added wire resistors could thus not be exploited.

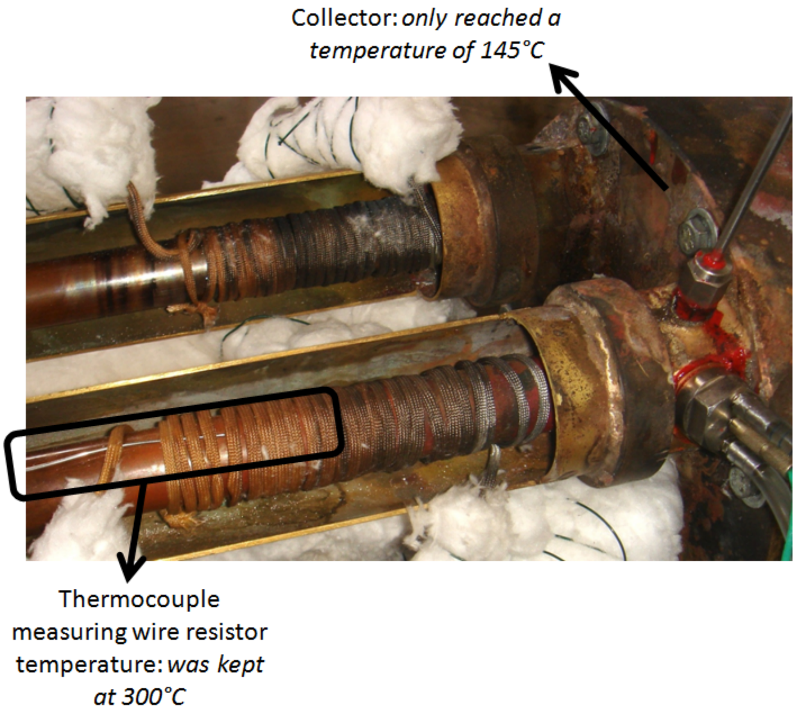

Figure 11.7: Temperatures at the hot side after warm-up

11.2.5 Dynamic tests

The same logic as in section 10.4.4, is followed to determine an estimation of heat input to the gas. After achieving steady state, the insulation plug at the cylinder entrance was removed and the dynamic testing started. To keep the resistor temperatures at 300°C, an additional heat input to the resistors was required. During the experiments heat input could go up from 320 W to 350 W (dependant of the working state). Again assuming that the energy fluxes calculated in the static engine did not change much, the energy balance during dynamic testing became:

$$P_{resistor} = Q_{surr} + Q'_{cooler} + Q_{table} + Q_{closure} + Q_{gas} \tag{11.14}$$

$$350\ W = 47.38\ W + Q'_{cooler} + 2.66\ W + 163.31\ W + Q_{gas} \tag{11.15}$$

The conductive heat losses to the cooler have decreased as the area was reduced by removal of the plug. The integral of equation 10.10, can be re-used but the integration borders should be changed. The integration should start at the outside diameter of the steel ring.

$$Q'_{insul} = \int_{r_{ring}}^{R} \frac{T_{collector}(r) - T_{cylinder}(r)}{R(r)} = 5.36\ W \tag{11.16}$$

This means that:

$$\begin{aligned} Q'_{cooler} &= Q_{insul} + Q_{ring} + Q_{bolts} \\ &= 5.36\ W + 35\ W + 66.08\ W \\ &= 106.44\ W \end{aligned} \tag{11.17}$$

From equation 11.14, we can now calculate the heat that left the heater through the gas path:

$$\begin{aligned} Q_{gas} &= (340\ W\ to\ 360\ W) - 47.38\ W - 106.44\ W - 2.66\ W - 163.31\ W \\ &= 30.21\ W \end{aligned} \tag{11.18}$$

As is evident from previous considerations, this value is an indication of the heat input that was delivered to the gas during the dynamic testing. During the tests pV-diagrams were obtained. We will discuss these in the following section.

11.3 pV-diagrams: results and analysis

11.3.1 7 Hz

Remark: As in experiment 1, the pV-diagrams show relative pressures. As the engine was not completely sealed, it was assumed that the lowest pressure in the cycle is equal to atmospheric pressure.

The pV-diagram of the engine at 7 Hz is shown in figure 11.8. The expansion line lies completely under the compression line. Unlike in the previous experiments, the cycle now represents a heat pump cycle. Heat is drawn from the cooler and delivered to the heater. During compression, the gas temperature is raised above heater temperature allow the gas to dump heat. During expansion, the gas temperature is pulled below that of the cooler allowing to take in heat from it. As opposed to the first experiment, the expansion line bends upwards around BDC. The gas was actually overexpanded beneath atmospheric pressure, as a popping sound could be heard from the rolling diaphragm seal. The seal was collapsing inward during the expansion stroke and recovered during compression. Around BDC the expansion curve bends upward taking in heat from the cooler, as opposed to the first experiment. This means that cooler performance had seriously deteriorated compared to the first experiments. The heater is again unable to keep up with the cycle at high frequencies.

To allow working as a heat pump, the cycle requires a net work input of 0.856 J of the electrical motor. The power input is 5.99 W with an error of 1.126 W.

As can be seen from the dynamic energy balance, when switching from static to dynamic testing, power input to the resistors could be increased by about 30 W. As the rig was behaving as a heat pump, this can not be seen as an indication of the heat input to the cycle, as net heat is dumped in the heater. The gas will have created an additional heat transfer path to draw heat from the resistors. This heat was then dissipated somewhere engine where the temperature lies below the gas temperature.

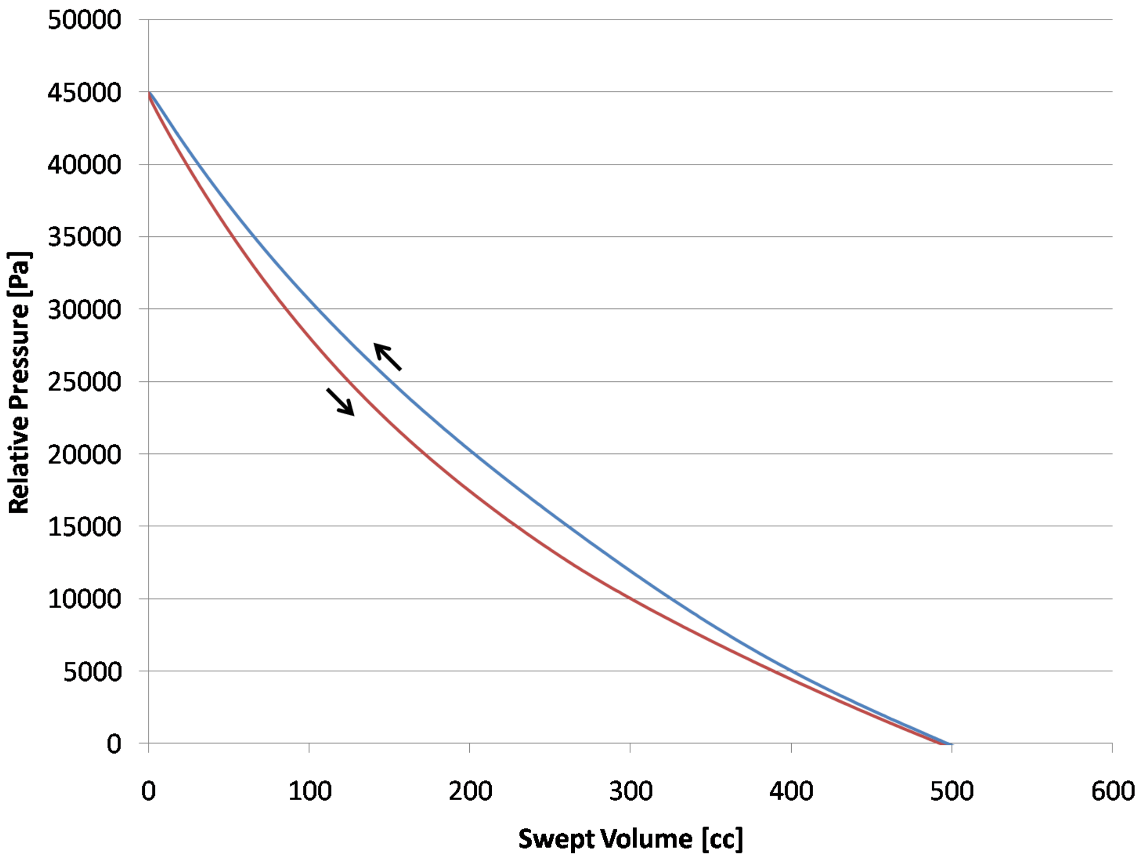

Figure 11.8: pV-diagram of the cycle at 7 Hz, 8 cm stroke and 23°C cooler temperature

11.3.2 5 Hz

The pV-diagram at 5 Hz is shown in figure 11.9. The same phenomena as in the previous situation can be observed. Heater nor cooler function properly and the rig again behaves as a heat pump.

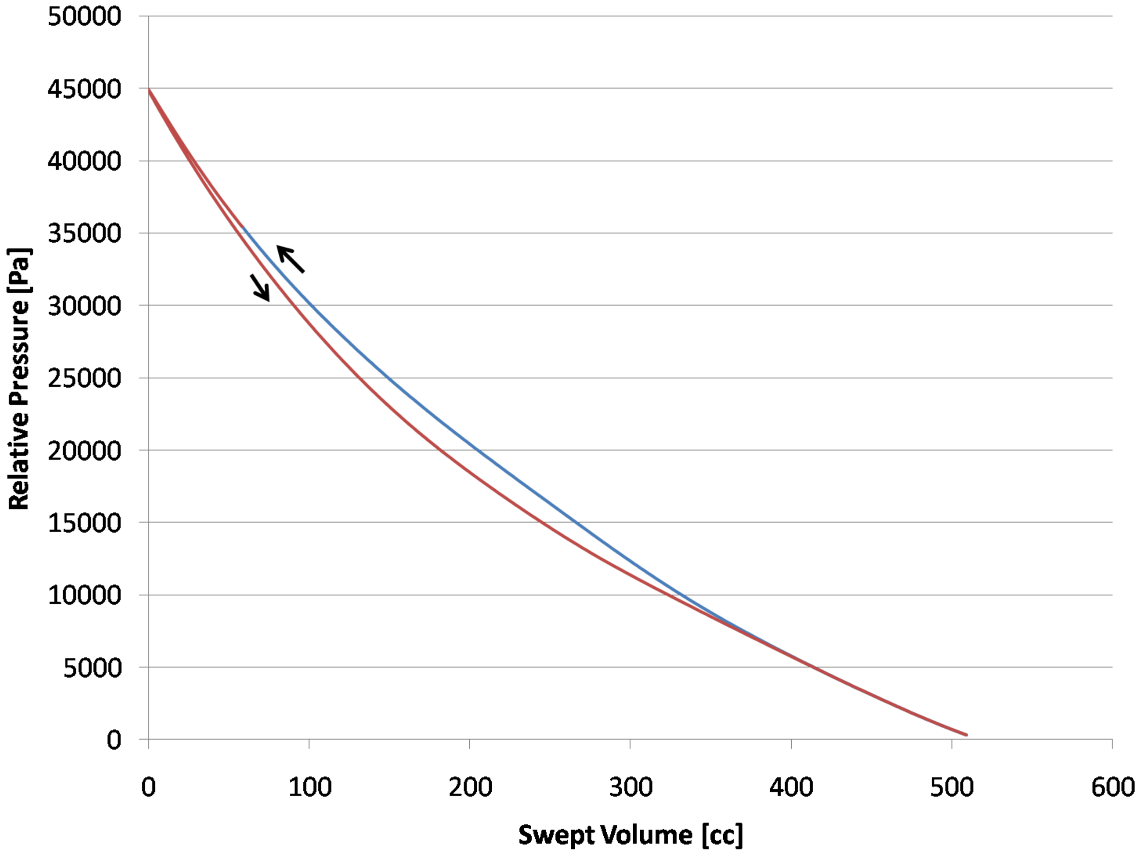

Figure 11.9: pV-diagram of the cycle at 5 Hz, 8 cm stroke and 23℃ cooler temperature

The lower frequency, however, gives the gas more time to exchange heat with heater and cooler. Comparing the compression line with that of the 7 Hz situation, see figure 11.10, it can be observed that the curves are parallel for the first half of the compression stroke (before (a)). At a certain moment, due to compression the gas temperature in the heater rises above heater temperature. Consequently, heat is dumped. As there is more time available in the 5 Hz cycle for this to happen, the 5 Hz compression line lies further below the 7 Hz line for the remaining part of the stroke (after (a)).

During expansion, an analog effect can be observed. The expansion lines map each other during most of the stroke (before (b)). Towards the end of expansion, the gas is taken in heat from the cooler as the gas temperature has dropped below cooler temperature. This causes pressure to rise. Again, this is more pronounced at lower frequency as more time is provided for heat transfer. As a result the expansion line of the 5 Hz cycle rises above the one at 7 Hz (after (b)).

To be able to work as a heat pump, the cycle requires a net work input of the electrical motor of 0.45 J. The indicated power input is 2.26 W. This is less than in the 7 Hz cycle as the area within the expansion and compression curves is smaller.

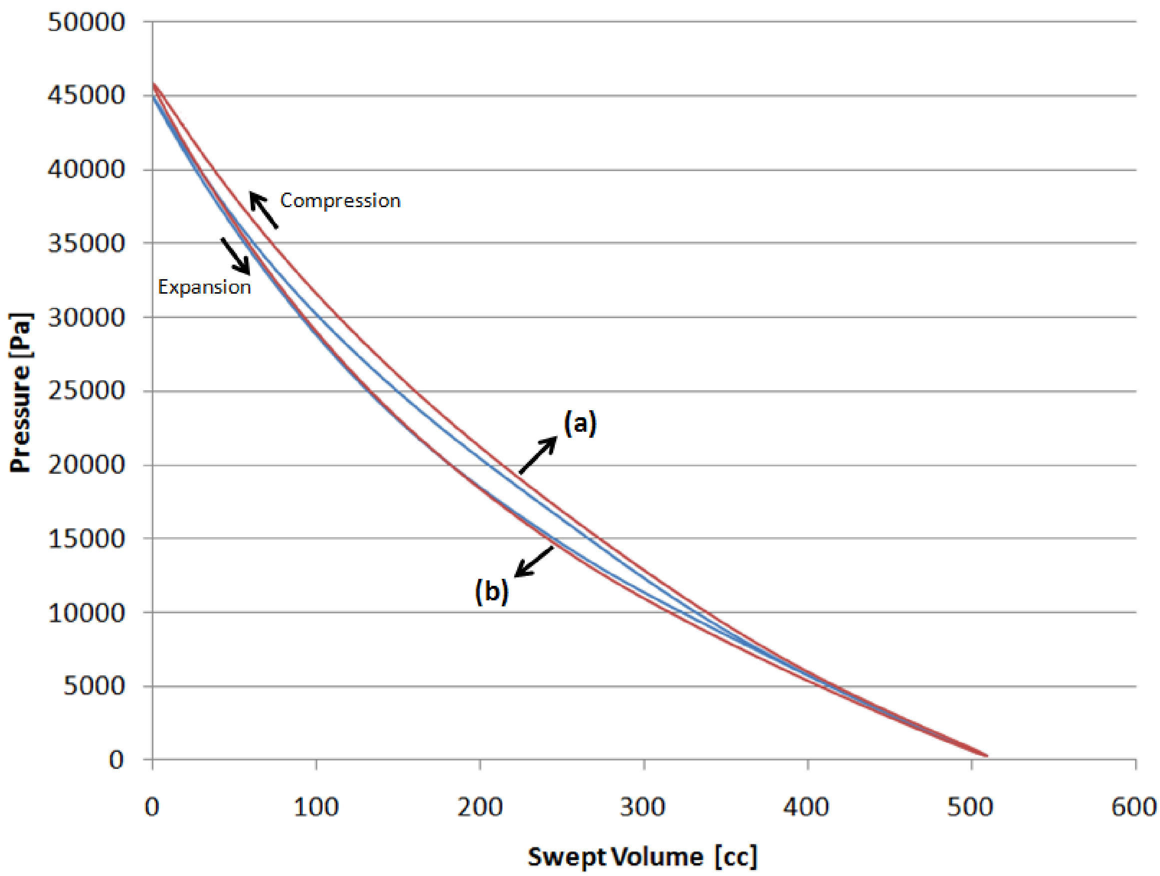

Figure 11.10: pV-diagrams at 5 Hz (blue) and 7 Hz (red) plotted over each other

11.3.3 3 Hz

The pV-diagram at 3 Hz is shown in figure 11.11. Over the whole cycle, there is a net work input, so the rig still behaves as a heat pump. However, around TDC a positive heater effect can be observed for the first time. The lower frequency allows the heater to deliver heat to the gas after the compression stroke, lifting the first part of the expansion line over the compression line. By delivering heat to the gas, the heater is thus able to compensate the pressure drop caused by expansion. At this lower engine speed, the heat transfer rate of the heater has becomes sufficient to have a more isothermal expansion. Further along the expansion stroke, the gas brought into the cylinder is cooled and pressure drops.

The cooler is still insufficient, that heat is still *taken* from the cooler around BDC. Pressure rises and the compression line returns above the expansion curve. The result is a butterfly shaped cycle. As opposed to the butterfly cycles of the first experiments, the loop near TDC now delivers a net work output and the loop near BDC requires work input. The negative loop dominates however, ensuring that the cycle still requires a net indicated work input of 0.39 J. In the case of a better cooler and heater where the heating effect is more pronounced and a cooling effect is achieved, the cycle would have opened up completely, allowing the rig to work as an engine.

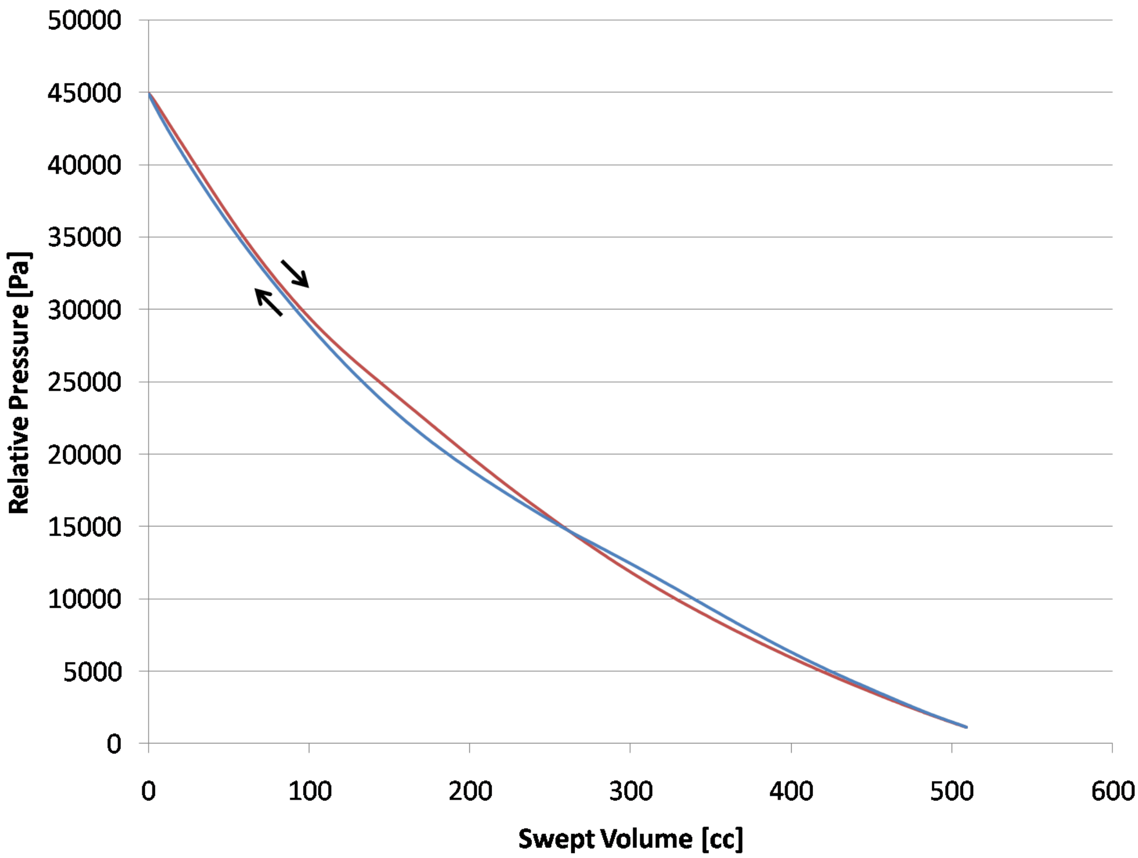

Figure 11.11: pV-diagram of the cycle at 3 Hz, 8 cm stroke and 23°C cooler temperature

11.3.4 Reduced cooling

When comparing these pV-diagrams with the ones of the first experiment, it is remarkable that no cooling effect can be observed at all. The differences between the two experiments performed at the same frequency of 5 Hz, for which the pV-diagrams are given in figures 10.8 and 11.9, are now listed:

- The piston stroke was 8 cm instead of 5.5 cm. This means that at BDC the gas was exposed to a cylinder wall area that was 45.4% larger.
- Cooling water temperature was $23°C$ instead of $15°C$. As the cylinder walls are made

out of brass and water flow was large, see section 10.2.2, it is reasonable to assume that cylinder wall temperature is equal to cooling water temperature.

- Collector temperature was raised by about 55℃ (from 85℃ to about 145℃).

Two reasons for the reduced cooling can be found.

The first reason is due to the increased stroke. As the volume increase during expansion is now significantly higher, the pressure drop increases as well. From the popping of the seal, it could even be observed that pressure dropped below atmospheric pressure. Heating is insufficient to compensate this pressure drop. Consequently, compared to the first experiments, gas temperature in the cooler will be lower at the end of expansion. This decreases the temperature difference between gas and cooler walls and cooling is reduced.

A second reason can be found when looking at the temperature profile of the engine more closely, see figure 11.12. It can be seen that the cylinder's front plate temperature has increased by 24℃. From the first experiments, where the positive cooling effect was observed, it could be seen that cooling only picked up significantly at a certain point *during* compression. If this, as was previously suggested, is a result from the induced circulating flow inside the cylinder, the reduced cooling in this experiment makes sense. Referring to figure 6.5(c), these vortices also increase gas velocities at the cylinder head. It can be thus expected that the role of the cylinder's front plate is more important for the cooling than previously assumed. The 24℃ increase in temperature at this front plate could thus have influenced cooling significantly. This presumption is supported by one of Tailer's remarks in his paper from 1995 [22]. He found that engine performance greatly improved when heat transfer area was added in front of the piston at the cylinder head, despite adding dead space.

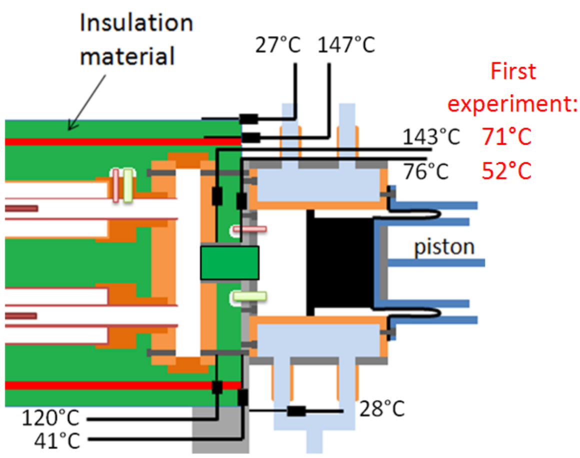

Figure 11.12: Part of the temperature profile of the engine during the second set of experiments.

11.3.5 Comparing the butterfly cycles

Two comparable butterfly cycles have been obtained from the experiments. The cycle at 3.2 Hz (5.5 cm stroke) and the cycle at 3 Hz (8 cm stroke). They look much alike, but illustrate the different working conditions of the first and second set of experiments. The first cycle was recorded with only the bar resistors at the far end of the heater tubes, but a decent cooling effect was achieved. The loop at TDC created a negative work output, the loop at BDC created a positive work output. Fortunately, the positive loop dominated and the rig behaved as an engine.

During the second experiment, another butterfly cycle was recorded, opposite to the first one however. The loop near TDC now created a positive heat input, the loop near BDC a negative one. In this case the negative loop dominated and a heat pump was obtained. If both effects could be combined in the same cycle, engine performance would be significantly enhanced.

The positive cooler effect of the first experiment was lost, but a positive heater effect was achieved. One might say that *one positive effect was traded for the other.* As discussed in section 11.2.4, due to the insulation problem, the full potential of the wire resistors could not be attained, however, and collector temperature was lower than had been hoped for. This would have increased heater performance even more.

11.3.6 Overview: results of the second set of experiments

An overview of indicated work and power of the pV-diagrams obtained from the second set of experiments is given in table 11.1. In figure 11.13 indicated work and power are plotted against frequency (with an 8 cm stroke). It is clear that the rig starts behaving more as an engine when frequency is reduced. The heater can then keep up better with the speed of the cycle raise expansion temperature.

Stroke length	**Frequency**	**Indicated work [J]**	**Indicated power [W]**	**Error [W]**
8	7	-0.856	-5.99	1.126
8	5	-0.45	-2.26	0.690
8	3	-0.39	-1.17	1.091

Table 11.1: Overview of indicated work and power derived from the obtained pV-diagrams

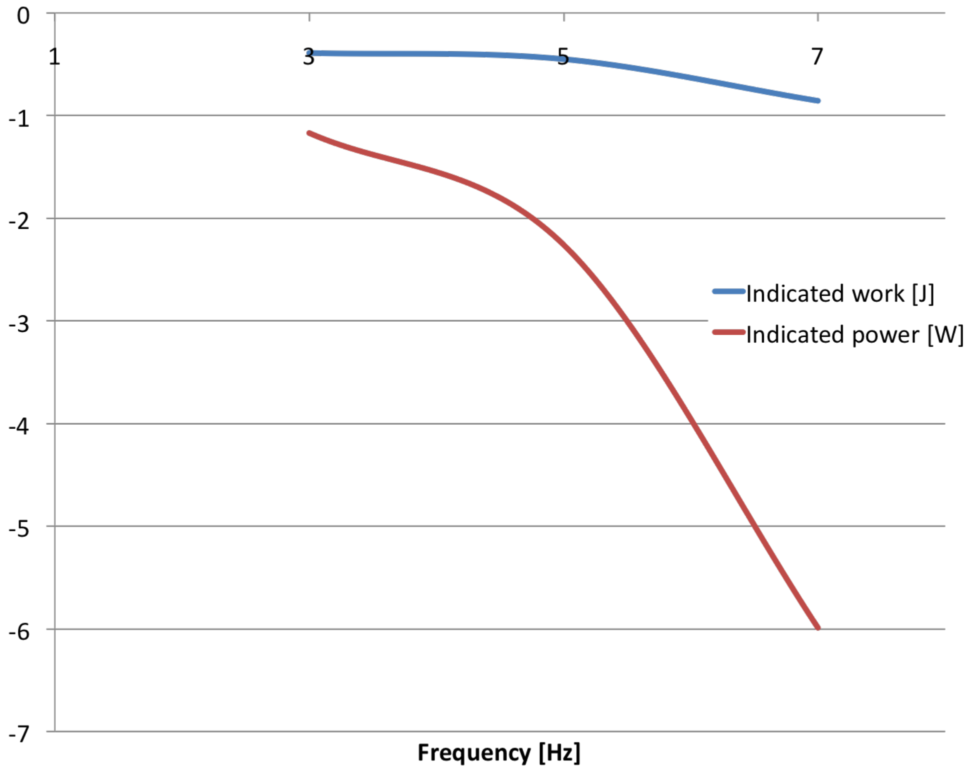

Figure 11.13: Indicated power and work - 8 cm stroke

11.4 Problems encountered with the pressure sensors

The results of the first set of experiments were based primarily on the signal of the pressure sensor in the cylinder head. The signal generated by the pressure sensor in the collector was very similar but suffered from significant distortion, see figure 11.14. For the clarity of the plot, the red signal is depicted with an offset in pressure. All the experiments of the first set have been recorded by both the sensors.

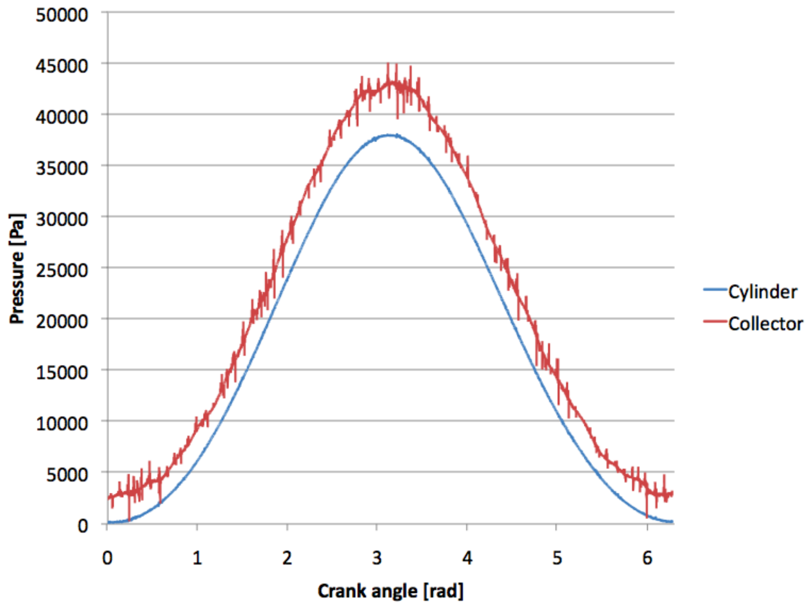

Figure 11.14: Comparison of the clean signal recorded in the cylinder head and the distorted signal recorded in the collector.

During the second set of experiments, a low pass filter was set to suppress the distortion on the signal from the sensor in the collector. After the data set with an 8 cm stroke was recorded at different frequencies, the signal from the pressure sensor in the cylinder head went in overload. For the remaining experiments, drift remained too high so the sensor could not be reset. The following cycles, with a stroke of 5 cm and 3 cm, were thus recorded by the second pressure sensor only.

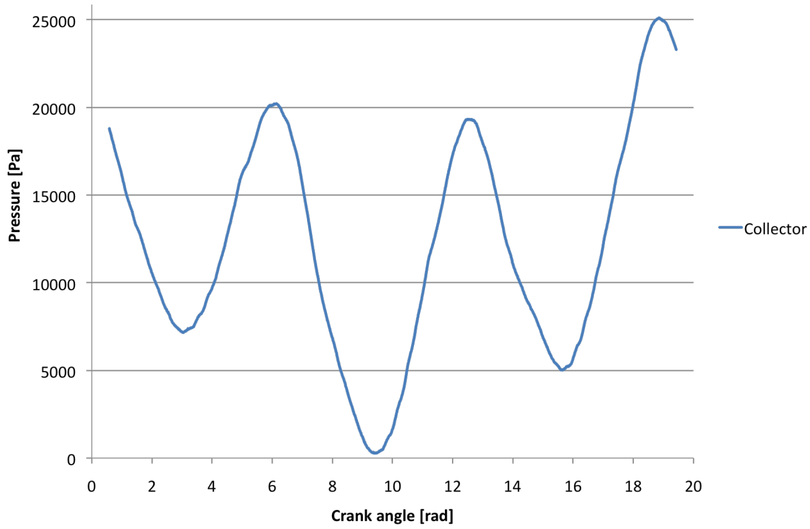

Figure 11.15: Seriously distorted pressure signal of the pressure sensor in the collector recorded during the last experiments.

After processing the data, the cycles recorded solely by the second sensor seemed unrealistic. Figure 11.15 shows the signal of the second sensor over three cycles. It is clear that these measurements are unreliable. If one of these signals are processed into a pV-diagram, figure 11.16 is obtained.

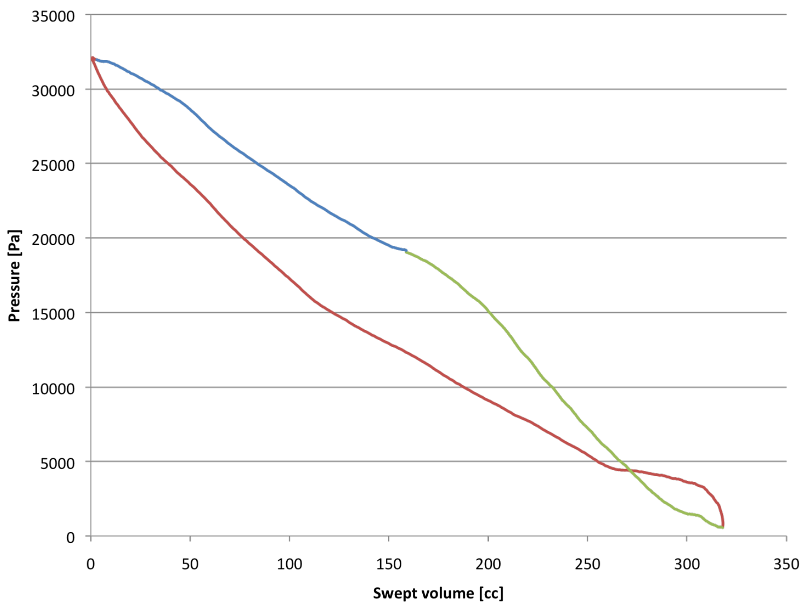

Figure 11.16: Unrealistic cycle recorded by the pressure sensor in the collector.

The signals of both pressure sensors that recorded the 8 cm cycles simultaneously are plotted on top of each ochter, see figure 11.17. This shows that the signal of the second sensor was already unreliable during the first experiments. As a result, the measurements of all experiments performed with a stroke of 3 cm and 5 cm are compromised.

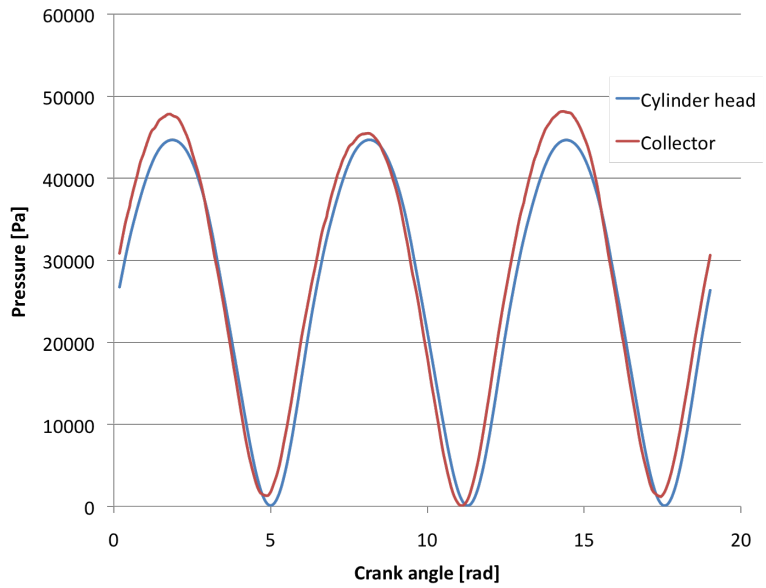

Figure 11.17: Comparison of the pressure signals during the 8 cm experiments.

Possible causes of this anomaly are:

- The low pass filter had an unwanted effect on the signal.
- The sensor suffers from drift. This seems unlikely when looking at the rate at which the signal shifts up and down over a limited amount of cycles.
- Because the sensor is placed in the collector there could be an effect of gas dynamics. Again, this seems unlikely, as there is absolutely no cyclic behaviour to be observed in the distortion. Also, the change in maximum pressure from one cycle to the next sometimes surpasses 25% of the amplitude!

Both the pressure sensors will be recalibrated and tested to hopefully solve and clarify the problem.

11.5 Conclusions

The propositions made after the first experiments were implemented. The method to measure the energy balance was made more accurate. The water leak from the pressure cooling circuit however, made it impossible to determine the error on the acquired energy balance. The insulation around the collector also got wet, which pulled its temperature down significantly. Although its temperature was higher than during the first experiments, the full potential of the added wire resistors could not be attained.

For the pV-diagrams, the misfortune occurred of the failing of the best pressure sensor. Therefore only the dataset with a stroke of 8 cm was reliable. The datasets of the 3 cm and 5 cm strokes could not be used.

From the observations made in this second experiment, it is suggested that the influence of the cylinder head is of more importance to the cooling than was previously assumed. This confirms the observation made by Tailer of having an improved engine when adding more heat transfer area at the cylinder head [22].

The importance of a good thermal barrier between hot and cold section has become clear, as raising of the heater temperature implies that cooler temperature goes up as well. Therefore, by improving the heater, the cooling effect is reduced. This negative side effect could be reduced by having a longer section between hot and cold space or the use of other materials such as ceramics, which have lower thermal conductivity.

From the experiments that have been performed, a positive heater and a positive cooler effect have been observed separately. If these effects are combined, work output can be increased. If the thermal barrier between hot and cold is improved this might be achieved with the current rig.

Part IV

Recommendations and Conclusions

Chapter 12

Review of Engine Design

In what follows, an evaluation is made of each section of the test rig that we designed and constructed.

12.1 Hot heat exchanger

From the outset of designing the hot heat exchanger, great importance was attached to its flexibility. Modelling of the engine at that time was still at an early stage, making it impossible to draw conclusions from simulations on how the engine should be built. A thorough literature study was performed on the very few engines that have been described: the ones built by Tailer and Organ. The parameters of their engines were found to be very dissimilar. Design thus focussed on covering the broadest range of configurations possible. The heater design with the different heater tubes was an exponent of that mindset. It offered the possibility of covering a very wide heater volume range as one or more tubes could be removed. In each tube, inserts could be placed to vary the tube volume and heat transfer area. Furthermore, the annular spaces filled with oil provided a very constant temperature heat source. The complete inner wall of the tubes would have been close to the designed heat temperature of 300℃.

In practice the design exhibited some shortages that were not easily overcome. Sealing was anticipated to be a tough task, but proved to be even more difficult within the time span of the project. Sealing threaded connections was problematic at high temperatures as 300℃ lies at the limit of what threadlockers available on the market today can handle. A lot of connections in the design depended on threads: thermocouples, resistor connections and even the heater tubes were designed to be screwed into the collector. Eventually, for the last experiment, the choice was made to solder all threaded connections shut. As a result, all the flexibility that was designed into this rig was lost completely.

Based upon these experiences it seems that a modular approach to the design of the hot heat exchanger is not the best solution. The increased complexity of a modular designs makes the heater too vulnerable to leakage. In future designs of the heater in TLE test rigs, it seems better to focus on simplicity and robustness. Instead of designing one heat exchanger to cover a very broad parameter range, the designer should prefer the use of multiple heaters that are easily interchanged.

The use of a simpler heater will avert a lot of the sealing problems. When designing from scratch, however, it is advised to locate the sealing mechanism closer to the cold heat exchanger. This will facilitate the use of more common rubbers or sealants.

The collector was designed to be a basis on which heater tubes could be inserted. As this engine is a low power application, energy fluxes throughout the rig are very small compared to conventional heat engines. Therefore this bulky collector piece greatly reduced the thermal response time of the entire engine. This increased the duration of the experiments greatly. Doing quick tests to check the functioning of other components became impossible as it took a few hours to get the collector to temperature.

12.2 Cold heat exchanger

The cold heat exchanger proved to be very reliable. The use of brass allowed the cylinder walls to be very close to cooling water temperature. A decent cooling effect was also observed during the experiments. The external water cooler that was connected to the cooling water circuit, however, was too powerful for the application. As it provided a high mass flow, no temperature difference could be observed between water inlet and outlet. This made it impossible to measure the heat removed by the cooler and a different solution was devised to obtain the energy balance.

Referring to the second experiment, chapter 11, it is suggested that the front plate of the cylinder is more important for the cooling than was assumed. As this is not discussed in previous literature, this had not been taken into account while designing the cold heat exchanger. As this would be an interesting subject for future research, designs should try to incorporate a way to vary the cooling capacity at this front wall, independently of that at the cylinder walls.

12.3 Thermal barrier - pulse tube

The discussion of the underlying physics, see chapter 6, showed that there are different opinions about the function of this section. Although the experiments that were performed have not reached the point to start varying this section, its properties and dimensions could be easily varied by replacing the whole piece or by putting inserts in it. It seems that this would be sufficient to investigate the claims that were made.

Additionally, this piece is very important as it acts as a thermal barrier between the hot and the cold space. If the thermal resistance created between the two sides is too low, it will be difficult to vary heater and cooler temperature independently. To separate and identify the effects that occur when heater or cooler temperature is varied, it is thus important that this section creates a high thermal resistance. It is therefore interesting to investigate the possibility of using different materials with a low thermal conductivity coefficient, such as ceramics.

12.4 Piston and piston sealing

Two pistons were constructed during the project. The first piston, which relied on a very low tolerance with the cylinder to provide sealing, was not adequate. Friction was low, but the leakage was too high. Furthermore, friction increased significantly with misalignment of the piston. A second piston was made smaller to achieve sealing with a rolling diaphragm seal. Hermetic sealing was attained without adding much friction. The functioning of the diaphragm seal is very dependent on the pressure inside the engine. When the engine is in overpressure the seal is 'blown up' and pressed against the walls and cylinder. There is no rubber to rubber contact and friction is very low. However, as the engine always suffered from leakage, over-pressure was never maintained. This resulted in increased frictional losses.

12.5 Driving mechanism

The driving mechanism was found adequate for the application. An improvement can be made by replacing the belt that drives the encoder shaft by a gear transmission. This would provide a more accurate TDC reference.

12.6 Instrumentation

The second experiment, discussed in chapter 11, revealed that the pressure sensor in the cylinder rendered the best pressure reading. This sensor is also preferred as it records the exact pressure that is exerted on the piston. In a TLE, a single gas-volume is being simultaneously heated and cooled. It would be interesting to measure instantaneous gas temperatures throughout the cycle in the heater and the cooler. The temperature cycles would provide direct information on the heat transfer functions in the heater and the cooler. Thermocouples, however, are not able to perform these measurements. A solution to this problem should thus be found using different technologies.

To know the absolute pressure in the engine, a pressure sensor that can measure the absolute pressures should be installed. The sensor that was available in the lab was not water cooled and could thus not be used in the rig.

Chapter 13

Recommendations for Further Research

The results presented in this master thesis are only a first step to fully understanding the driving phenomena of the TLE. A path is now proposed in which future research should be headed.

13.1 Operating conditions

The first step that needs to be taken is to make the engine work in a wider range of conditions. To achieve this, both a positive cooler and heater effect should be observed in the pV-diagrams. Both heater and cooler need to be optimised.

13.1.1 Heater

First, the entire hot heat transfer area needs to be put at the desired temperature. Once this is achieved, the heat transfer capacity should be improved to obtain isothermal gas behaviour during expansion. For that, the influence of two heater parameters should be evaluated.

Thermal capacity As the heat input to the gas is not constant during a cycle, heater temperature will fluctuate during the cycle. To have a quasi constant temperature in the heater, the thermal inertia of the heater should be sufficient.

Heat transfer area As discussed in section 6.2, there is an optimum to be found in the heat transfer capacity of the heater. It should be high to support isothermal gas behaviour during expansion but limited to minimise heat input during compression. From this perspective, an ideal heater would consist of two sections: an isothermal section to enable optimal isothermal expansion and a non-isothermal section into which the cold gas can be compressed. This could be achieved by having a varying heat transfer area throughout the engine.

13.1.2 Cooler

To optimise cooler performance, research should focus on the surfaces that contribute to a positive cooling effect: the cylinder walls or the cylinder head. A positive cooling effect occurs when the most intense cooling regime takes place *at the right time* during the cycle: during compression.

An experiment comes to mind to evaluate the influence of the front wall of the cylinder: first a pV-diagram should be obtained when the engine runs with some free space left in front of the piston at the cylinder head. Then an insert should be placed at the cylinder head, which does not cover the entrance to the cylinder. The insert should be in contact with the front wall and increase its heat transfer area. By using different inserts with steadily increased heat transfer area, the recorded pV-diagrams can be compared to evaluate if the cooling improves during compression.

13.2 Trends

After optimisation of the heater and the cooler to the extent that the rig works as an engine over a range of working conditions, different engine configurations can be compared. Work output and pV-diagrams should be evaluated while varying the following engine parameters:

- Piston stroke
- Engine speed
- Ratio of hot to cold volume

Analysing these trends will give insight in the engine configurations that achieve optimal engine performance. It will also help to identify which adjustments to the rig have the highest potential of increasing engine performance further.

13.3 Optimisation

At this stage, it would be interesting to investigate the claims that have been made in literature. The experiments of both Tailer and Organ should be reproduced in the same test engine. As discussed in the underlying physics, see chapter 6, there are multiple ways to implement the thermal lag effect that dephases heat transfer and volume function. To optimise engine performance, the focus of the research should lie in identifying which implementations tend to create the optimal 90° phase shift, and thus maximise efficiency.

In a last stage of optimisation, improvements that propelled Stirling technology to higher power outputs, such as increasing internal pressure, should be investigated. However, not all improvements in Stirling engine technology can be assumed to be beneficial in the TLE. For example, having a regenerator between the hot and the cold section will not always improve work output.

A last recommendation originates from both literature and the experiments that were performed in this project. Both West and Tailer stated that improvements in work output could be obtained when the speeds at which expansion and compression occur are varied [11] [20]. In the experiments described in chapter 10, the influence of the limited flywheel inertia is shown. Influencing the speeds at which compression and expansion occur, by varying flywheel inertia or using cams, will be an interesting field of research.

13.4 Mindset

Experiments that are designed to investigate certain effects in the TLE should not be approached in the same way as for conventional heat engines. The processes that occur within the engine cannot easily be separated in time. Heat transfer functions in both cooler and heater are continuous in time and influence each other to a great extent. Therefore they cannot be treated independently. For example, if the heat transfer capacity of the heater is improved, the gas that enters the cylinder during expansion will be hotter. This will also increase the cooler's performance as the temperature difference between gas and wall is increased. When designing experiments, one should thus be aware that when changing a single parameter it is likely that more processes in the engine will be influenced. These interactions make it difficult to give the correct interpretation of the observations that are made.

Chapter 14

Conclusions

A literature study was performed to identify the state of the art concerning the Thermal Lag Engine (TLE). Only a handful of researchers have worked on the subject: Peter Tailer, the inventor of the TLE [11], Colin D. West and Allan Organ being the most important. At first sight, the claims that had been made about the driving mechanism of the engine seemed very contradictory. This culminated in the statement of Organ that the TLE patent that Tailer had been granted in 1995 seemed inconsistent with how the engine works [24]. Tailer and West consider bulk shifts of mass between the hot and the cold space [19] [20]. Organ, however, considers shifts in gas temperature profiles based on the pulse tube principle [24]. Only Tailer and Organ have made the effort of building a TLE on which measurements could be performed. Furthermore these experiments view the engine as a black box from which only work output is observed. Engine parameters were changed and the effect on engine performance was observed and interpreted. No correspondance can be made between the different experiments as both engines have subtle differences in configuration and the published results lack crucial information. Organ made a numerical analysis of his engine, but again little correspondance can be found between his results.

Different working principles were claimed, but all of these researchers lack the experimental proof to back up their statements. Thorough analysis of the proposed working mechanisms further revealed that they are not explicitly contradictory, but represent different implementations of the same effect. Discussions in literature about minor differences in effects overlook the essence, which is the dephasing of the heat transfer and the movement of the piston. Future research should investigate the different claims that have been made in literature to identify which implementation of the thermal lag effect can maximise engine performance.

To be able to validate the claims that are made about the driving mechanisms of this engine, a thermal lag test engine was designed and built to perform experiments and to measure the first pressure versus volume diagrams of this type of engine. The requirements for the test rig were based on the claims concerning the possible working principles and descriptions of previously built engines in literature. The design incorporates the possibility to adopt the engine configurations of both Organ and Tailer. It allows to reproduce their experiments and investigate optimal operating conditions. Furthermore, the rig is equipped with a variety of sensors to measure inside the engine in order to derive pV-diagrams and acquire a more profound insight in the inner workings of the TLE.

Two experiments have been conducted in which energy balances and pV-diagrams were obtained. The first energy balance did not close sufficiently and improvements were proposed. The heater proved insufficient but a distinct cooler effect was observed, allow the cycles to provide a net work output. The observations indicate an intensified cooling regime occurring at a certain point *during* compression, suggesting that cooling picks up due to increased circulating gas flow. Neither Tailer, West or Organ have predicted or anticipated this cooling behaviour. They all state that the major pressure drop of the gas, due to cooling, happens during the dwell time *at* bottom dead centre. The experiments also illustrate the important influence of engine speed on the cycle. When optimising a TLE, the engine speed should be adapted to the ratio of heat transfer capacities of the heater and cooler.

In the second experiment, the method to measure the energy balance was made more accurate. A water leak from the pressure sensor cooling circuit, however, made it impossible to determine the error on the acquired energy balance. The heater was improved by adding heating elements but was still not sufficient. Nonetheless, a positive heater affect was observed on the pV-diagram during expansion. The cooling effect, however, was lost. Furthermore, the additional heating elements raised the temperature of the cylinder head. A suggestion was made concerning the influence of the cylinder head on the cooling. This confirms the observation made by Tailer that an increased heat transfer area in the cylinder head improves engine performance [22].

The results presented in this master thesis are an important first step in understanding the driving phenomena of the TLE based on measurements inside the engine. A wide range of recommendations was given regarding future research. It reveals that this field of research is still wide open.

With the experiences of the experiments, a critical review was given on the test rig design. The flexibility that was included in the design proved to be a limiting factor due to unforeseen problems, such as the difficulty of sealing the engine. Design should be focused on simplicity and robustness. Instead of using a single complex heater, multiple simple heaters that are interchangeable are recommended.

The developments and challenges cited uncover vast opportunities the TLE to become a sustainable engine for the future.

Part V

Appendices

Appendix A

Oil Reservoir

The heat source for the test engine consists of an annular space, formed by an inner and outer copper tube. This space is filled with a thermal oil - Therminol 66 - at ambient temperature and pressure (20 °C and 1.013 bar). Under working conditions the oil is heated up to 300°C by thermal resistors which are immersed in the oil. As the oil tends to expand with the elevated temperature, pressure in the annular space goes up. Let us first calculate this pressure rise:

'Therminol 66' has the following physical properties[1], required for this problem:

- Volumetric thermal expansion coefficient at 200 °C: $\alpha = 0.000819\ /°C$
- Compressibility at 300°C: $\beta = 2.0 \times 10^{-9}\ m^2/N$

Remark: The compressibility of Therminol 66 was obtained after an inquiry with the producing company. At the time they did not have exact data available, but gave this value as a rough estimation. Using these properties, an approximation of the pressure increase can be found:

$$\begin{aligned} \Delta p &= \frac{\alpha}{\beta}\ \Delta T \\ &= \frac{0.000819\ /°C}{2.0 \times 10^{-9}\ m^2/N} \times (300°C - 20°C) \\ &= 114.66\ MPa \end{aligned} \tag{A.1}$$

This clearly is unacceptable. The copper tubes will never be able to withstand this rise of pressure. Therefore it is necessary to allow the oil to expand. A solution is to make an expansion tank which is connected to the oil in each heated tube. This also seals off the oil from the surrounding atmosphere, preventing gases to escape. We will now calculate the necessary volume of the expansion tank. The first problem is to calculate the volume increase of the oil.

[1] Therminol 66: http://www.therminol.com/pages/products/66.asp

The annular space has an outer diameter of 46 mm (inside diameter of outer tube), an inner diameter of 22 mm (outside diameter of inner tube) and a length of 400 mm. This gives:

$$\begin{aligned} V_{oil,tube} &= \pi \times \frac{(0.046\ m)^2 - (0.022\ m)^2}{4} \times 0.4\ m \\ &= 5.13\ 10^{-4}\ m^3 = 0.513\ liter \end{aligned} \tag{A.2}$$

Due to the temperature rise of 20°C to 300°C, the oil volume increase of each tube is approximated by:

$$\begin{aligned} \Delta V_{oil,tube} &= \alpha \times V_0 \times \Delta T \\ &= 0.000819\ /°C \times 0.513\ liter \times (300°C - 20°C) \\ &= 0.118\ liter \end{aligned} \tag{A.3}$$

The total increase of oil volume in the reservoir will be five times this amount, $\Delta V_{tot} = 0.59\ liter$. The problem is described in figure A.1. The oil volume increase will be buffered by the air that experiences a pressure rise. We need to keep this pressure rise low enough to be able to contain it safely.

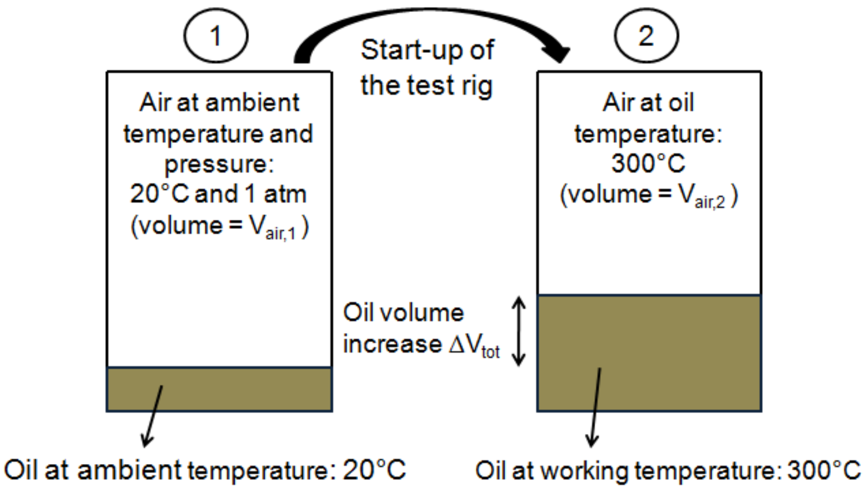

Figure A.1: Physical Problem

Going from state 1 to 2, the air undergoes two changes: volume decreases with ΔV_{tot} and the temperature rises from 20°C to 300°C, that is from 293.15 K to 573.15 K. The tank is assumed to be closed at atmospheric pressure. To determine the pressure in state 2, the two states are linked with the ideal gas law and constant mass:

$$m_{air} = \frac{p_1 \times V_1}{R_{air} \times T_1} = \frac{p_2 \times (V_1 - \Delta V_{tot})}{R_{air} \times T_2} \tag{A.4}$$

Solving for p_2 gives:

$$\begin{aligned} p_2 &= p_1 \times \frac{V_1 \times T_2}{(V_1 - \Delta V_{tot}) \times T_1} \\ &= 1.013\ bar \times \frac{V_1 \times 573.15\ K}{(V_1 - 0.59\ liter) \times 293.15\ K} \end{aligned} \tag{A.5}$$

Pressure p_2 however will be less than the actual pressure in the tank. By going to a higher temperature, some of the oil will also evaporate to reach the two-phase equilibrium with its vapour. The vapour pressure of the oil at 300°C should be added to p_2 to form the actual resulting pressure p_{end}. Vapour pressure of Therminol 66 at 300°C is 0.3073 bar. The resulting air pressure p_{end} is plotted against the initial volume V_1 in figure A.2.

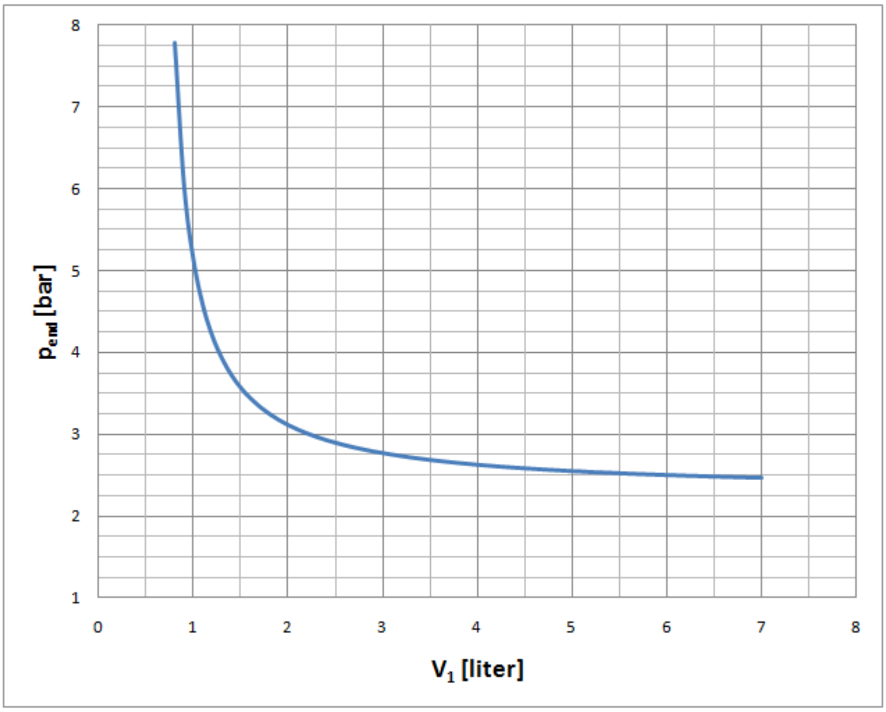

Figure A.2: Pressure p_{end} versus Volume V_1

The expansion tank is designed as a cylinder, as this is the best geometry to handle internal pressures. To close the tank, a plate is welded at the top and bottom of the cylinder. The internal diameter and height of the cylinder are respectively 15 cm and 30 cm. If we assume the initial oil level in the tank to be 1 cm, we get:

$$V_1 = \frac{\pi \times 0.15\ m^2}{4} \times 0.29\ m = 5.125\ liter \tag{A.6}$$

The resulting end pressure p_{end} will, according to figure A.2, be 2.545 bar. The expansion tank walls are designed to be 5 mm, so that this internal pressure is easily handled. The oil from the heater tubes is collected by small copper pipes, who congregate, and led to the bottom of the expansion tank. Right before it enters the tank, the pipe makes a U shape downwards. This creates a temperature inversion, so that the oil can not flow into the tank because of its buoyancy. The support of the tank ensures that its bottom stands higher than the heater tubes. This way, the tubes can be filled by pouring the oil in the tank. To allow this, a threaded hole is made in the top of the tank. Small holes are needed in the heater tubes to allow the air to escape during filling. A CAD-drawing can be seen in figure A.3.

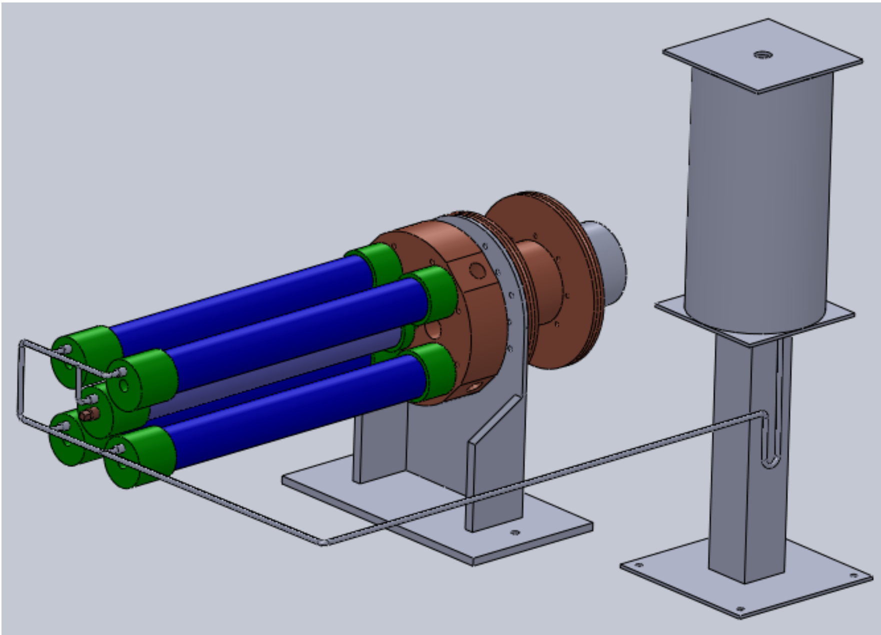

Figure A.3: Heater Tubes With Oil Reservoir

Appendix B

Oil Temperature Fluctuation

The power supply to the resistors is constant, 1 kW. During an engine cycle, the heat drawn from the resistors will not be constant however. This will be a function of time. As there is no experimental data available at the moment about the nature of the heat output function, assumptions must be made. In this case, the ideal TLE cycle with the assumption of a sinusoidal heat transfer and volume function will be used, see figure B.1. This has been discussed in detail in section 6.1.

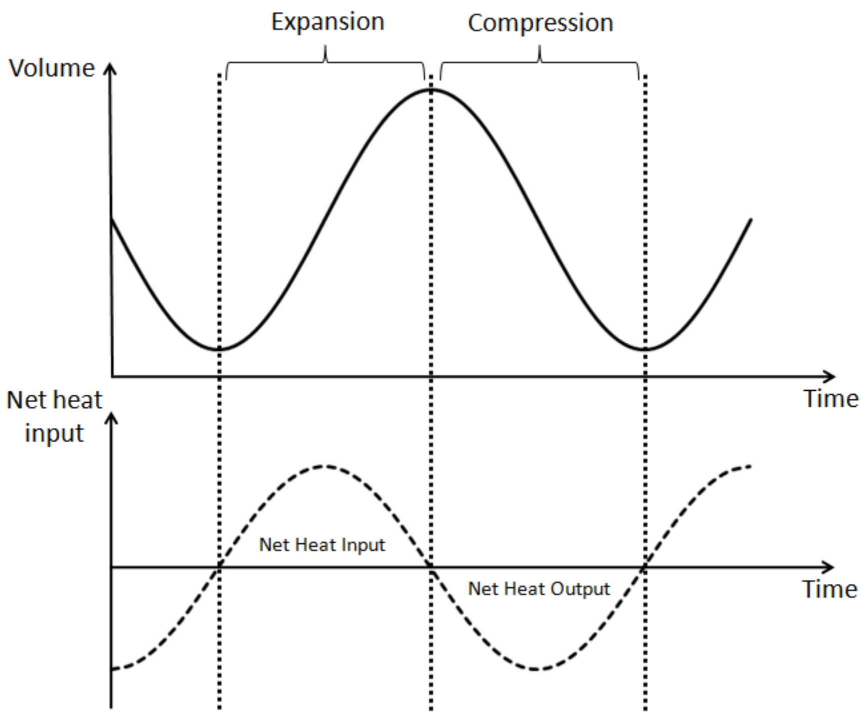

Figure B.1: Heat Transfer and Volume function in an ideal TLE with assumed sinusoidal behaviour

As can be seen, there is no heat input to the gas during compression. All the heat input to the gas is delivered during expansion which stretches over half of the cycle period (because of the assumed sinusoidal behaviour). In a test engine, the heat input should be provided by a constant temperature source. This will not be the case with the resistors alone, as they have a small mass. Resistor temperature will fluctuate throughout the cycle because the instantaneous electrical power input does not equal the instantaneous heat output. To reduce this hot source temperature fluctuation, the resistors are immersed in a oil bath. The mass of the oil forms a thermal buffer. To calculate the temperature swing of the oil, we must consider the problem described in figure B.2. We will now calculate the oil temperature function in time and the resulting temperature fluctuation.

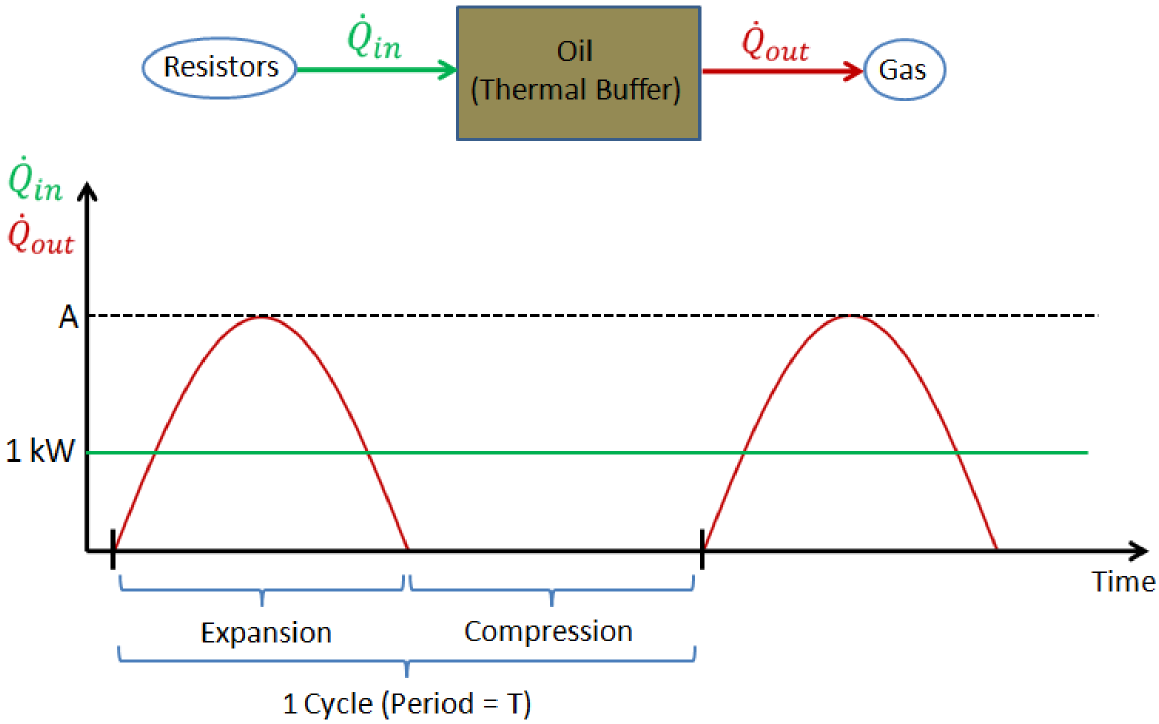

Figure B.2: Physical Problem with Oil as Thermal Buffer

To make sure that the mean temperature of the oil stays constant, heat input and heat output must be equal during each cycle. With this consideration we can determine the amplitude A of the heat output from integrating the energy balance over one cycle with period T (time t = 0 at the beginning of this cycle):

$$\int_0^T \dot{Q}_{in}(t)dt = \int_0^T \dot{Q}_{out}(t)dt \tag{B.1}$$

The heat transfer functions are:

$$\dot{Q}_{in}(t) = 1 \ kW \tag{B.2}$$

$$\dot{Q}_{out}(t) = \begin{cases} A \sin\left(\frac{2\pi}{T} \times t\right) & , \ 0 \leq t \leq T/2 \\ 0 & , \ T/2 \leq t \leq T \end{cases} \tag{B.3}$$

Substituting (B.2) and (B.3) in equation (B.1) and solving for A gives:

$$A = \pi \ kW \tag{B.4}$$

To determine the temperature fluctuation, we must solve the time rate form of the energy balance:

$$\frac{\partial U_{oil}(t)}{\partial t} = \dot{Q}_{in}(t) - \dot{Q}_{out}(t) \tag{B.5}$$

With $U_{oil}(t)$ the internal energy of the oil mass, integrating this equation in time gives:

$$\int_0^t \frac{\partial U_{oil}(t)}{\partial t} dt = U_{oil}(t) - U_{oil}(0) = \int_0^t \dot{Q}_{in}(t)dt - \int_0^t \dot{Q}_{out}(t)dt \tag{B.6}$$

Substituting (B.2), (B.3) and (B.4) in equation (B.6) and solving for U(t) gives:

$$U_{oil}(t) = \begin{cases} U_{oil}(0) + 1 \ kW \times t - \frac{T}{2}(1 - \cos(\frac{2\pi}{T} \times t)) \ kW & , \ 0 \leq t \leq T/2 \\ U_{oil}(0) + 1 \ kW \times t - T \ kW & , \ T/2 \leq t \leq T \end{cases} \tag{B.7}$$

The initial condition $U_{oil}(0)$ must now be found. This can be done by expressing that the mean temperature of the oil throughout the cycle is 300℃ = 573.15 K. With $U_{oil}(t) = m_{oil} \times c_{oil} \times T_{oil}(t)$:

$$\frac{1}{T} \int_0^T T_{oil}(t)dt = \frac{1}{T} \int_0^T \frac{U_{oil}(t)}{m_{oil} \times c_{oil}} dt = 573.15 \ K \tag{B.8}$$

The heat capacity of the oil is assumed to be constant. Substituting (B.7) in (B.8):

$$\frac{1}{T \times m_{oil} \times c_{oil}} \left(U_{oil}(0) \times T - \frac{T^2}{4} \ kW \right) = 573.15 \ K \tag{B.9}$$

The thermal oil used is Therminol 66[1]. At 300℃, the heat capacity is $c_{oil} = 2.569 \ kJ/kgK$. The oil in each tube sits in an annular space with an internal diameter of 22 mm, an external diameter of 46 mm and a length of 400 mm. As there are 5 tubes and Therminol has a density of 808.5 kg/m^3, the total oil mass m_{oil} becomes:

$$\begin{aligned} m_{oil} &= \rho_{oil} \times V_{oil} \\ &= 808.5 \ kg/m^3 \times 5 \times \frac{\pi \times (0.046^2 - 0.022^2) \ m^2}{4} \times 0.4 \ m \\ &= 0.41452 \ kg \end{aligned} \tag{B.10}$$

[1] Therminol 66: http://www.therminol.com/pages/products/66.asp

Solving equation (B.9) for $U_{oil}(0)$ gives:

$$\begin{aligned} U_{oil}(0) &= m_{oil} \times c_{oil} \times 573.15\ K + \frac{T}{4}\ kW \\ &= 0.41452\ kg \times 2.569\ kJ/kgK \times 573.15\ K + \frac{T}{4}\ kW \\ &= 610.35\ kJ + \frac{T}{4}\ kW \end{aligned} \tag{B.11}$$

The initial condition $U_{oil}(0)$ is now found. Substituting this result in equation (B.7) gives the fluctuation of the internal energy of the oil during the cycle, in function of its period T:

$$U_{oil}(t) = \begin{cases} 610.35\ kJ + \frac{T}{4}\ kW + 1\ kW \times t - \frac{T}{2}(1 - \cos(\frac{2\pi}{T} \times t)) & ,\ 0 \leq t \leq T/2 \\ 610.35\ kJ + \frac{T}{4}\ kW + 1\ kW \times t - T\ kW & ,\ T/2 \leq t \leq T \end{cases} \tag{B.12}$$

Dividing $U_{oil}(t)$ by $m_{oil} \times c_{oil}$ and substracting 273.15 K from it, gives the temperature fluctuation during the cycle in °C. Notice that this temperature fluctuation is a function of time and of the period T of the cycle. We design the engine for a frequency range of 1 Hz to 10 Hz. This means a cycle period of 0.1 s to 1 s. The oil temperature fluctuations are plotted for 3 Hz and 7 Hz in respectively figure B.3 and figure B.4.

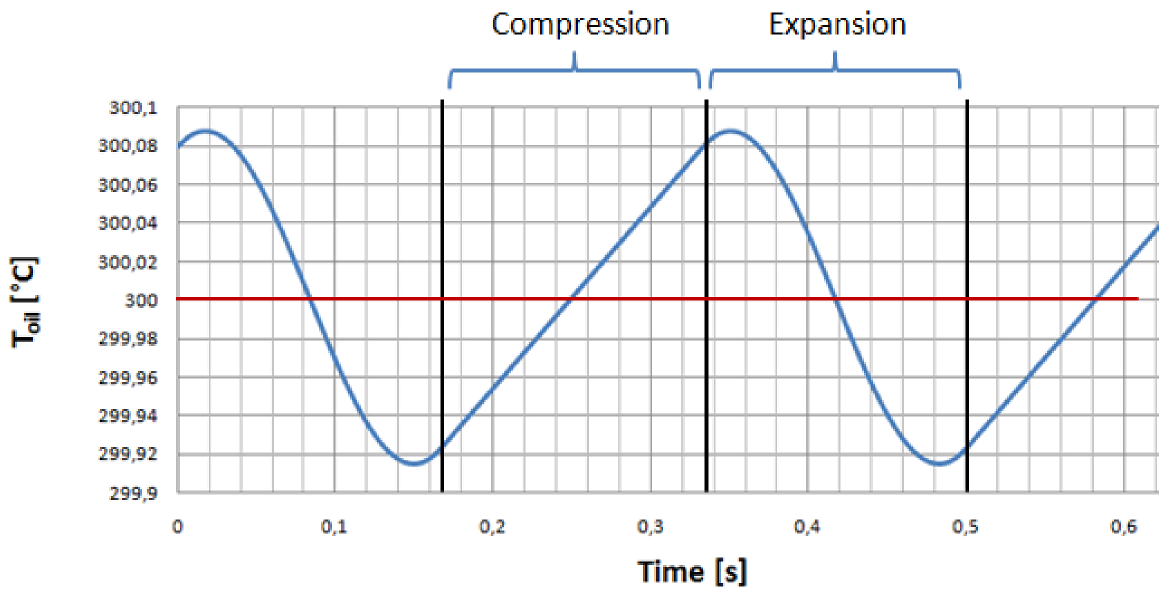

Figure B.3: Oil Temperature Fluctuation when Engine runs at 3 Hz

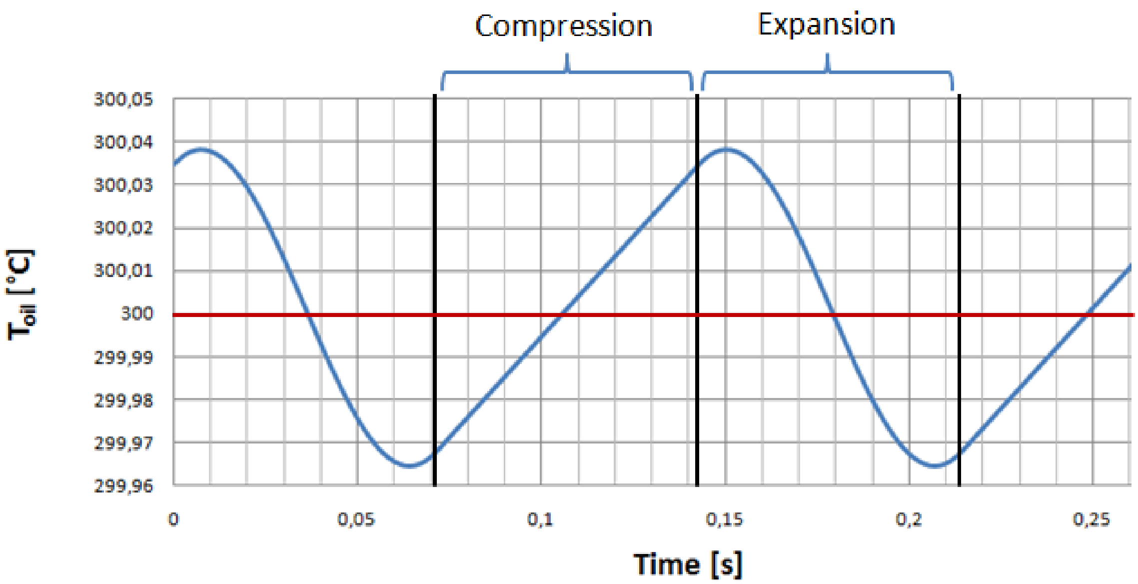

Figure B.4: Oil Temperature Fluctuation when Engine runs at 7 Hz

To understand these waveforms, one must look simultaneously at figure B.2. At the start of expansion, $\dot{Q}_{out}$ is smaller than $\dot{Q}_{in}$. Therefore the oil temperatures rises. It does not take long however for $\dot{Q}_{out}$ to rise above $\dot{Q}_{in}$ and as a result the oil temperature drops. This stays the case during most of the expansion. It is only at the end of expansion that $\dot{Q}_{out}$ again decreases below $\dot{Q}_{in}$, allowing the oil temperature to increase. During the compression, the gas draws no heat from the oil and the power input is used to refill the oil's energy reservoir.

Notice that the amplitude of the temperature fluctuation is bigger when the frequency is smaller. The reason for this is that the differences between $\dot{Q}_{in}$ and $\dot{Q}_{out}$ are maintained for a longer time, as the period T increases. As a result, the biggest temperature fluctuations will occur at the lowest frequency: 1 Hz. With the help of equation (B.12), the minimum and maximum oil temperature at 1 Hz (T = 1 s) are calculated to be respectively 300.260℃and 299.743℃. Relative to the mean temperature, the temperature swing is:

$$\begin{aligned} Relative\ Temperature\ Swing &= \frac{T_{oil,max} - T_{oil,min}}{T_{oil,mean}} \\ &= \frac{300.260°C - 299.743°C}{300°C} \\ &= 0.1723\% \end{aligned} \tag{B.13}$$

This temperature swing is acceptable for our application.

Appendix C

Frictional Losses of Piston Sealing: Viton O-ring

A piston running in a cylinder is traditionally sealed by sliding piston or rod rings. These can be either metal or rubber O-rings. This sealing method has two main disadvantages, however. First, when working with gas, a significant leakage rate for our application is unavoidable. Second, the rings slide against the cylinder walls, generating serious frictional losses. To have an indication of the order of magnitude of this loss, a calculation was made based on formulas and data taken from the Parker O-ring Handbook [?]. The calculations focus on running friction. It can be assumed break-out friction is a multiple of this number. The following formulas are used to estimate the frictional loss, with a glossary of the used abbreviations in table C.1:

$$\begin{aligned} F_c &= f_c \times L_r \\ F_h &= f_h \times A_r \\ F &= F_c \times F_h \end{aligned} \tag{C.1}$$

Abbreviation	**Description**
A_r	Projected area of seal for rod groove applications
F	Total seal friction in pounds
F_c	Total friction due to seal compression
F_h	Total friction due to hydraulic pressure on the seal
f_c	Friction due to O-ring compression obtained from figure X
f_h	Friction due to fluid pressure obtained from figure X
L_r	Length of seal rubbing surface in inches for rod groove applications

Table C.1: Abbreviations used in friction calculations

The dimensions, projected areas and friction factors are taken from the Parker O-ring Handbook. It is important to remark that the values of f_c and f_h taken from the plots in figure C.1 are different for every application. This calculation offers only an indication of the order of magnitude of the frictional loss.

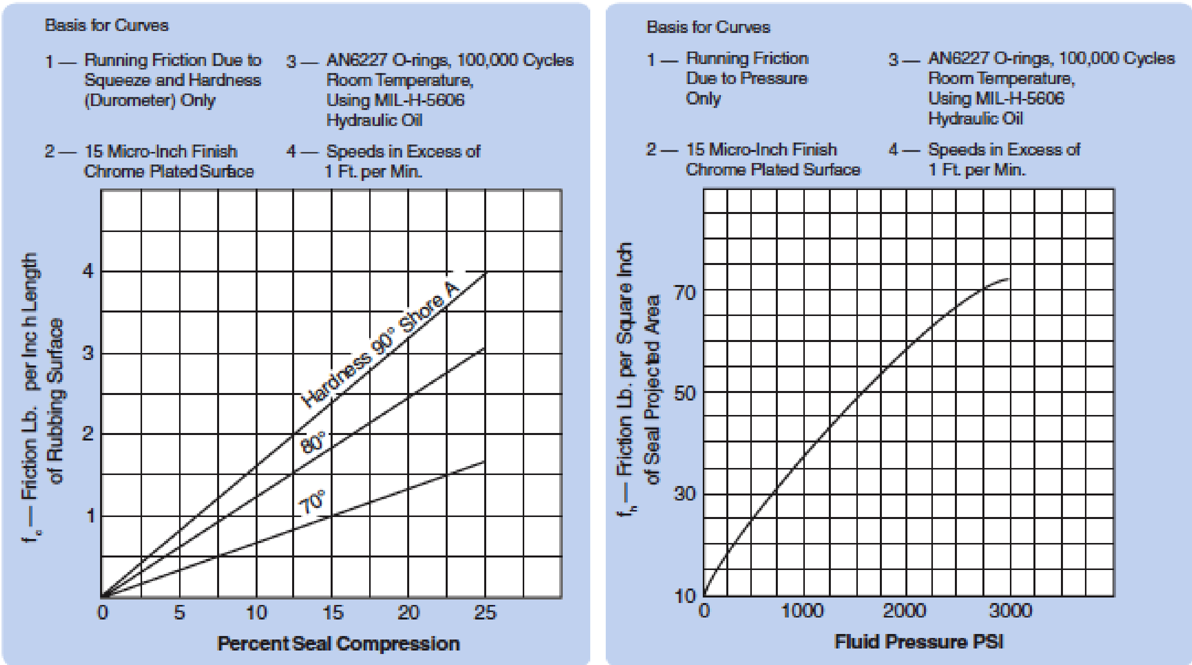

(a) Friction due to O-ring compression

(b) Friction due to fluid pressure

Figure C.1: Friction coefficients taken from the Parker O-ring Handbook

We assume no fluid pressure, average rubber hardness (70°-80°) and 5% seal compression. The following values are derived from the plots in figure C.1 and dimension tables in the Parker O-ring Handbook.

$$Ar = 2.17\ sq.\ in.$$
$$Lr = 10.99\ in.$$
$$fc = 0.5\ \frac{Lb.}{in.}$$
$$fh = 10\ \frac{Lb.}{\text{sq. in.}}$$

The occurring forces can now be calculated according to the formulas in C.1.

$$Fc = 0.5 \times 10.99 = 5.495 Lb.$$
$$Fh = 10 \times 2.17$$
$$F = Fc = 27.195 Lb.$$

This force multiplied by the average piston speed gives an indication of power loss by friction.

$$\begin{aligned} P &= \frac{F\ Lb. \times 0.08\ m \times 5\ Hz}{0.3048\ m/ft} \\ &= 35.69\ \frac{ft.Lb.}{s} \\ &= 48.4\ W \end{aligned}$$

High frictional loss, unavoidable leakage and expected wear of the brass cylinder make the option of sliding rings unsuitable for the application.

Appendix D

Heat Losses

A rectangular wooden box is placed around the hot section of the engine, which is formed by collector and heater tubes. Inside the box an insulation layer is glued with a thickness of 10 cm. With the following procedure, an indication of the heat losses to the surroundings can be found. To calculate the maximum heat loss, we assume the collector and heater tubes walls to be at 300°C.

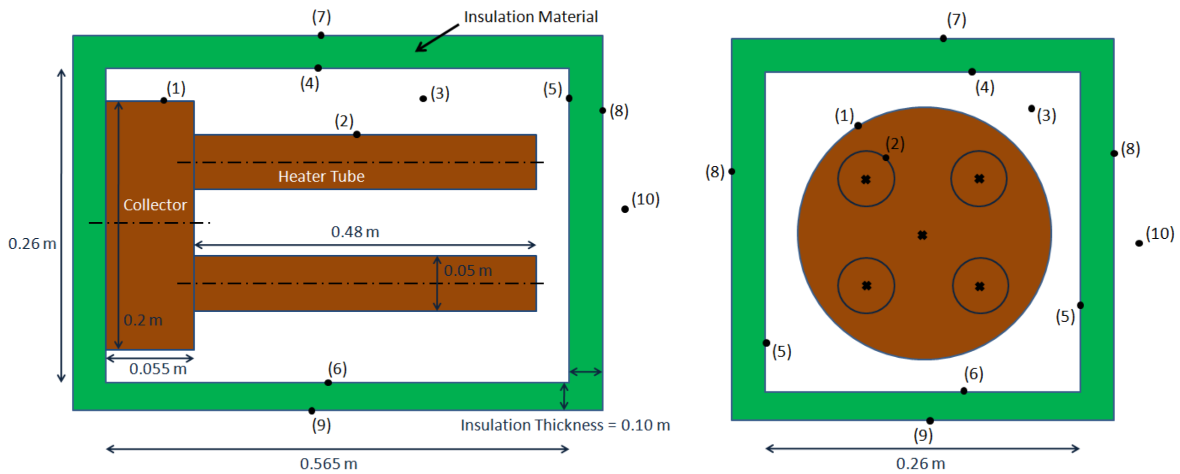

(a) Side View

(b) Front View

Figure D.1: Simplified Problem

A simplification of the physical situation is given in figureD.1(a) and D.1(b). The surfaces and fluids are numbered. The air inside the insulation is labeled as (3). The atmospheric air (10) is assumed to be at 20°C. The heat that is lost through the wall that touches the collector is not considered here. This heat loss flows to the cooler. The thermal resistance network that is used to solve the problem is given in figure D.2.

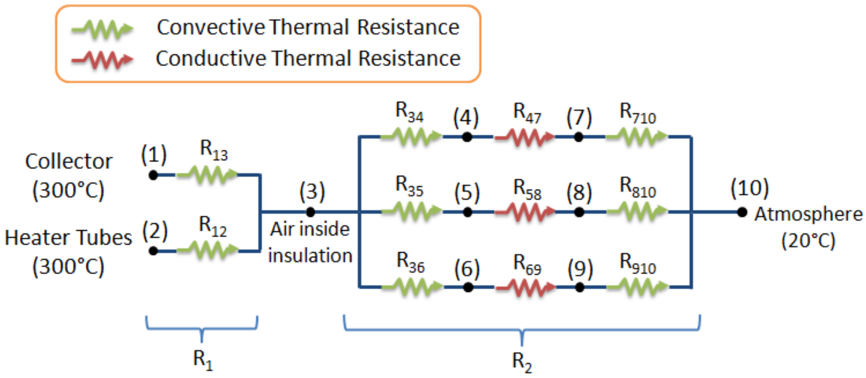

Figure D.2: Thermal Resistance Network

When all thermal resistances are known, the resulting heat loss to the surroundings will be given by:

$$Q = \frac{\Delta T}{R_1 + R_2} = \frac{280\ K}{R_1 + R_2} \tag{D.1}$$

In all correlations used below, air properties must be evaluated at film temperature $T_f = (T_s + T_\infty)/2$.

R_{47} - R_{58} - R_{69} The used insulation material is rockwool. The product that is used in this design is Rockwool Rockfit 431 Adapt[1]. Thermal conductivity from the datasheet is 0.036 W/mK. With a thickness t of 10 cm, the conductive thermal resistances can be calculated as:

$$\begin{aligned} R_{47} &= \frac{t}{k_{rw} \times A_{47}} = \frac{0.10\ m}{0.036\ \frac{W}{mK} \times 0.26\ m \times 0.565\ m} \\ &= 18.909\ \frac{K}{W} \\ R_{69} &= \frac{t}{k_{rw} \times A_{69}} = \frac{0.10\ m}{0.036\ \frac{W}{mK} \times 0.26\ m \times 0.565\ m} \\ &= 18.909\ \frac{K}{W} \\ R_{58} &= \frac{t}{k_{rw} \times A_{58}} = \frac{0.10\ m}{0.036\ \frac{W}{mK} \times (2 \times 0.26\ m \times 0.565\ m + 0.26\ m \times 0.26\ m)} \\ &= 7.686\ \frac{K}{W} \end{aligned} \tag{D.2}$$

The area A_{58} incorporates both inner side walls of the box and the inner wall at the free end of the heater.

R_{13} - R_{23} For the convective resistances R_{13} and R_{23} (convection from the engine to the air inside the insulation) the convection coefficients must be determined. This is done by using

[1]Rockwool Rockfit 431 Adapt: http://www.rockwool.be/

the correlation of Churchill and Chu for 'natural convection around long horizontal cylinders' [29]. The resulting values will be nothing but an approximation of the actual convection coefficients because of the following reasons:

- The collector is not a long cylinder so there is an influence of the end faces on the flow pattern.
- The heater tubes are in close proximity of each other and thus the air flow differs from the case of an individual cylinder.
- The cylinders are not placed in free space, but in a closed box.

Churchill and Chu propose the following correlation in the range of $10^{-5}<Ra_D<10^{12}$:

$$Nu_D = \left(0.60 + \frac{0.387\ Ra_D^{1/6})}{\left[1+(0.559/Pr)^{9/16}\right]^{8/27}}\right)^2 = \frac{h \times D}{k_f} \tag{D.3}$$

The Rayleigh number is given by:

$$Ra_D = \frac{g\beta\ (T_s - T_\infty)\ D^3}{\nu^2} \times Pr \tag{D.4}$$

For the thermal resistances we get:

$$R_{13} = \frac{1}{h_{13} \times A_{13}} = \frac{1}{h_{13} \times \pi \times 0.2\ m \times 0.055\ m} \tag{D.5}$$

$$R_{23} = \frac{1}{h_{23} \times A_{23}} = \frac{1}{h_{23} \times 5 \times \pi \times 0.05\ m \times 0.48\ m} \tag{D.6}$$

R_{34} - R_{710} For the resistances R_{34} and R_{710} the correlations should be used for natural convection along a horizontal plate. In the case of R_{34} this is a 'cold surface facing down'. For R_{710} this is a 'hot surface facing up'. To find the convection coefficients, the correlation of McAdam is used [29]:

$$Nu_L = 0.54\ \sqrt[4]{Ra_L} = \frac{h \times L}{k_f} \tag{D.7}$$

The Rayleigh number is given by:

$$Ra_L = \frac{g\beta\ |T_s - T_\infty|\ L^3}{\nu^2} \times Pr \tag{D.8}$$

L is the ratio of area to perimeter. We get:

$$L_{34} = \frac{(0.26\ m \times 0.565\ m)}{2 \times (0.26\ m + 0.565\ m)} = 0.08903\ m \tag{D.9}$$

$$L_{710} = \frac{(0.26\ m + 2 \times 0.10\ m) \times (0.565\ m + 2 \times 0.10\ m)}{2 \times (0.26\ m + 0.565\ m + 4 \times 0.10\ m)} = 0.14363\ m \tag{D.10}$$

The thermal resistances are then obtained by:

$$R_{34} = \frac{1}{h_{34} \times A_{34}} = \frac{1}{h_{34} \times 0.26\ m \times 0.565\ m} \tag{D.11}$$

$$R_{710} = \frac{1}{h_{710} \times A_{710}} = \frac{1}{h_{710} \times (0.26\ m + 2 \times 0.10\ m) \times (0.565\ m + 2 \times 0.10)} \tag{D.12}$$

R_{36} - R_{910} The correlations used for these convection coefficients are also given by McAdam [29]. These are correlations for 'cold surfaces facing up' or 'hot surfaces facing down':

$$Nu_L = 0.27\ \sqrt[4]{Ra_L} = \frac{h \times L}{k_f} \tag{D.13}$$

The Rayleigh number is also given by equation (D.8). Again, L is the ratio of area to perimeter:

$$L_{36} = L_{34} = 0.08903\ m \tag{D.14}$$

$$L_{910} = L_{710} = 0.14363\ m \tag{D.15}$$

The thermal resistances become:

$$R_{36} = \frac{1}{h_{36} \times A_{36}} = \frac{1}{h_{36} \times 0.26\ m \times 0.565\ m} \tag{D.16}$$

$$R_{910} = \frac{1}{h_{910} \times A_{910}} = \frac{1}{h_{910} \times (0.26\ m + 2 \times 0.10\ m) \times (0.565\ m + 2 \times 0.10)} \tag{D.17}$$

R_{35} - R_{810} For these thermal resistances, correlations must be used for natural convection along a vertical plate. Churchill and Chu proposes the following expression for the Nusselt number [29]:

$$Nu_L = \left(0.825 + \frac{0.387\ Ra_L^{1/6})}{\left[1 + (0.429/Pr)^{9/16}\right]^{8/27}}\right)^2 = \frac{h \times L}{k_f} \tag{D.18}$$

Here, L is the vertical height of the plate. $L_{35} = 0.26\ m$ and $L_{810} = 0.26\ m + 2 \times 0.10\ m = 0.46\ m$. The Rayleigh number is again given by equation (D.8). The thermal resistances can be then calculated:

$$R_{35} = \frac{1}{h_{35} \times A_{35}} = \frac{1}{h_{35} \times (2 \times 0.26\ m \times 0.565\ m + 0.26\ m \times 0.26\ m)} \tag{D.19}$$

The area A_{810} must incorporate both outer side walls of the box and the outer wall at the free end of the heater:

$$\begin{aligned} A_{810} &= (0.26\ m + 2 \times 0.10\ m)^2 + 2 \times (0.565\ m + 2 \times 0.10\ m) \times (0.26\ m + 2 \times 0.10\ m) \\ &= 0.9154\ m^2 \end{aligned} \tag{D.20}$$

Thermal resistance R_{810} then becomes:

$$\begin{aligned} R_{810} &= \frac{1}{h_{810} \times A_{810}} \\ &= \frac{1}{h_{810} \times 0.9154\ m^2} \end{aligned} \tag{D.21}$$

R_1 **-** R_2 The combined thermal resistances, as defined in figure D.2, can be calculated from:

$$R_1 = \left(\frac{1}{R_{13}} + \frac{1}{R_{23}}\right)^{-1} \tag{D.22}$$

$$R_2 = \left(\frac{1}{R_{34} + R_{47} + R_{710}} + \frac{1}{R_{35} + R_{58} + R_{810}} + \frac{1}{R_{36} + R_{69} + R_{910}}\right)^{-1} \tag{D.23}$$

When these thermal resistances are known, the total heat loss can be calculated from equation D.1.

Solution Method To solve the previous problem, air properties should be evaluated at film temperatures which are not known initially as the surface temperatures are not known. Therefore the solution must be obtained through iteration. First, an estimation of all the wall temperatures and the air temperature inside the insulation is made. The necessary air properties can then be inserted in the above equations to find the convective thermal resistances. The conductive thermal resistances stay the same as, according to the datasheet, the thermal conductivity of the rockwool is the same for a wide temperature range. After this first iteration, a first indication of the heat loss Q is known. The estimated temperatures should be checked however. This can be done using the following formulas:

$$T_3 = 300\text{°C} - Q \times R_1 \tag{D.24}$$

To check the remaining temperatures, the heat flow through the top of the box Q_{up}, through the side walls Q_{side} and through the bottom of the box Q_{down} is calculated:

$$Q_{up} = \frac{T_3 - 20\text{°C}}{R_{34} + R_{47} + R_{710}} \tag{D.25}$$

$$Q_{down} = \frac{T_3 - 20\text{°C}}{R_{36} + R_{69} + R_{910}} \tag{D.26}$$

$$Q_{side} = \frac{T_3 - 20\text{°C}}{R_{35} + R_{58} + R_{810}} \tag{D.27}$$

The remaining wall temperatures are then found from:

$$T_4 = T_3 - Q_{up} \times R_{34} \tag{D.28}$$

$$T_5 = T_3 - Q_{side} \times R_{35} \tag{D.29}$$

$$T_6 = T_3 - Q_{down} \times R_{36} \tag{D.30}$$

$$T_7 = T_4 - Q_{up} \times R_{47} \tag{D.31}$$

$$T_8 = T_5 - Q_{side} \times R_{58} \tag{D.32}$$

$$T_9 = T_6 - Q_{down} \times R_{69} \tag{D.33}$$

After the calculation of these temperatures, a second iteration must be performed. Using the new obtained temperatures, air properties must be re-evaluated, which will result in differenct convection coefficients. The same procedure as above will then yield new temperatures that can be used for a third iteration, etc. After a few iterations, the temperatures will be converging and a final solution is found. The results of each iteration is found in table D.3.

The resulting heat loss to the surroundings is thus 52 W. 12 W goes through the top of the box, 29 W through the side walls and 11 W through the bottom of the box. These losses are acceptable for our application. They are however significant relative to the given input power, 1 kW. Hence, measurement of the actual heat losses are necessary. This is easy to do with the box configuration. With a thermocouple on the inside and outside of each wall, the heat losses through that wall can be calculated accurately with the conduction formula. The maximum temperature on the outside of the box will be 34℃.

	[Unit]	Iteration nr. 1	Iteration nr. 2	Iteration nr. 3	Iteration nr. 4
$T_1=T_2$	[°C]	300	300	300	300
T_3	[°C]	280	269	272	272
T_4	[°C]	220	256	254	255
T_5	[°C]	220	253	250	251
T_6	[°C]	220	245	244	244
T_7	[°C]	60	38	27	28
T_8	[°C]	60	40	27	29
T_9	[°C]	60	47	31	34
T_{10}	[°C]	20	20	20	20
$Ra_{D,15}$	[]	879100	$0.142\ 10^7$	$0.127\ 10^7$	
$Nu_{D,15}$	[]	13.94	15.96	15.46	
h_{15}	[W/m²K]	3.119	3.541	3.437	
R_{15}	[K/W]	9.278	8.172	8.419	
$Ra_{D,25}$	[]	13736	22197	19821	
$Nu_{D,25}$	[]	4.696	5.278	5.133	
h_{25}	[W/m²K]	4.202	4.685	4.566	
R_{25}	[K/W]	0.631	0.566	0.581	
$Ra_{L,34}$ []	[]	468064	91700	126969	
$Nu_{L,34}$	[]	14.12	9.397	10.193	
h_{34}	[W/m²K]	6.679	4.531	4.915	
R_{34}	[K/W]	1.019	1.508	1.385	
$Ra_{L,710}$	[]	$0.129\ 10^8$	$0.684\ 10^7$	$0.290\ 10^7$	
$Nu_{L,710}$	[]	32.38	27.62	22.27	
h_{710}	[W/m²K]	6.108	5.068	4.024	
R_{710}	[K/W]	0.465	0.561	0.706	
$Ra_{L,36}$	[]	468064	187226	218430	
$Nu_{L,36}$	[]	7.062	5.616	5.837	
h_{36}	[W/m²K]	3.340	2.656	2.760	
R_{36}	[K/W]	2.038	2.563	2.466	
$Ra_{L,910}$	[]	$0.129\ 10^8$	$0.960\ 10^7$	$0.441\ 10^7$	
$Nu_{L,910}$	[]	16.19	15.08	12.37	
h_{910}	[W/m²K]	3.054	2.788	2.247	
R_{910}	[K/W]	0.930	1.019	1.265	
$Ra_{L,35}$	[]	$0.117\ 10^8$	$0.284\ 10^7$	$0.387\ 10^7$	
$Nu_{L,35}$	[]	32.42	21.848	23.77	
h_{35}	[W/m²K]	5.250	3.599	3.925	
R_{35}	[K/W]	0.527	0.769	0.705	
$Ra_{L,810}$	[]	$0.424\ 10^9$	$0.246\ 10^9$	$0.951\ 10^8$	
$Nu_{L,810}$	[]	94.47	80.064	60.16	
h_{810}	[W/m²K]	5.565	4.595	3.393	
R_{810}	[K/W]	0.196	0.238	0.322	
R_1	[K/W]	0.591	0.529	0.543	
R_2	[K/W]	4.680	4.827	4.841	
Q	[W]	53.12	52.28	52	
Q_{up}	[W]	12.19	12.03	11.99	
Q_{side}	[W]	29.57	29.03	28.89	
Q_{down}	[W]	11.36	11.22	11.12	

Figure D.3: Result of iterations

Appendix E

Error Analysis

The experimental results presented in sections 10 and 11 are subject to statistical and systematic errors. In this section, the statistical error of indicated work and power derived from the pV-diagrams are calculated.

To compose a pV-diagram, pressure and crank angle measurements are performed simultaneously. The incremental encoder generates a thousand pulses for each revolution, dividing a cycle in a thousand parts by crank angle. Because pressure measurements are taken with a sample rate of 100000 samples per second, a certain number of pressure values are identified with the same crank angle.

$$N_i = \frac{100000}{1000 \times f_{motor}} = \frac{\#\ pressure\ measurements}{crank\ angle} \tag{E.1}$$

Each measurement of this population has a standard deviation to the mean value, given by formula (E.2). The standard deviation of the mean value itself is given by equation (E.3)

$$\sigma_{p_i} = \sqrt{\frac{\left(\Sigma_j \left(p_j - p_{gem}\right)\right)^2}{N_i - 1}} \tag{E.2}$$

$$\sigma_{p_i,gem} = \frac{\sigma_{p_i}}{\sqrt{N_i}} \tag{E.3}$$

The standard deviation of the mean can be regarded as the error on the pressure measurement of a given crank angle. The (swept) volume function of the cycle is related to crank angle as shown in equation (E.4).

$$V\left(\alpha\right) = \left(k + r - r\cos\left(\alpha\right) - \sqrt{k^2 - r^2\left(\sin\left(\alpha\right)\right)^2}\right) A_{piston} \tag{E.4}$$

The error on this function is the product of its derivative to crank angle and the error on crank angle itself. The error on crank angle is taken as the encoder accuracy, or $2 * \pi$ radians divided by the number of pulses.

$$\sigma_{V_i} = \left(\frac{d}{d\alpha} V\left(\alpha\right)\right) \sigma_\alpha \tag{E.5}$$

with

$$\frac{d}{d\alpha}V(\alpha) = \left(r\sin(\alpha) + \frac{r^2\cos(\alpha)\sin(\alpha)}{\sqrt{k^2 - r^2(\sin(\alpha))^2}} \right) A_{piston} \tag{E.6}$$

$$\sigma_{alpha} = \frac{2\pi}{1000\ pulses} \tag{E.7}$$

Once the pV-diagram is constructed, indicated work can be calculated by using the trapezium rule:

$$W = 1/2\,\Sigma\,(p_i + p_{i+1})\,(V_{i+1} - V_i) \tag{E.8}$$

The formula to calculate the error on a function with multiple variables is given in equation (E.9). Applied to the trapezium rule to calculate indicated work, this gives equation (E.10).

$$\sigma_q = \sqrt{\Sigma_i \left(\frac{d}{dx_i} q(x_i)\right)^2 {\sigma_{x_i}}^2} \tag{E.9}$$

$$\delta\, W_i = 1/2\sqrt{(\Sigma\,(V_{i+1} - V_i))^2\left({\sigma_{p_{i,gem}}}^2 + {\sigma_{p_{i+1,gem}}}^2\right) + \left({p_{i,gem}}^2 + {p_{i+1,gem}}^2\right){\sigma_{V_i}}^2} \tag{E.10}$$

Because indicated power is the product of indicated work and frequency (a constant), the error is the same as for indicated work.

Appendix F

Radial Clearance

The piston and cylinder are allowed to expand freely when subject to a temperature increase. The general formula to calculate the change in radial dimensions due to a (uniform) elevated temperature is given by equation (F.1) [30]. The change in dimensions with respect to the dimensions in the cold state are calculated separately for the piston and the cylinder. A simple comparison of the new dimensions results in the radial clearance between piston and cylinder under working conditions, see equation (F.5).

$$u_r(r) = \alpha \, \frac{1+\nu}{1-\nu} \, \frac{1}{b^2-a^2} \, [(1-2\,\nu)\, r + \frac{a^2}{r}] \int_a^b T\, r dr + \alpha \, \frac{1+\nu}{1-\nu} \, \frac{1}{r} \int_a^r T r dr \tag{F.1}$$

Abbreviation	**Dimension**	**Description**
u_r	m	Radial displacement
r	m	Radius
T	K	Radial temperature profile (assumed constant)
α	$\frac{m}{mK}$	Thermal expansion coefficient
ν	-	Poisson ratio
a	m	Inner radius (a=0 for discs)
b	m	Outer radius

Table F.1: Glossary of used abbreviations

The values that are used in the situations of the copper cylinder and aluminium piston are listed in table F.2. The dimension of the cylinder and piston were measured with the use of a micrometer at atmospheric temperature.

Factor	**Dimension**	**value**
T	K	393.15 (120°C)
α_{copper}	$\frac{m}{m\times}$	17.64
$\alpha_{aluminium}$	$\frac{m}{m\times}$	23.58
ν_{copper}	-	0.37
$\nu_{aluminium}$	-	0.35
a_{copper}	m	0.044995
b_{copper}	m	0.0455
$a_{aluminium}$	m	0
$b_{aluminium}$	m	0.04492

Table F.2: Glossary of used abbreviations

The results of equ F.1 for both situations are:

$$u_{cylinder} = 108.739\ [\mu m] \tag{F.2}$$

$$u_{piston} = 142.994\ [\mu m] \tag{F.3}$$

With the obtained values of displacement, the radii of both piston and cylinder in the hot state can be calculated. Subtracting the radii gives the new radial clearance:

$$radial\ clearance_{cold} = 75\ [\mu m] \tag{F.4}$$

$$radial\ clearance_{hot} = 40.745\ [\mu m] \tag{F.5}$$

Appendix G

MATLAB Code

G.1 Code for first data set

```
function [mdta,sdta] = readdata(rawdta,r)

%initializing the data
dta1 = zeros(length(rawdta),5);

%triming the lines of the raw data that will not be analysed
dta1(:,1) = rawdta(:,1);
dta1(:,2:5) = rawdta(:,6:9);

%select the number of loop to study (lastloop = number of loop + 1)
lastLoop = 2; %max(dta1(:,2));

%trimming the undesired data so we only keep the number of loops
c0 = 0;
cl = 0;
for i = 1:length(dta1)
    if dta1(i,3) == 0
        c0 = c0 + 1;
    elseif dta1(i,3) >= lastLoop
        cl = cl + 1;
    else
    end
end

dta = zeros(length(dta1) - (cl+c0),5);
```

```
dta(:,:) = dta1(c0+1:length(dta1)-cl,:);

%scaling and inverting for pressures
dta(:,4:5) = (dta(:,4:5)*-1 + 30)*40000;

minP1 = min(dta(:,4));
minP2 = min(dta(:,5));

dta(:,4) = dta(:,4) - minP1;
dta(:,5) = dta(:,5) - minP2;

%indentifying the reference
[rP1,cP1] = find(dta(:,4) == 0,1);
[rP2,cP2] = find(dta(:,5) == 0,1);

pls1 = dta(rP1,2);
pls2 = dta(rP2,2);

%introducing angle values for the two pressures references
dta(:,6) = pi + 2*pi/1000*(dta(:,2)-pls1);
dta(:,7) = pi + 2*pi/1000*(dta(:,2)-pls2);

%Introducing volume reading for the two pressure references
k = 0.206;
Ap = 0.0063617;
dta(:,8) = (k + r -(r.*cos(dta(:,6)) + sqrt(k^2 - r^2.*sin(dta(:,6)).^2)))*Ap;
dta(:,9) = (k + r -(r.*cos(dta(:,7)) + sqrt(k^2 - r^2.*sin(dta(:,7)).^2)))*Ap;

%averaging the pressure readings to 1000 points per cycle.
i = min(dta(:,2));
k = 1;
g = 0;
y = 0;
while i ~= max(dta(:,2))
    if dta(k,2) == i
        g = g + 1;
        k = k + 1;
    else
```

```
        p = dta(k-g:k,:);
        y = y + 1;
        mdta(y,:) = mean(p);
        sdta(y,:) = std(p);
        i = i + 1;
        g = 0;
    end
end

fmdta = zeros(1000,9);
sfmdta = zeros(1000,9);

%Fold all mean cycle points of the experiment into a single mean cycle.
%for i = 1:1000
%    for j = 1:lastLoop-2
%        p(j,:) = mdta(1000*(j-1) + i,:);
%    end
%    fmdta(i,:) = mean(p);
%    sfmdta(i,:) = std(p);
%end

%close the cycle for calculating the indicates work
%fmdta(length(fmdta)+1,:) = fmdta(1,:);
%sfmdta(length(sfmdta)+1,:) = sfmdta(1,:);

%calculate work
Work = trapz(mdta(:,9),mdta(:,5))
```

G.2 Code for second data set

```
function [mdta,sdta] = readdata(rawdta)

%initializing the data
dta1 = zeros(length(rawdta),5);

%triming the lines of the raw data that will not be analysed
dta1(:,1) = rawdta(:,1);
dta1(:,2:5) = rawdta(:,9:12);
```

```
%select the number of loops to study (lastloop = number of loop + 1)
lastLoop = 4; %max(dta1(:,2));

%trimming the undesired data so we only keep the number of loops
c0 = 0;
cl = 0;
for i = 1:length(dta1)
    if dta1(i,3) == 0
        c0 = c0 + 1;
    elseif dta1(i,3) >= lastLoop
        cl = cl + 1;
    else
    end
end

dta = zeros(length(dta1) - (cl+c0),5);

dta(:,:) = dta1(c0+1:length(dta1)-cl,:);

%scaling and inverting for pressures
dta(:,4:5) = (dta(:,4:5) + 30)*40000;

minP1 = min(dta(:,4));
minP2 = min(dta(:,5));

dta(:,4) = dta(:,4) - minP1;
dta(:,5) = dta(:,5) - minP2;

%indentifying the reference
[rP1,cP1] = find(dta(:,4) == 0,1);
[rP2,cP2] = find(dta(:,5) == 0,1);

pls1 = dta(rP1,2);
pls2 = dta(rP2,2);

%introducing angle values for the two pressures references
dta(:,6) = pi + 2*pi/1000*(dta(:,2)-pls1);
dta(:,7) = pi + 2*pi/1000*(dta(:,2)-pls2);
```

```
%Introducing volume reading for the two pressure references
k = 0.206;
r = 0.025;
Ap = 0.0063617;
dta(:,8) = (k + r -(r.*cos(dta(:,6)) + sqrt(k^2 - r^2.*sin(dta(:,6)).^2)))*Ap;
dta(:,9) = (k + r -(r.*cos(dta(:,7)) + sqrt(k^2 - r^2.*sin(dta(:,7)).^2)))*Ap;

%averaging the pressure readings to 1000 points per cycle.
i = min(dta(:,2));
k = 1;
g = 0;
y = 0;
while i ~= max(dta(:,2))
    if dta(k,2) == i
        g = g + 1;
        k = k + 1;
    else
        p = dta(k-g:k,:);
        y = y + 1;
        mdta(y,:) = mean(p);
        sdta(y,:) = std(p);
        i = i + 1;
        g = 0;
    end
end

%fmdta = zeros(1000,9);
%sfmdta = zeros(1000,9);

%Fold all mean cycle points of the experiment into a single mean cycle.
%for i = 1:1000
%    for j = 1:lastLoop-2
%        p(j,:) = mdta(1000*(j-1) + i,:);
%    end
%    fmdta(i,:) = mean(p);
%    sfmdta(i,:) = std(p);
%end
```

```
%close the cycle for calculating the indicates work
fmdta(length(fmdta)+1,:) = fmdta(1,:);
sfmdta(length(sfmdta)+1,:) = sfmdta(1,:);

%calculate work
Work = trapz(mdta(:,9),mdta(:,5))
```

Bibliography

[1] IPCC: *Intergovernmental panel on climate change*, 2009. http://www.ipcc.ch/.

[2] United Nations: *Kyoto Protocol to the United Nations Framework Convention on Climate Change*, 1998.

[3] *Citizen's summary eu climate and energy package*, 2008. European Communities http://ec.europa.eu/environment/climat/climateaction.htm.

[4] REN21: *Renewables global status report update*, 2009. http://www.ren21.net/.

[5] *Frost & sullivan: Offshore wind energy set to boom in the next few years.* 2009. PR Newswire http://sev.prnewswire.com/.

[6] (WWEA), World Wind Energy Association, 2009. http://www.wwindea.org/home/index.php/.

[7] Sier, R.: *Reverend Robert Stirling D.D.: A Biography of the Inventor of the Heat Economiser and Stirling Cycle Engine.* L.A. Mair, 1995.

[8] Beale, W.T.: *The development of stirling engines at sunpower inc.* In *2nd International Conference on Stirling Engines*, Shanghai, China, 1983.

[9] Meier, R.C.: *Development of the general electric stirling engine gas heat pump.* Technical report, General Electric Company, year unknown.

[10] *A brief stirling engine history*, 2007. http://www.stirlingengine.co.uk/.

[11] Tailer, P.: *Thermal lag machine.* U.S. Patent, May 1995. Patent No 5414997.

[12] *Beta type stirling engines*, 2009. http://www.ent.ohiou.edu/urieli/stirling/engines/beta.html/.

[13] Nightingale, N. P.: *Automotive stirling engine mod ii design report.* Technical report, Mechanical Technology Inc., October 1986.

[14] Hsu, S., Lin, F., and Chiou, J.: *Heat-transfer aspects of stirling power generation using incinerator waste energy.* Renewable Energy, 28:59–69, 2003.

[15] Rifkin, W., Vincent, R., and Benson, O.: *Application of free piston stirling engine.* American Institute of Aeronautics and Astronautics, 809401:1982–6, 1980.

[16] Swift, G.: *Thermoacoustic engines and refrigerators.* Physics Today, July 1995.

[17] Tailer, P., Hastings, R., and Malkus, P.: *Internally pressurized annular rolling seal.* In *Proceedings of the 26th Intersociety Energy Conversion Engineering Conference*, volume 5, Boston, USA, August 1991. American Nuclear Society.

[18] Chen, N.C.J. and West, C.D.: *A single-cylinder valveless heat engine.* In *Proceedings of the 22nd Intersociety Energy Conversion Engineering Conference*, Philadelphia, USA, January 1987. American Society of Mechanical Engineers.

[19] Tailer, P.: *External combustion otto cycle thermal lag engine.* In *Proceedings of the 28th Intersociety Energy Conversion Engineering Conference*, volume 1, Atlanta, USA, August 1993. American Society of Mechanical Engineers.

[20] West, C.D.: *Some single-piston closed-cycle machines and peter tailer's thermal lag engine.* In *Proceedings of the 28th Intersociety Energy Conversion Engineering Conference*, volume 1, Atlanta, USA, August 1993. American Society of Mechanical Engineers.

[21] Wicks, F. and Caminero, C.: *The peter tailer external combustion thermal lag piston/-cylinder engine analysis and potential applications.* In *Proceedings of the 29th Intersociety Energy Conversion Engineering Conference.* American Society of Mechanical Engineers, August 1994.

[22] Tailer, P.: *Thermal lag test engines evaluated and compared to equivalent stirling engines.* In *Proceedings of the 30th Intersociety Energy Conversion Engineering Conference*, Orlando, FL, USA, July-August 1995. American Society of Mechanical Engineers.

[23] Altamirano, C. Fernandez Aballi, Paepe, M. De, Verhelst, S., and Bayon, J.J. Gonzalez: *Control volume energy based model for a thermal lag engine.* 2009.

[24] Organ, A.: *The Air Engine.* Woodhead Publishing Ltd, 2007. Part 2 Some light on the inner workings of the thermal lag engine.

[25] Paepe, M. De and Mertens, D.: *Micro-chp systems for residential applications.* Energy Conversion and Management, 47:3435–3446, 2006.

[26] Farrel, J. and Morris, D.: *Energy self-reliant states second and expanded edition.* October 2009. New Rules Project, Institute for Local Self-Reliance.

[27] Newman, M.: *World mapper - electricity access*, 2009. http://www.worldmapper.org/display.php?selected=346#/.

[28] Hamaguchi, K., Futagi, H., Yazaki, T., and Chen, R.: *Measurement of work generation and improvement.* Journal of Power and Energy Systems, 2:1267–1275, 2008.

[29] Welty, J., Wicks, C. E., Wilson, R. E., and Rorrer, G. L.: *Fundamentals of Momentum, Heat and Mass Transfer.* Wiley, 2007.

[30] Paepegem, W. Van: *Mechanica van Materialen.* Ghent University, 2007.

List of Figures